GAS EMISSIVITIES AND RADIATIVE TRANSFER STUDIES

Thesis by

Daniel B. Olfe

In Partial Fulfillment of the Requirements

For the Degree of

Doctor of Philosophy

California Institute of Technology

Pasadena, California

1960

ACKNOWLEDGEMENT

The author wishes to express his sincere appreciation to Dr. S. S. Penner for suggesting these studies and for many valuable discussions and suggestions.

Financial assistance during the time this work was carried out was provided by a Daniel and Florence Guggenheim Jet Propulsion Fellowship for the 1957-58 and 1958-59 academic years and by a National Science Foundation Cooperative Fellowship for the 1959-60 academic year. Portions of the work in this thesis were supported by the U. S. Navy (Office of Naval Research) under Contract Nonr-220(03), NR 015 401 and the U. S. Air Force under Contract AF 18(603)-2. Grateful acknowledgement is made to these organizations.

The author is grateful to Mrs. Barbara Rickert and Mrs. L. Lozoya for the expert typing of this thesis.

ABSTRACT

In Chapter 1 theoretical expressions are derived for the relations between gas absorptivities and emissivities for the limit of zero optical depth and for various models of vibration-rotation bands. Some of the band models for which useful results are obtained are bands with constant average absorption coefficients and well-defined widths, bands composed of non-overlapping spectral lines with dispersion or Doppler contour, and bands composed of randomly distributed lines with dispersion contour. The theoretical formulae are shown to provide a good correlation for the available experimental data on CO_2, H_2O and CO .

Representative estimates for the radiant energy emission from the combustion products formed by a burning ammonium perchlorate propellant grain are made in Chapter 2. The listed compilations of data may be used to estimate the radiant heat transfer to the burning propellant surface, as well as the radiant energy loss from the combustion products, since emission and absorption of radiation by the gases in the reaction zone are shown to be negligibly small.

The study in Chapter 3 on radiant energy transfer from non-isothermal molecular emitters with non-overlapping dispersion lines complements earlier work done on overlapping lines and on randomly distributed dispersion lines. In addition to the transparent gas

approximation for gases of small optical depth, a "square root" approximation is found to be valid for large optical depths, provided the temperature gradient in the slab of gas nearest to the observer is not too large. These approximations are used to derive explicit expressions for the radiant energy flux from two adjacent isothermal regions at different temperatures.

In Chapter 4, the important equilibrium emission processes in a hydrogen plasma are investigated in the temperature range between 300°K and 10,000°K for pressures up to several hundred atmospheres. It is found that the pressure-induced spectrum of the H_2 molecule makes an important emissivity contribution at the lower temperatures (below approximately 4500°K) whereas, at the higher temperatures, the bound-free and free-free transitions of the H^- ion and the continuum and line spectrum of the H atom are the most important contributors to the emissivity. The problems of the very broad wings of the Lyman α line and of the lowering of the ionization potentials by the fields of the plasma ions are considered.

TABLE OF CONTENTS

CHAPTER 1

RELATIONS BETWEEN MOLECULAR GAS ABSORPTIVITIES AND EMISSIVITIES

I. INTRODUCTION

Theoretical expressions between gas absorptivities and emissivities for various representations of molecular vibration-rotation bands are of fundamental interest and may also be useful for extending available gas emissivity compilations to different conditions of temperature and pressure because it is often easier to measure absorptivities than emissivities. Representative results for selected band models have been described in previous publications.[1-5] In this chapter we present an exhaustive review and extension of this earlier work in which the most important restriction is the following: the temperatures used for making absorptivity and emissivity estimates must be sufficiently close to justify the assumption that neither the spectral line shape nor the band model are changed in character.

Theoretical relations for important band models are derived in the following Section II. The correlation of available experimental data for CO_2, H_2O and CO, in terms of appropriate theoretical expressions, is described in Section III.

II. RELATIONS BETWEEN ABSORPTIVITIES AND EMISSIVITIES

The total absorptivity α_{ab} of a gaseous absorber at the temperature T_g for blackbody radiation emitted at the temperature T_s is defined by the relation

$$a_{ab} = \frac{1}{\sigma T_s^4} \int_0^\infty R^o_{\omega, T_s} \left[1-\exp-(P_{\omega, T_g} X)\right] d\omega \qquad (1)$$

where σ is the Stefan-Boltzmann constant, R^o_{ω, T_s} is the spectral blackbody radiancy at T_s in the wave number range between ω and $\omega + d\omega$, P_{ω, T_g} represents the spectral absorption coefficient (in cm^{-1}-$atmos^{-1}$) of the gas at T_g and ω, and X denotes the optical depth. Since the vibration-rotation bands of molecular emitters lie in well-defined spectral regions, we may replace Eq. (1) by the approximate expression

$$a_{ab} \simeq \frac{1}{\sigma T_s^4} \sum_i R^o_{\omega_i, T_s} \int_{\Delta\omega_{i, T_g}} \left[1-\exp(-P_{\omega, T_g} X)\right] d\omega \qquad (2)$$

where ω_i is the wave number at the center of the ith vibration-rotation band which has an "effective" width $\Delta\omega_{i, T_g}$ at the temperature T_g of the gaseous absorbers and $R^o_{\omega_i, T_s}$ is the spectral blackbody radiancy evaluated at ω_i and T_s.

A. Emission from a Blackbody and Absorption by Transparent Gases[2-5]

For optically thin layers of absorbing gases, Eq. (2) becomes

$$a_{ab} \simeq \frac{1}{\sigma T_s^4} \sum_i R^o_{\omega_i, T_s} X \int_{\Delta\omega_{i, T_g}} P_{\omega, T_g} d\omega$$

or

$$a_{ab} \simeq \frac{1}{\sigma T_s^4} \sum_i R^o_{\omega_i, T_s} a_{i, T_g} X \qquad (3)$$

since

$$a_{i,T} \equiv \int_{\Delta\omega_{i,T}} P_{\omega,T}\, d\omega \tag{4}$$

represents the integrated absorption (in cm^{-2}-$atmos^{-1}$) for the ith vibration-rotation band of the gas at T. But*

$$\frac{a_{i,T}}{a_{i,T_g}} = \frac{T_g}{T} \tag{5}$$

whence Eq. (3) becomes

$$a_{ab} \simeq \frac{T_s}{T_g}\, \mathcal{E}(T_s, X) \tag{6}$$

since the emissivity of transparent gases at the temperature T_s and optical depth X is defined by the expression

$$\mathcal{E}(T_s, X) = \lim_{X\to 0} \frac{1}{\sigma T_s^4} \int_0^\infty R^o_{\omega,T_s} \left[1-\exp(-P_{\omega,T_s} X)\right] d\omega$$

$$\simeq \lim_{X\to 0} \frac{1}{\sigma T_s^4} \sum_i R^o_{\omega_i,T_s} \int_{\Delta\omega_{i,T_s}} \left[1-\exp(-P_{\omega,T_s} X)\right] d\omega$$

or

$$\mathcal{E}(T_s, X) \simeq \frac{1}{\sigma T_s^4} \sum_i R^o_{\omega_i,T_s}\, a_{i,T_s} X. \tag{7}$$

---

* Equation (5) depends essentially only on the validity of the ideal gas law, i.e., on the assumption that the number of absorbers at constant pressure in a fixed geometric length is inversely proportional to the temperature if the Boltzmann population factor may be neglected.

It is apparent that Eq. (6) is independent of any band model and of the spectral line shape and depends, in fact, only on the temperature dependence of the integrated intensity specified through Eq. (5). Accordingly, we expect that all of the theoretical formulae derived in subsequent sections for special band models and line shapes must reduce to Eq. (6) if they apply in the limit of zero optical depth. In this connection it is important to note that

$$\lim_{X \to 0} \mathcal{E}(T, \beta X) = \beta \mathcal{E}(T, X). \tag{8}$$

B. Emission from a Blackbody and Absorption by Vibration-Rotation Bands Characterized by Constant Average Absorption Coefficients[1-5]

When the ith vibration-rotation band is characterized by the constant absorption coefficient $\overline{P}_i$ over the effective width $\Delta\omega_{i,\,T_g}$, then Eq. (2) is replaced by the expression

$$a_{ab} \simeq \frac{1}{\sigma T_s^{\,4}} \sum_i R^o_{\omega_i,\,T_s}\, \Delta\omega_{i,\,T_g} \left[1 - \exp(-\overline{P}_{i,\,T_g} X)\right]. \tag{9}$$

However, to the order of approximation that constant average absorption coefficients may be used, it is easily shown[5] that

$$\frac{\Delta\omega_{i,\,T}}{\Delta\omega_{i,\,T_g}} = \left(\frac{T}{T_g}\right)^{1/2} \tag{10}$$

whence

$$\frac{\overline{P}_{i,\,T}}{\overline{P}_{i,\,T_g}} = \frac{(a_{i,\,T}/\Delta\omega_{i,\,T})}{(a_{i,\,T_g}/\Delta\omega_{i,\,T_g})} = \left(\frac{T_g}{T}\right)^{3/2} \tag{11}$$

where use had been made of Eq. (5). From Eqs. (9), (10) and (11) it now follows that

$$\alpha_{ab} \simeq \left(\frac{T_g}{T_s}\right)^{1/2} \frac{1}{\sigma T_s^4} \sum_i R^o_{\omega_i, T_s} \Delta\omega_{i, T_s} \left\{ 1-\exp\left[-\bar{P}_{i, T_s} \left(\frac{T_s}{T_g}\right)^{3/2} X \right] \right\}$$

or

$$\alpha_{ab} \simeq \left(\frac{T_g}{T_s}\right)^{1/2} \varepsilon\left[T_s, \left(\frac{T_s}{T_g}\right)^{3/2} X \right] \qquad (12)$$

since

$$\varepsilon\left[T_s, \left(\frac{T_s}{T_g}\right)^{\frac{3}{2}} X \right] \simeq \frac{1}{\sigma T_s^4} \sum_i R^o_{\omega_i, T_s} \int_{\Delta\omega_{i, T_s}} \left\{ 1-\exp\left[-P_{\omega, T_s} \left(\frac{T_s}{T_g}\right)^{\frac{3}{2}} X \right] \right\} d\omega$$

$$\simeq \frac{1}{\sigma T_s^4} \sum_i R^o_{\omega_i, T_s} \Delta\omega_{i, T_s} \left\{ 1-\exp\left[-P_{i, T_s} \left(\frac{T_s}{T_g}\right)^{\frac{3}{2}} X \right] \right\} \qquad (13)$$

for the assumed band model.

Equation (12) is a relation between the absorptivity α_{ab} for molecular absorbers at the temperature T_g and optical depth X and the emissivity of the same gas at the temperature T_s and the optical depth $(T_s/T_g)^{3/2} X$. Within the limitations of the assumed band model, Eq. (12) and other similar expressions suggest the possible determination of (infrared) emissivities from lower temperature absorptivity measurements.

C. Emission from a Blackbody and Absorption by Vibration-Rotation Bands Composed of Just-Overlapping Spectral Lines

For just-overlapping spectral lines it may be shown* that

$$\int_{\Delta\omega_{i,\,T_g}} \left[1-\exp(-P_{\omega,\,T_g} X)\right] d\omega \simeq \Delta\omega_{i,\,T_g} \left\{ h\left(\frac{a_{i,\,T_g} X}{\Delta\omega_{i,\,T_g}}\right)\left[1-\exp(-a_{i,\,T_g} X/\Delta\omega_{i,\,T_g})\right]\right\}^{\frac{1}{2}} \tag{14}$$

where

$$h(x) = \ln Cx - Ei(-x),$$

C is Euler's constant, and

$$-Ei(-x) = \int_x^\infty \frac{1}{t} \exp(-t)dt$$

is the exponential integral. Using Eqs. (5) and (10), it is apparent that

$$\int_{\Delta\omega_{i,\,T_g}} \left[1-\exp(-P_{\omega,\,T_g} X)\right] d\omega \simeq \left(\frac{T_g}{T_s}\right)^{\frac{1}{2}} \Delta\omega_{i,\,T_s} \left\{ h\left[\frac{a_{i,\,T_s} X(T_s/T_g)^{3/2}}{\Delta\omega_{i,\,T_s}}\right] \right.$$

$$\left. X\left[1-\exp-\frac{a_{i,\,T_s} X(T_s/T_g)^{3/2}}{\Delta\omega_{i,\,T_s}}\right]\right\}^{\frac{1}{2}} \simeq \left(\frac{T_g}{T_s}\right)^{\frac{1}{2}} \int_{\Delta\omega_{i,\,T_s}} \left\{1-\exp\left[-P_{\omega,\,T_s} X\left(\frac{T_s}{T_g}\right)^{\frac{3}{2}}\right]\right\} d\omega.$$

Hence Eq. (2) becomes

---

* Reference 5, Eq. (58-37); the validity of Eq. (15) is independent of the approximation contained in Eq. (14), as may be verified readily by using the exact integral representation for the just-overlapping line model.

$$\alpha_{ab} \simeq \left(\frac{T_g}{T_s}\right)^{\frac{1}{2}} \frac{1}{\sigma T_s^{\,4}} \sum_i R^o_{\omega_{i,T_s}} \int_{\Delta\omega_{i,T_s}} \left\{1-\exp\left[-P_{\omega,T_s} X\left(\frac{T_s}{T_g}\right)^{\frac{3}{2}}\right]\right\} d\omega$$

or

$$\alpha_{ab} \simeq \left(\frac{T_g}{T_s}\right)^{\frac{1}{2}} \varepsilon\left[T_s, \left(\frac{T_s}{T_g}\right)^{\frac{3}{2}} X\right] . \qquad (15)$$

Comparison of Eqs. (12) and (15) shows that the constant absorption coefficient approximation and the just-overlapping line approximation lead to the same relation between absorptivity and emissivity. This result is not unexpected since the assumed physical models are similar and since it is known that these two representations lead to practically identical emissivity estimates for diatomic molecules.[3, 5]

D. Emission from a Blackbody and Absorption by Vibration-Rotation Bands with Non-Overlapping Dispersion Lines[2, 5]

For non-overlapping spectral lines, Eq. (2) becomes

$$\alpha_{ab} \simeq \frac{1}{\sigma T_s^{\,4}} \sum_i R^o_{\omega_{i,T_s}} \sum_{j=0}^{\infty} 2\pi\, b_{i,j,T_g} f\left(\frac{S_{i,j,T_g} X}{2\pi\, b_{i,j,T_g}}\right) \qquad (16)$$

where b_{i,j,T_g} is the dispersion half-width of the jth line in the ith band at T_g, S_{i,j,T_g} is the corresponding integrated line intensity, and

$$f(x) = x\left[\exp(-x)\right]\left[J_o(ix) - iJ_1(ix)\right]$$

with J_o and J_1 representing Bessel functions of the first kind of order zero and one, respectively. The relation between absorptivity and

emissivity may be determined for two cases depending on the form of $S_{i,j}$.

(1). Bands with Regular Spacing and Constant Collision Half-Width

We may now use* the following approximation to S_{i,j,T_g} for each branch of a vibration-rotation band:

$$S_{i,j,T_g} = a_{i,T_g}\sqrt{\frac{hcB_{e_i}}{kT_g}}\; g\left(\sqrt{\frac{hcB_{e_i}}{kT_g}}\; j\right) \qquad (17)$$

where

$$g(x) = x\exp(-x^2) \qquad (18)$$

and B_{e_i} is the usual rotational spectroscopic constant for the ith band. Hence Eq. (16) becomes, for $b_{i,j,T_g} = b_{i,T_g}$,

$$\alpha_{ab} \simeq \frac{1}{\sigma T_s^4}\sum_i R^o_{\omega_i,T_s}\, 2\sum_{j=0}^{\infty} 2\pi b_{i,T_g} f\left[\frac{a_{i,T_g}\sqrt{\frac{hcB_{e_i}}{kT_g}}\; g\left(\sqrt{\frac{hcB_{e_i}}{kT_g}}\; j\right) X}{2\pi b_{i,T_g}}\right]$$

$$\simeq \frac{1}{\sigma T_s^4}\sum_i R^o_{\omega_i,T_s}\, 2\int_0^{\infty} 2\pi b_{i,T_g}\sqrt{\frac{kT_g}{hcB_{e_i}}}\; f\left[\frac{a_{i,T_g}\sqrt{\frac{hcB_{e_i}}{kT_g}}\; g(u)}{2\pi b_{i,T_g}} X\right] du$$

where the factor 2 preceding the sum over j accounts for the two branches of the vibration-rotation band. Using Eq. (5) and the relation

$$\frac{b_{i,T}}{b_{i,T_g}} = \left(\frac{T_g}{T}\right)^{1/2} \qquad (19)$$

* Reference 5, Eq. (58-35).

the preceding relation reduces to

$$a_{ab} \simeq \frac{1}{\sigma T_s^4} \sum_i R^o_{\omega_i, T_s}{}^2 \int_0^\infty 2\pi b_{i, T_s} \sqrt{\frac{kT_s}{hcB_{e_i}}}\, f\left[\frac{a_{i, T_s}\sqrt{\frac{hcB_{e_i}}{kT_s}}\, g(u)}{2\pi b_{i, T_s}} \cdot \frac{T_s}{T_g} X\right] du$$

$$\simeq \frac{1}{\sigma T_s^4} \sum_i R^o_{\omega_i, T_s}{}^2 \sum_j 2\pi b_{i, T_s}\, f\left[\frac{a_{i, T_s}\sqrt{\frac{hcB_{e_i}}{kT_s}}\, g\left(\sqrt{\frac{hcB_{e_i}}{kT_s}}\, j\right)}{2\pi b_{i, T_s}} \frac{T_s}{T_g} X\right]$$

or

$$a_{ab} \simeq \varepsilon\left(T_s, \frac{T_s}{T_g} X\right) . \tag{20}$$

(2). Bands with Equally Intense Spectral Lines and Constant Collision Half-Width

If all of the spectral lines of the ith band have the same integrated intensity $\overline{S}_{i, T_g}$ and the same half-width b_{i, T_g} and there are N_{i, T_g} lines contributing, then Eq. (16) becomes

$$a_{ab} \simeq \frac{1}{\sigma T_s^4} \sum_i R^o_{\omega_i, T_s} N_{i, T_g} 2\pi b_{i, T_g} f\left(\frac{\overline{S}_{i, T_g} X}{2\pi b_{i, T_g}}\right) . \tag{21}$$

By definition,

$$N_{i, T_g} = \frac{\Delta\omega_{i, T_g}}{d_{i, T_g}} \tag{22}$$

if d_{i,T_g} represents the average line spacing in the ith band at T_g. If we assume that

$$\frac{d_{i,T_g}}{d_{i,T_s}} = \left(\frac{T_s}{T_g}\right)^{\eta} \tag{23}$$

and use Eq. (10), then

$$\frac{N_{i,T_g}}{N_{i,T_s}} = \left(\frac{T_g}{T_s}\right)^{\eta+(1/2)} \tag{24}$$

and

$$\frac{\overline{S}_{i,T_g}}{\overline{S}_{i,T_s}} = \frac{(a_{i,T_g}/N_{i,T_g})}{(a_{i,T_s}/N_{i,T_s})} = \left(\frac{T_s}{T_g}\right)^{\eta+(3/2)} . \tag{25}$$

From Eqs. (21) to (25) it follows that

$$a_{ab} \simeq \frac{1}{\sigma T_s^4}\left(\frac{T_g}{T_s}\right)^{\eta} \sum R^{o}_{\omega_i, T_s} N_{i,T_s} 2\pi b_{i,T_s} f\left[\frac{\overline{S}_{i,T_s}}{2\pi b_{i,T_s}}\left(\frac{T_s}{T_g}\right)^{\eta+1} X\right]$$

or

$$a_{ab} \simeq \left(\frac{T_g}{T_s}\right)^{\eta} \varepsilon\left[T_s, X\left(\frac{T_s}{T_g}\right)^{\eta+1}\right]. \tag{26}$$

E. Emission from a Blackbody and Absorption by Randomly Distributed Spectral Lines with Dispersion Contour[4]

For the statistical model of a vibration-rotation band, it may be shown[2, 5-7] that

$$\int_{\Delta\omega_{i,T_g}} \left[1-\exp(-P_\omega X)\right] d\omega \simeq \Delta\omega_{i,T_g}\left[1-\exp-\left(\frac{\overline{A}_{i,T_g}}{d_{i,T_g}}\right)\right] \tag{27}$$

where

$$\overline{A}_{i,\,T_g} = \int_0^\infty A_L \, \mathcal{P}(\overline{S}_i/S) \, d(\overline{S}_i/S) \tag{28}$$

is the weighted mean value of the line absorption A_L with respect to the normalized intensity probability distribution function $\mathcal{P}(\overline{S}_i/S)$. For dispersion lines of half-width b, it is well-known[5] that

$$A_L \simeq SX \quad \text{for} \quad \frac{SX}{2\pi b} < \frac{2}{\pi} \tag{29}$$

and

$$A_L \simeq 2\sqrt{SbX} \quad \text{for} \quad \frac{SX}{2\pi b} > \frac{2}{\pi} \ . \tag{30}$$

Thus, for the range of values in which Eq. (29) applies for the contributing spectral lines, the relation between absorptivity and emissivity is determined by the optically thin gas approximation given in Eq. (6). On the other hand, for the square root region,

$$\overline{A}_i = 2\sqrt{b_i X} \int_0^\infty \mathcal{P}(\overline{S}_i/S) \sqrt{S} \, d(\overline{S}_i/S) = \text{constant} \sqrt{\overline{S}_i b_i X} \, . \tag{31}$$

Hence, assuming that $\overline{S}_i = a_i/(\Delta\omega_i/d_i)$ and using the previously specified temperature dependence for a_i [see Eq. (5)], $\Delta\omega_i$ [see Eq. (10)] and d_i [see Eq. (23)], we obtain

$$\frac{\overline{A}_{i,\,T_g}}{d_{i,\,T_g}} = \text{constant} \, \frac{\left[\overline{S}_{i,\,T_s} \, b_{i,\,T_s} \left(\frac{T_s}{T_g}\right)^{2-\eta} X\right]^{1/2}}{d_{i,\,T_s}} \ . \tag{32}$$

Introduction of Eqs. (27) and (32) into Eq. (2) leads to the result

$$\alpha_{ab} \simeq \left(\frac{T_g}{T_s}\right)^{1/2} \mathcal{E}\left[T_s, X\left(\frac{T_s}{T_g}\right)^{2-\eta}\right]. \tag{33}$$

It is important to observe that Eq. (33) does not reduce to Eq. (6) as X goes to zero. This result is not surprising in view of the fact that Eq. (33) has been derived specifically for the square root region, i.e., for values of X which are sufficiently large to justify use of the line absorption formula given in Eq. (30).

F. Emission from a Blackbody and Absorption by Non-Overlapping Spectral Lines with Doppler Contour

For spectral lines with Doppler broadining, it is well known* that

$$\int_{\Delta\omega_{i,j}} \left[1-\exp(-P_\omega X)\right] d\omega = \omega_{i,j} \left(\frac{2\pi kT}{mc^2}\right)^{1/2} \sum_{n=1}^{\infty} -\frac{1}{n!\sqrt{n}} (-P'_{i,j}X)^n \tag{34}$$

where the integration interval over the jth line of the ith band $\Delta\omega_{i,j}$ has been extended from the band center $\omega_{i,j}$ to $-\infty$ and $+\infty$, m represents the mass of the radiator, and

$$P'_{i,j} = \frac{S_{i,j}}{\omega_{i,j}} \left(\frac{mc^2}{2\pi kT}\right)^{1/2} \tag{35}$$

is the spectral absorption coefficient at the center of the jth line in the ith band. In view of Eqs. (34) and (35), Eq. (2) becomes

$$\alpha_{ab} \simeq \frac{1}{\sigma T_s^4} \sum_i R^o_{\omega_i, T_s} \left\{ \sum_j \omega_i \left(\frac{2\pi kT_g}{mc^2}\right)^{\frac{1}{2}} \sum_{n=1}^{\infty} -\frac{1}{n!\sqrt{n}} \left[-\frac{S_{i,j,T_g} X}{\omega_i} \left(\frac{mc^2}{2\pi kT}\right)^{\frac{1}{2}}\right]^n \right\} \tag{36}$$

---

* Reference 5, Eq. (16-8).

where we have used the wave number at the band center ω_i for all of the $\omega_{i,j}$. We proceed to consider two special cases which are analogous to those treated for non-overlapping dispersion lines.

(1). Diatomic Molecules with Regular Spacing

The rotational line intensities are again given by Eq. (17). Hence, proceeding as before,

$$a_{ab} \simeq \frac{1}{\sigma T_s^4} \sum_i R^o_{\omega_i, T_s} 2\omega_i \left(\frac{2\pi k T_g}{mc^2}\right)^{1/2} \left\{ \sum_{j=0}^{\infty} \sum_{n=1}^{\infty} - \frac{1}{n!\sqrt{n}} \left[\frac{-a_{i,T_g} X}{\omega_i} \sqrt{\frac{hcB_{e_i}}{kT_g}}\, g(u) \left(\frac{mc^2}{2\pi k T}\right)^{1/2} \right]^n \right\}$$

where

$$u = \sqrt{\frac{hcB_{e_i}}{kT_g}}\, j;$$

thus

$$a_{ab} \simeq \frac{1}{\sigma T_s^4} \sum_i R^o_{\omega_i, T_s} 2\omega_i \left(\frac{2\pi k T_g}{mc^2}\right)^{1/2} \int_0^{\infty} \sqrt{\frac{kT_g}{hcB_{e_i}}} \left\{ \sum_{n=1}^{\infty} - \frac{1}{n!\sqrt{n}} \left[\frac{-a_{i,T_g}}{\omega_i} \sqrt{\frac{hcB_{e_i}}{kT_g}}\, g(u) \left(\frac{mc^2}{2\pi k T_g}\right)^{1/2} X \right]^n \right\} du$$

$$\simeq \left(\frac{T_g}{T_s}\right) \frac{1}{\sigma T_s^4} \sum_i R^o_{\omega_i, T_s} 2\omega_i \left(\frac{2\pi k T_s}{mc^2}\right)^{1/2} \int_0^{\infty} \sqrt{\frac{kT_s}{hcB_{e_i}}}$$

$$\left\{ \sum_{n=1}^{\infty} - \frac{1}{n!\sqrt{n}} \left[\frac{-a_{i,\,T_s}}{\omega_i} \sqrt{\frac{hcB_{e_i}}{kT_s}} \left(\frac{mc^2}{2\pi kT_s} \right)^{1/2} X \left(\frac{T_s}{T_g} \right)^2 g(u) \right] \right\} du$$

or

$$a_{ab} \simeq \left(\frac{T_g}{T_s} \right) \varepsilon \left[T_s, \left(\frac{T_s}{T_g} \right)^2 X \right]. \tag{37}$$

(2). Molecules with Equally Intense Spectral Lines

For equally intense spectral lines, we may introduce Eqs. (24) and (25) into Eq. (36). Hence

$$a_{ab} \simeq \frac{1}{\sigma T_s^4} \sum_i R^o_{\omega_i,\,T_s} N_{i,\,T_g} \omega_i \left(\frac{2\pi kT_g}{mc^2} \right)^{1/2} \sum_{n=1}^{\infty}$$

$$- \frac{1}{n!\sqrt{n}} \left[- \frac{\overline{S}_{i,\,T_g} X}{\omega_i} \left(\frac{mc^2}{2\pi kT_g} \right)^{1/2} \right]^n$$

$$\simeq \left(\frac{T_g}{T_s} \right)^{\eta+1} \frac{1}{\sigma T_s^4} \sum_i R^o_{\omega_i,\,T_s} N_{i,\,T_s} \omega_i \left(\frac{2\pi kT_s}{mc^2} \right)^{1/2} \sum_{n=1}^{\infty}$$

$$- \frac{1}{n!\sqrt{n}} \left[- \frac{\overline{S}_{i,\,T_s}}{\omega_i} \left(\frac{mc^2}{2\pi kT_s} \right)^{1/2} X \left(\frac{T_s}{T_g} \right)^{\eta+2} \right]^n$$

or

$$a_{ab} \simeq \left(\frac{T_g}{T_s} \right)^{\eta+1} \varepsilon \left[T_s, X \left(\frac{T_s}{T_g} \right)^{\eta+2} \right]. \tag{38}$$

G. Emission from a Blackbody and Absorption by Randomly Distributed Spectral Lines with Doppler Contour

Equations (27) and (28) apply for the specified model with the line absorption determined explicitly through Eqs. (34) and (35). Hence

$$\overline{A}_i = \int_0^\infty A_L \, \mathcal{P}(\overline{S}_i/S) \, d(\overline{S}_i/S)$$

$$= \omega_i \left(\frac{2\pi kT}{mc^2}\right)^{1/2} \int_0^\infty \mathcal{P}(\overline{S}_i/S) \, d(\overline{S}_i/S) \sum_{n=1}^\infty - \frac{1}{n!\sqrt{n}} \left[\frac{-SX}{\omega_i}\left(\frac{mc^2}{2\pi kT}\right)^{1/2}\right]^n$$

$$= \omega_i \left(\frac{2\pi kT}{mc^2}\right)^{1/2} \sum_{n=1}^\infty - \frac{1}{n!\sqrt{n}} \left[-\frac{X}{\omega_i}\left(\frac{mc^2}{2\pi kT}\right)^{1/2}\right]^n \int_0^\infty S^n \, \mathcal{P}(\overline{S}_i/S) \, d(\overline{S}_i/S)$$

$$= \omega_i \left(\frac{2\pi kT}{mc^2}\right)^{1/2} \sum_{n=1}^\infty - \frac{1}{n!\sqrt{n}} \left[-\frac{\overline{S}_i X}{\omega_i}\left(\frac{mc^2}{2\pi kT}\right)^{1/2}\right]^n c_n$$

where

$$c_n = \int_0^\infty \left(\frac{S}{\overline{S}_i}\right)^n \mathcal{P}\left(\frac{\overline{S}_i}{S}\right) d\left(\frac{\overline{S}_i}{S}\right) . \qquad (39)$$

If we assume again that

$$\frac{\overline{S}_{i,\,T_g}}{\overline{S}_{i,\,T_s}} = \frac{a_{i,\,T_g}/(\Delta\omega_{i,\,T_g}/d_{i,\,T_g})}{a_{i,\,T_s}/(\Delta\omega_{i,\,T_s}/d_{i,\,T_s})} = \left(\frac{T_s}{T_g}\right)^{\eta+(3/2)}$$

then

$$\bar{A}_{i,T_g} = \sqrt{\frac{T_g}{T_s}}\,\omega_i\left(\frac{2\pi k T_s}{mc^2}\right)^{\frac{1}{2}} \sum_{n=1}^{\infty} -\frac{c_n}{n!\sqrt{n}}\left[-\frac{\bar{S}_{i,T_s}}{\omega_i}\left(\frac{mc^2}{2\pi k T_s}\right)^{\frac{1}{2}} X\left(\frac{T_s}{T_g}\right)^{\eta+2}\right]^n$$

and

$$\frac{\bar{A}_{i,T_g}}{d_{i,T_g}} = \left(\frac{T_g}{T_s}\right)^{(1/2)+\eta}\omega_i\left(\frac{2\pi k T_s}{mc^2}\right)^{\frac{1}{2}} \sum_{n=1}^{\infty} -\frac{c_n}{n!\sqrt{n}}\left[\frac{\bar{S}_{i,T_s}}{\omega_i}\left(\frac{mc^2}{2\pi k T_s}\right)^{\frac{1}{2}} X\left(\frac{T_s}{T_g}\right)^{\eta+2}\right]^n . \tag{40}$$

In view of Eq. (27), the absorptivity is now given by the relation

$$a_{ab} \simeq \sqrt{\frac{T_g}{T_s}}\,\frac{1}{\sigma T_s^4}\sum_i R^o_{\omega_i,T_s}\left[1-\exp-\left(\frac{\bar{A}_{i,T_g}}{d_{i,T_g}}\right)\right] \tag{41}$$

where it is impossible to express $\bar{A}_{i,T_g}/d_{i,T_g}$ in terms of $\bar{A}_{i,T_s}/d_{i,T_s}$ with a suitably modified optical depth $X(T_s/T_g)^{\varepsilon}$ except in the unlikely case that $\eta = -1/2$. In this special case

$$a_{ab} \simeq \sqrt{\frac{T_g}{T_s}}\quad\left[T_s, X\left(\frac{T_s}{T_g}\right)^{3/2}\right], \quad \eta = -\frac{1}{2}. \tag{42}$$

Thus, in general, it is not feasible to obtain an explicit relation between emissivity and absorptivity for randomly distributed spectral lines with Doppler contour.

H. Emission from a Blackbody and Absorption by Non-Overlapping Spectral Lines with Combined Doppler and Collision Broadening and with Constant Collision Half-Width

For combined Doppler and collision broadening the line absorption depends on P'X, on the Doppler half-width b_D, and on the line-shape parameter $a \simeq \frac{b_C}{b_D}\sqrt{\ell n 2}$, viz.,

$$\frac{A_L\sqrt{\ell n 2}}{2b_D} = F(P'X;a) \tag{43}$$

where $b \equiv b_C$ is the collision half-width and the function F is the ordinate of the curves of growth.[5] Hence

$$\alpha_{ab} \simeq \frac{1}{\sigma T_s^4}\sum_i R^o_{\omega_i, T_s}\sum_j \frac{2b_{D,i,T_g}}{\sqrt{\ell n 2}} F\left[\frac{S_{i,j,T_g}}{\omega_i}\left(\frac{mc^2}{2\pi k T_g}\right)^{\frac{1}{2}} X;\ a_{i,j,T_g}\right]. \tag{44}$$

(1). Bands with Regular Spacing

For molecules with regular spacing, Eq. (17) applies and Eq. (44) becomes

$$\alpha_{ab} \simeq \frac{1}{\sigma T_s^4}\sum_i R^o_{\omega_i, T_s}\sum_j \frac{2b_{D,i,T_g}}{\sqrt{\ell n 2}} F\left[\frac{a_{i,T_g}}{\omega_i}\sqrt{\frac{hcB_{e_i}}{kT_g}}\, g(u)\left(\frac{mc^2}{2\pi k T_g}\right)^{\frac{1}{2}} X; a_{i,T_g}\right]$$

where g(x) is again defined by Eq. (18) and $u = \sqrt{hcB_{e_i}/kT_g}\ j$. Since[5]

$$\frac{b_{D,T_g}}{b_{D,T_s}} \simeq \left(\frac{T_g}{T_s}\right)^{1/2}$$

and

$$\frac{a_{i,\,T_g}}{a_{i,\,T_s}} = \left(\frac{T_s}{T_g}\right),$$

the preceding expression becomes

$$\alpha_{ab} \simeq \left(\frac{T_g}{T_s}\right)\frac{1}{\sigma T_s^4}\sum_i R^o_{\omega_i,\,T_s}\int_0^\infty \frac{2b_{D,\,i,\,T_s}}{\sqrt{\ell n 2}}$$

$$F\left[\frac{a_{i,\,T_s}}{\omega_i}\sqrt{\frac{hcB_{e_i}}{kT_s}}\,g(u)\left(\frac{mc^2}{2\pi kT_s}\right)^{1/2} X\left(\frac{T_s}{T_g}\right)^2;\right.$$

$$\left. a_{i,\,T_s}\left(\frac{T_s}{T_g}\right)\right]\sqrt{\frac{kT_s}{hcB_{e_i}}}\;du$$

or

$$\alpha_{ab} \simeq \frac{T_g}{T_s}\;\mathcal{E}\left[T_s, X\left(\frac{T_s}{T_g}\right)^2; a_{T_g}\right]. \qquad (45)$$

According to Eq. (45), the absorptivity at T_g depends on the emissivity at T_s for an optical depth $X(T_s/T_g)^2$ with the line-shape parameter $a_{T_g} = a_{T_s}(T_s/T_g)$ evaluated at T_g.

(2). Bands with Equally Intense Spectral Lines

For equally intense spectral lines with constant collision half-width, Eq. (44) becomes

$$a_{ab} \simeq \frac{1}{\sigma T_s^4} \sum_i R^o_{\omega_i, T_s} N_{i, T_g} \frac{2b_{D, i, T_g}}{\sqrt{\ell n 2}} F\left[\frac{\overline{S}_{i, T_g} X}{\omega_i}\left(\frac{mc^2}{2\pi k T_g}\right)^{\frac{1}{2}} ; a_{i, T_g}\right] .$$

Using the previously specified temperature dependence for the various terms occurring in the preceding relation, we find that

$$a_{ab} \simeq \left(\frac{T_g}{T_s}\right)^{\eta+1} \frac{1}{\sigma T_s^4} \sum_i R^o_{\omega_i, T_s} N_{i, T_s} \frac{2b_{D, i, T_s}}{\sqrt{\ell n 2}} F\left[\frac{\overline{S}_{i, T_s}}{\omega_i}\left(\frac{mc^2}{2\pi k T_s}\right)^{\frac{1}{2}} X\left(\frac{T_s}{T_g}\right)^{\eta+2} ; a_{i, T_s} \frac{T_s}{T_g}\right]$$

or

$$a_{ab} \simeq \left(\frac{T_g}{T_s}\right)^{\eta+1} \mathcal{E}\left[T_s, X\left(\frac{T_s}{T_g}\right)^{\eta+2} ; a_{T_g}\right] . \qquad (46)$$

I. Effect of Total Pressure on the Relation Between Absorptivities and Emissivities

The preceding theoretical relations all involve the implicit assumption that the absorptivity and emissivity data refer to the same total pressure p. In practice it is, however, often advantageous to measure absorptivities and emissivities at different total pressures p_1 and p_2, respectively. In this case all of the theoretical relations involving collision broadening must be modified. Appropriate relations can be derived without difficulty if the effective collision half-width depends linearly on the pressure, i.e., the line broadening agent is

assumed to be the same for the absorption and for the emission measurements. Thus

$$\frac{b_{i,\,T_g,\,p_1}}{b_{i,\,T_s,\,p_2}} = \frac{p_1}{p_2}\sqrt{\frac{T_s}{T_g}} \quad . \tag{47}$$

The use of Eq. (47) leads to the revised relations summarized below.

(1). Transparent Gases

The derivation of Eq. (6) does not involve the spectral line shape and, therefore, Eq. (6) applies irrespective of the total pressures of the absorbing and emitting gases.

(2). Constant Average Absorption Coefficients and Just-Overlapping Lines

As long as both p_1 and p_2 are sufficiently large to justify the use of one of the postulated models, Eq. (12) [and the same expression which has been repeated in Eq. (15)] applies.

(3). Non-Overlapping Dispersion Lines with Regular Spacing and Constant Collision Half-Width

The use of Eq. (47) in place of Eq. (19) shows that the factor p_1/p_2 will occur outside the sum over bands and p_2/p_1 will occur as a multiplicative factor to X, i.e., Eq. (20) becomes

$$a_{ab} \equiv a_{ab}(T_s \longrightarrow T_g, X, p_1) \simeq \frac{p_1}{p_2}\ \varepsilon\left[T_s, X\left(\frac{T_s}{T_g}\right)\left(\frac{p_2}{p_1}\right),\ p_2\right]. \tag{20a}$$

(4). Non-Overlapping Dispersion Lines of Equal Intensity with Constant Collision Half-Width

Proceeding as before, it is apparent that Eq. (26) should be replaced by the expression

$$\alpha_{ab}(T_s \longrightarrow T_g, X, p_1) \simeq \left(\frac{p_1}{p_2}\right)\left(\frac{T_g}{T_s}\right)^{\eta} \cdot \varepsilon\left[T_s, X\left(\frac{T_s}{T_g}\right)^{\eta+1}\left(\frac{p_2}{p_1}\right), p_2\right]. \quad (26a)$$

(5). Randomly Distributed Spectral Lines with Dispersion Contour

Equation (33) is now replaced by the expression

$$\alpha_{ab}(T_s \longrightarrow T_g, X, p_1) \simeq \left(\frac{T_g}{T_s}\right)^{\frac{1}{2}} \varepsilon\left[T_s, X\left(\frac{T_s}{T_g}\right)^{2-\eta}\left(\frac{p_1}{p_2}\right), p_2\right] \quad (33a)$$

since the collision half-width multiplies X in Eq. (31).

(6). Non-Overlapping Spectral Lines with Doppler Contour

As long as the postulated model remains applicable, the total pressure cannot affect the results since it has no influence on the Doppler half-width. Thus Eqs. (37), (38) and (42) hold independently of the values of p_1 and p_2.

(7). Non-Overlapping Spectral Lines with Combined Doppler and Collision Broadening, Constant Collision Half-Width, and Regular Line Spacing

Examination of the relations preceding Eq. (45) shows that

$$\alpha_{ab}(T_s \longrightarrow T_g, X, p_1) \simeq \left(\frac{T_g}{T_s}\right) \varepsilon\left[T_s, X\left(\frac{T_s}{T_g}\right)^{2}; a_{T_g, p_1}; p_2\right], \quad (45a)$$

i.e., the line-shape parameter must be evaluated at T_g and p_1. Here

$$a_{T_g, p_1} = a_{T_s, p_2} \left(\frac{T_s}{T_g}\right)\left(\frac{p_1}{p_2}\right) .$$

(8). Non-Overlapping Spectral Lines with Combined Doppler and Collision Broadening, Constant Collision Half-Width, and Lines of Equal Intensity

It is easily seen that

$$a_{ab}(T_s \longrightarrow T_g, X, p_1) \simeq \left(\frac{T_g}{T_s}\right)^{\eta+1} \mathcal{E}\left[T_s, X\left(\frac{T_s}{T_g}\right)^{\eta+2} ; a_{T_g, p_1} ; p_2\right] . \quad (46a)$$

III. DISCUSSION OF RESULTS AND CORRELATION OF EXPERIMENTAL DATA

In accord with the general result obtained in Eq. (6), it is apparent that the absorptivity at T_g and the emissivity at T_s for $p_1 = p_2 = p$ must be related, in general, in such a way that

$$a_{ab} = \left(\frac{T_g}{T_s}\right)^{\beta-1} \mathcal{E}\left[T_s, X\left(\frac{T_s}{T_g}\right)^{\beta} ; a_{T_g}\right] \quad (48)$$

provided it has not been explicitly postulated that X cannot be arbitrarily small [compare Eq. (33)]. The absolute values of β depend on the assumed band model and are summarized in Table I for the cases considered in Section II. It should be noted that $\mathcal{E}$ depends on the line-shape parameter a only in the special case of combined Doppler and collision broadening. The following interesting summary statements may be made:

Table I. Summary of theoretical relations between absorptivities at T_g and emissivities at T_s for $p_1 = p_2 = p$.

Model:	Physical Conditions for which the Model Applies:	β in Eq. (48)	Remarks
constant average absorption coefficients for vibration-rotation bands. just-overlapping spectral lines.	at elevated pressures where the rotational fine structure is smeared out.	3/2	
non-overlapping dispersion lines with regular spacing and constant collision half-width.	molecules without Q-branch at moderate temperatures for sufficiently low pressures.	1	
non-overlapping dispersion lines of equal intensity and constant half-width.	molecules without Q-branch at elevated temperatures for sufficiently low pressures.	$1 + \eta$	At moderate temperatures, $\eta = 0$, and this case reduces to the preceding limiting conditions.
non-overlapping Doppler lines with regular line spacing.	moderate temperatures and sufficiently low pressures to make $b_C << b_D$.	2	
non-overlapping Doppler lines of equal intensity.	elevated temperatures and sufficiently low pressures to make $b_C << b_D$.	$2 + \eta$	At moderate temperatures, $\eta = 0$, and this case reduces to the preceding limiting conditions.

(Table I continued)

Model:	Physical Conditions for which the Model Applies:	β in Eq. (48)	Remarks
non-overlapping spectral lines with regular spacing, constant collision half-width, and combined Doppler and collision broadening.	moderate temperatures and pressures which are sufficiently small to justify the neglect of overlapping between spectral lines.	2	
combined Doppler and collision broadening for non-overlapping lines of equal intensity with constant half-width.	elevated temperatures and moderate pressures for molecules with large rotational spacing.	$2+\eta$	At moderate temperatures, $\eta=0$, and this case reduces to the preceding limiting condition.
randomly distributed dispersion lines of equal intensity for sufficiently large optical depths to make the dominant line absorption vary as the square root of the optical depth.	complicated molecules (e.g., H_2O) at moderate or large pressures for temperatures sufficiently low to make $b_C >> b_D$.	$\alpha_{ab}=\sqrt{\frac{T_g}{T_s}}\ \varepsilon\left[T_s, X\left(\frac{T_s}{T_g}\right)^{2-\eta}\right]$ and Eq. (48) does not apply.	
randomly distributed Doppler lines.	--	$\beta = 3/2$ for $\eta = -1/2$	This case is of no physical interest.

(1) For otherwise comparable assumptions, $\beta = 1$ or $1 + \eta$ for dispersion lines and $\beta = 2$ or $2 + \eta$ for lines with Doppler broadening or combined Doppler and collision broadening.*

(2) For overlapping lines $\beta = 3/2$.

We now proceed to consider briefly the correlation of available experimental data by means of our theoretical formulae.

A. Carbon Dioxide

Hottel and Mangelsdorf[8] have obtained the empirical relation

$$(a_{ab,CO_2})_{H\text{-}M} \simeq \left(\frac{T_g}{T_s}\right)^{2/3} \varepsilon\left[T_s, X\left(\frac{T_s}{T_g}\right)\right]. \qquad (49)$$

It is apparent that Eq. (49) cannot apply in the limit of zero optical depth since it does not reduce to Eq. (6). Hence it is reasonable to assume that the important contributions to a_{ab} and ε are made by dispersion lines which are sufficiently strong so that the emissivity varies as the square root of the optical depth. On this assumption, we may use the relation obtained for randomly distributed dispersion lines in Eq. (33) for the derivation of an effective value of η for CO_2, viz.,

$$a_{ab} \simeq \left(\frac{T_g}{T_s}\right)^{1/2} \varepsilon\left[T_s, \sqrt{X\left(\frac{T_s}{T_g}\right)\left(\frac{T_s}{T_g}\right)^{1-\eta}}\right]$$

* The value of β for combined Doppler and collision broadening is not directly comparable to β for the other cases because the absorptivity is related to an emissivity at the temperature T_s but with a line-shape parameter a evaluated at T_g. This is not a physically realizable case, and is therefore not directly useful. If we were able to refer the absorptivity to an emissivity at T_s with the line-shape parameter evaluated at T_s then β would depend on the optical depth and the line-shape parameter, and would equal 2 or $2+\eta$ only in the limiting case of collision broadened lines.

or

$$\alpha_{ab} \simeq \left(\frac{T_g}{T_s}\right)^{\eta/2} \mathcal{E}\left[T_s, \sqrt{X\left(\frac{T_s}{T_g}\right)}\right] .$$

On the other hand, Eq. (49) becomes

$$(\alpha_{ab, CO_2})_{H\text{-}M} \simeq \left(\frac{T_g}{T_s}\right)^{2/3} \mathcal{E}\left[T_s, \sqrt{X\left(\frac{T_s}{T_g}\right)}\right]$$

and

$$(\eta)_{CO_2} \simeq 4/3.$$

The fact that Eq. (33) with $\eta = 4/3$ provides a good correlation of the available experimental results is illustrated in Fig. 1. It is interesting to observe that the choice $\eta = 1$, which is the appropriate value for water in the statistical model, leads to notably poorer correlation of data than $\eta = 4/3$.

Although η is independent of X, Eq. (33) with $\eta = 4/3$ should not be used either for very large or for very small values of X since it was derived by using the line absorption relation appropriate for the square root region [compare Eq. (31)] .

B. Water[4]

A comparison of observed and calculated results is shown in Fig. 2 for water vapor. Reference to Fig. 2, and to data for larger values of X which are not plotted, shows that Eq. (33) gives a fair representation for X greater than about 0.1 or 0.2 ft-atmos; $\beta = 3/2$ holds for very small values of X and also for X greater than about 0.5 ft-atmos; $\beta = \eta + 1 = 2$

applies for X less than about 0.2 ft-atmos.* Equation (33) is seen to apply when the absorption is dominated by dispersion lines in the square root region irrespective of the extent of overlapping between lines.

C. Carbon Monoxide

Careful absorptivity measurements for carbon monoxide have been performed recently in our laboratory by U. P. Oppenheim.[10] The experimental results obtained at very low pressures where $\beta = 1$, and at elevated pressures where $\beta = 3/2$, are shown in Figs. 3 and 4, respectively. Reference to the data plotted in Figs. 3 and 4 shows very satisfactory agreement with theoretical predictions. It is interesting to observe (see Fig. 4) that the overlapping line models fail to apply at elevated temperatures for constant pressure and optical depth. This conclusion is in accord with predictions since both the collision half-width and the number of absorbers in the light path decrease for the specified conditions, i.e., the requirements for use of an overlapping line model must break down at sufficiently high temperatures. The relative positions for broadening with He or A are in accord with the known pressure dependence and absolute values of the collision half-width for these broadening agents.[11] Finally, the observed lower temperature deviations from an overlapping line model at smaller optical depths serve to emphasize the fact that both the product of integrated intensity with optical depth and the effective half-width are important in

* The estimate $\eta = 1$ for water vapor has been derived from correlation of measured emissivity data by means of the statistical model.[2, 5]

determining the range of validity of an overlapping line model.

D. Use of the Total Pressure Dependence of the Relation for Non-Overlapping Lines with Combined Doppler and Collision Broadening

Reference to Eqs. (45a) and (46a) shows that the following relations hold for non-overlapping lines with combined Doppler and collision broadening and constant collision half-width:

$$\alpha_{ab}(T_s \rightarrow T_g, X; p_1) \simeq \left(\frac{T_g}{T_s}\right) \varepsilon \left[T_s, X\left(\frac{T_s}{T_g}\right)^2; a_{T_g, p_1}; p_2\right], \tag{45a}$$

for regular line spacing, and

$$\alpha_{ab}(T_s \rightarrow T_g, X; p_1) \simeq \left(\frac{T_g}{T_s}\right)^{\eta+1} \varepsilon \left[T_s, X\left(\frac{T_s}{T_g}\right)^{\eta+2}; a_{T_g, p_1}; p_2\right] \tag{46a}$$

for lines of equal intensity. It is observed from Eqs. (45a) and (46a) that the absorptivity is related to an emissivity at temperature T_s and total pressure p_2 but with a line-shape parameter evaluated at T_g and p_1. In order for this emissivity to be an actual emissivity for the gas, the line-shape parameter must be equal to the value at T_s and p_2. It is evident from the relation

$$a_{T_g, p_1} = a_{T_s, p_2}\left(\frac{T_s}{T_g}\right)\left(\frac{p_1}{p_2}\right)$$

that we must therefore consider the case

$$\frac{p_1}{p_2} = \frac{T_g}{T_s} \quad .$$

Thus one can obtain a value for the emissivity of a gas at temperature T_s and pressure p_2 by performing an absorption experiment for a gas temperature T_g and pressure p_1, provided the lines are non-overlapping for both gas conditions and provided $p_1 = p_2(T_g/T_s)$.

CHAPTER 2

RADIANT ENERGY EMISSION FROM A BURNING AMMONIUM PERCHLORATE PROPELLANT*

I. INTRODUCTION

In connection with current experimental and theoretical studies on burning mechanism and flammability limits of composite solid propellants, it is of interest to estimate radiation losses from the combustion products and radiant heat transfer to the burning propellant surface. We consider this problem in the present analysis for a rectangular parallelepiped of $NH_4Cl O_4$ burning in a rectangular enclosure with a square base, as is shown in Fig. 5; the translation of our results to other geometric configurations may be accomplished readily by using listed compilations of mean beam lengths.

The reaction zone of height d is assumed to consist of NH_3 and $HCl O_4$ at temperatures between 900 and 1200°K, while the stable combustion products (H_2O, HCl, N_2, and O_2) occupy a region of height h and are assumed to be at a temperature of 1433°K (see reference 12).

In Section II we determine the mean beam length for a uniform gas enclosed by a rectangular parallelepiped; the development of corresponding results for other geometric configurations may be accomplished

---

* This research was supported by the United States Air Force through the Air Force Office of Scientific Research of the Air Research and Development Command under Contract AF49(638)-412.

The author enjoyed discussion with W. Nachbar on this problem.

readily by using known prescriptions for the computation of mean beam lengths. The analysis given in Section III shows that emission and absorption of radiant energy in the reaction zone may be neglected. In Sections IV and V we compute the emissivities of $HC\ell$ and H_2O, respectively, under the pressure and temperature conditions which are of interest for the present study. The effect on the total emissivity of overlapping between the emission spectra of $HC\ell$ and H_2O is considered in Section VI for appropriate mixture compositions. Representative estimates of radiant energy loss from the combustion products and of radiant heat transfer to the burning propellant surface are obtained in Section VII.

II. MEAN BEAM LENGTHS

We consider an enclosure in the form of a rectangular parallelepiped. The radiant energy flux dR to an area dA from a gas volume contained within a solid angle $d\omega'$ and bounded by radius vectors of lengths x and x + dx is given by[13]

$$dR = \frac{\sigma T^4}{\pi} d\omega' \cos\varphi \, dA \, \frac{d\varepsilon}{dx} \, dx \qquad (1)$$

where φ is the angle between x and the normal to dA, T is the (uniform) temperature of the gas volume, σ denotes the Stefan-Boltzmann constant, and ε is the hemispherical emissivity of the gas volume. Thus the radiant energy flux from the isothermal volume to the portion of its containing surface of area A is

$$R = \frac{\sigma T^4}{\pi} \int_A \int_C^{x_{max}} \int_{\omega'} \cos\varphi \, d\omega' \, \frac{d\varepsilon}{dx} \, dx \, dA \qquad (2)$$

where we have integrated over the complete solid angle and over A.

The mean beam length L is defined through the expression

$$\sigma T^4 A \varepsilon_L \equiv R = \frac{\sigma T^4}{\pi} \int_A \int_0^{x_{max}} \int_{\omega'} \cos\varphi \, d\omega' \, \frac{d\varepsilon}{dx} \, dx \, dA \tag{3}$$

where ε_L is the hemispherical emissivity for a gas of depth L, i.e., $\sigma T^4 \varepsilon_L$ is the radiant energy flux from a hemispherical gas volume of radius L at the temperature T to the center of its base, per unit area of the base. When the optical depth $p_g L$ (p_g = partial pressure of the emitting gas) becomes sufficiently small, self-absorption by the emitting gas may be neglected and, therefore, ε_L becomes directly proportional to $p_g L$. Let L^o be the mean beam length evaluated for transparent gases, i.e., in the limit for $p_g L \longrightarrow 0$. Then

$$\varepsilon_{L^o} = \left[\lim_{x \to 0} \left(\frac{d\varepsilon}{dx} \right) \right] L^o \tag{4}$$

where $\lim_{x \to 0} (d\varepsilon/dx)$ is a constant which may be taken outside of the integrals in Eq. (3). Therefore Eq. (3) leads to the result

$$L^o = \frac{1}{A\pi} \int_A \int_0^{x_{max}} \int_{\omega'} \cos\varphi \, d\omega' \, dx \, dA. \tag{5}$$

The computation of L^o for radiation to the entire confining enclosure is discussed, for example, in reference (13). In this special case we may write the integrand in Eq. (5) as

$$(x^2 d\omega' dx) \cdot \left(\frac{\cos\varphi \, dA}{x^2} \right) = dV d\Omega \tag{6}$$

where $d\Omega$ is the solid angle subtended by dA at the emitting volume dV. Since we are considering radiation to the entire surface of the enclosure,

$$\int_V \int_\Omega dV d\Omega = 4\pi \int_V dV = 4\pi V, \tag{7}$$

and we obtain the result

$$L^o = \frac{4V}{A} \quad . \tag{8}$$

For a rectangular parallelepiped of height h and square base with side lengths r, Eq. (8) becomes

$$L^o = \frac{2}{(1/h) + (2/r)} \quad . \tag{9}$$

Equation (9) is an expression for the mean beam length for radiation to all faces of the parallelepiped in the limit of zero optical depth. Equation (9) may be used to compute the mean beam lengths for radiation to individual faces of the parallelepiped for three particular cases. When $h >> r$, $L^o \simeq r$; L^o now represents the mean beam length for radiation to the long rectangular sides with lengths h and r since, for $h >> r$, practically all of the radiant energy transfer occurs to the side faces. For $h = r$, $L^o = 2r/3$, which is the mean beam length for any of the faces singly since, in this case, the side faces, top face and base are all squares with side lengths r. When $h << r$, $L^o \simeq 2h$, which is the mean beam length for radiation to the base or top face since practically all of the radiation occurs to the base and top face for $h << r$.

In addition to the special cases given above, the mean beam lengths for radiation to the side faces and to the base of a rectangular parallele-

piped with h = 4r are listed in reference (13). The resulting values are

L^o (to the side faces) = 0.90r

and

L^o (to the base) = 0.86r

for h = 4r. For h > 4r, we may use the preceding estimate of L^o for radiation to the base at h = 4r in Eq. (5) in order to compute the actual mean beam length. Thus

$$L^o(\text{to the base}) \simeq 0.86r + \frac{1}{A\pi} \int_A \int_{4r}^{h} \int_{\omega'} d\omega' \, dA \, dx \qquad (10)$$

since $\cos\varphi \simeq 1$ for $x > 4r$. Furthermore, the solid angle subtended at dA by the slab of gas between x and x + dx for x > 4r is, approximately, r^2/x^2 and is practically independent of the position in the base at which the element dA is located. Therefore

$$L^o \text{ (to the base)} \simeq 0.86r + \frac{1}{A\pi} \int_{4r}^{h} \frac{r^2}{x^2} \cdot A\,dx = \left[0.86 + \frac{1}{\pi}\left(\frac{1}{4} - \frac{r}{h}\right)\right] r$$

$$= \left[0.94 - \frac{1}{\pi(h/r)}\right] r \quad \text{for } h > 4r. \qquad (11)$$

Useful results for the computation of mean beam lengths L^o are summarized in Table II on p. 52 and in Fig. 6.

The mean beam length L for finite values of $p_g L$ may be obtained* by using Fig. 7 which has been reproduced from Hottel's work.[13] In

---

* The exact value of the ratio L/L^o must depend on the temperature. Theoretical studies are currently in progress in order to determine the ratio $L_{H_2O}/L^o_{H_2O}$ as a function of T and $p_{H_2O}L^o_{H_2O}$.

Fig. 7 the quantity L/L^o is plotted as a function $p_{H_2O}L = p_{H_2O}L_{H_2O}$. The data shown in Fig. 7 should apply at the high pressures with which we are concerned since the calculations given in Section V show that the emissivity of H_2O is a monotone function of $p_{H_2O}L_{H_2O}$ for the mean beam lengths of interest to us.

For HCl we have no detailed numerical results which permit computation of L/L^o in terms of $p_{HCl}L_{HCl}$. However, since L differs appreciably from L^o only for large optical depths for which the emissivity is a weak function of L, and since our emissivity estimates for HCl are usually small (see Section IV), it is reasonable to use L^o for the mean beam length of HCl for most of the values of $p_{HCl}L_{HCl}$ considered in the present calculations. Furthermore, since the emissivity contributions of HCl are smaller than those of H_2O, an error in the appropriate optical depths for HCl will exert only a relatively small influence on the calculated results.

III. EMISSION AND ABSORPTION OF RADIATION IN THE REACTION ZONE

The decomposition of ammonium perchlorate involves the reaction

$$NH_4ClO_4 \longrightarrow NH_3 + HClO_4 . \qquad (12)$$

We shall assume that only the species NH_3 and $HClO_4$ occur in the reaction zone. For reasonable values of the pressure, the reaction zone thickness is smaller than about 10^{-4} cm, i.e., the corresponding mean beam length is less than about 2×10^{-4} cm for radiation to the propellant grain. We shall now show that the equilibrium emissivities and absorptivities of NH_3 are very much smaller than the corresponding values for HCl and H_2O. In the absence of quantitative data to the contrary, it is reasonable to assume that the equilibrium emissivities and absorptivities of $HClO_4$

are similarly small. Finally, we note that for reasonable values of the pressure, the absolute emissivities and absorptivities of the chemical species in the reaction zone must be negligibly small unless unpredictable and unknown non-equilibrium (chemiluminescent) radiation of surprising intensity is present.

The general expression for the hemispherical emissivity of a gaseous emitter is[5]

$$\varepsilon_L \equiv \varepsilon = \frac{1}{\sigma T^4} \int_0^{\omega} R_\omega^o \left[1-\exp(-P_\omega p_g L)\right] d\omega \qquad (13)$$

where ω is the wave number, R_ω^o is the spectral blackbody radiancy, P_ω represents the spectral absorption coefficient, p_g denotes the partial pressure of the emitter, and L identifies again the mean beam length. For small values of $p_g L$, the exponential in Eq. (13) may be expanded to give

$$\varepsilon \simeq \sum_i \frac{1}{\sigma T^4} R_{\omega_i}^o \, a_i p_g L = 15 \left(\frac{hc}{\pi k T}\right)^4 p_g L \sum_i \frac{\omega_i^3 \, a_i}{\left[\exp(hc\omega_i/kT)\right] - 1} \qquad (14)$$

where

$$a_i \equiv \int_{\text{ith band}} P_\omega d\omega$$

is the integrated intensity of the ith band. The sum in Eq. (14) should include all of the bands. In Eq. (14) we have expressed the blackbody radiancy at the center of the ith band in terms of the wavenumber of the band center ω_i, Planck's constant h, the velocity of light c, the Boltzmann constant k, and the temperature T. In Table III we have listed the known values for the integrated intensities of the fundamental vibration-rotation

bands of NH_3 at room temperature. These bands should account for most of the emitted radiation from NH_3 under the conditions existing in the reaction zone. Therefore, from Eq. (14),

$$\varepsilon \simeq 6.3 \times 10^{-6}\, p_T \text{ (for } T = 900^{\circ}K \text{ and } L = 2 \times 10^{-4} \text{cm)}$$

and

$$\varepsilon \simeq 2.72 \times 10^{-6}\, p_T \text{ (for } T = 1200^{\circ}K \text{ and } L = 2 \times 10^{-4} \text{cm)},$$

where we have used the fact that the integrated intensities of fundamental bands vary, approximately, inversely with the temperature. The temperature in the reaction zone has been assumed[12] to lie between 900 and 1200°K and, in accord with Eq. (12), the equilibrium relation $p_{NH_3} = \frac{1}{2} p_T$ has been used. Reference to Sections IV and V shows that the emissivities of NH_3 in the reaction zone are negligibly small compared with the emissivities of $HC\ell$ and H_2O, except when the height h of the stable combustion products becomes smaller than about 10^{-2} cm. In the present analysis we are actually concerned with $h \gtrsim 0.1$ cm.

If the emissivity of NH_3 cannot be computed from the transparent gas approximation given in Eq. (14), then the actual value is necessarily smaller than the estimate derived from Eq. (14).[5] Thus the preceding numbers are, in any case, conservative upper limits.

The absorptivity a_{ab} of NH_3 for radiation emitted by the combustion products at T = 1433°K can be estimated from the formula (see Chapter 1)

$$a_{ab} \simeq \frac{1433}{T_{NH_3}}\, \varepsilon_{NH_3}(1433^{\circ}K) \lesssim 10^{-5} p_T.$$

Since we shall limit our considerations to $p_T \leq 300$ atmos, the ammonia

may be considered to be transparent with respect to radiation emitted by the products of combustion.

Because NH_3 has relatively intense bands near the blackbody peaks at 900 and 1200°K, we expect that the emissivities and absorptivities of $HCl O_4$ are of the same order of magnitude or smaller than those for NH_3. Therefore, we may neglect the influence of the reaction zone in radiant heat transfer calculations.

IV. EMISSIVITY CALCULATIONS FOR HCl

The chemical species in the reaction zone decompose ultimately according to the relation

$$NH_3 + HCl O_4 \longrightarrow \frac{3}{2} H_2O + HCl + \frac{1}{2} N_2 + \frac{5}{4} O_2 \, . \qquad (16)$$

According to the geometric arrangement assumed in Fig. 5, these stable products of combustion are confined within a parallelepiped of height h and base R = r at a temperature of 1433°K. The homopolar species N_2 and O_2 cannot contribute measurably to the radiant heat transfer.

The emissivity of HCl may be computed by summing the contributions from the fundamental and first overtone bands. For the specified range of total pressures (i.e., $p_T \leq 300$ atmos) and small values of p_{HCl} and mean beam lengths L_{HCl}, the spectral lines do not overlap and it is permissible to use emissivity expressions derived for nonoverlapping lines.[5] At very large values of p_{HCl} and L_{HCl}, the spectral lines are effectively "well overlapped" and we may use an average absorption coefficient for each band ("box model").[5]

For nonoverlapping spectral lines, the emissivity of $HC\ell$ is given by the expression

$$\varepsilon = \varepsilon_F + \varepsilon_O = \sum_{n=0}^{\infty} \varepsilon_{n\rightarrow n+1} + \sum_{n=0}^{\infty} \varepsilon_{n\rightarrow n+2} \qquad (17)$$

where ε_F is the emissivity of the fundamental bands, ε_O is the emissivity of the first overtone bands, and $\varepsilon_{m\rightarrow n}$ is the emissivity for a transition between states with vibrational quantum numbers m and n. For small values of $L_{HC\ell}$, $\varepsilon_{m\rightarrow n}$ is a linear function of $p_{HC\ell}L_{HC\ell}$ or of $\eta_{NC\ell}p_T L_{HC\ell}$ where $p_{HC\ell} = \eta_{HC\ell}p_T$ if $\eta_{HC\ell}$ is the mole fraction of $HC\ell$; at higher values of $L_{HC\ell}$, $\varepsilon_{m\rightarrow n}$ becomes proportional to $p_T\sqrt{\eta_{HC\ell}L_{HC\ell}}$ and, for constant values of $\eta_{HC\ell}$, $\varepsilon_{m\rightarrow n}$ is simply proportional to $p_T\sqrt{L_{HC\ell}}$. We may obtain an estimate for $\varepsilon_{m\rightarrow n}/p_T$ by drawing a curve which always falls on or beneath the curves which make $\varepsilon_{m\rightarrow n}/p_T$ proportional to $L_{HC\ell}$ and to $\sqrt{L_{HC\ell}}$ (see Figs. 8 to 10). The values of $\varepsilon_{m\rightarrow n}$ may then be summed to yield ε_F/p_T and ε_O/p_T (see Figs. 11 to 14). The explicit relations* used for the calculation of $\varepsilon_{m\rightarrow n}/p_T$ are the following:(5)

$$(\varepsilon_{0\rightarrow 1})_{\ell.r.} = 15\left(\frac{u}{\pi}\right)^4 \frac{1}{\omega^*}\Big[\exp(-u)\Big]\Big[1-\exp(-u)\Big]\, a_F \eta_{HC\ell}\, p_T L_{HC\ell}$$

$$= 1.438 \times 10^{-3}\, p_T L_{HC\ell},$$

$$(\varepsilon_{0\rightarrow 1})_{s.r.r.} = 0.6345u^5\Big[\exp(-u)\Big]\,(\gamma u)^{-3/4}\,\frac{1}{\omega^*}\left[\gamma b\,\frac{a_F}{u}\,\eta_{HC\ell}\,p_T L_{HC\ell}\right]^{\frac{1}{2}}$$

$$= 1.560 \times 10^{-3}\, p_T\sqrt{L_{HC\ell}},$$

* The subscript $\ell.r.$ identifies results appropriate for the linear region; the subscript s.r.r. applies to the square-root region.

$$(\varepsilon_{n\to n+1})_{\ell.r.} = (n+1)\left[\exp(-nu)\right](\varepsilon_{0\to 1})_{\ell.r.},$$

$$(\varepsilon_{n\to n+1})_{s.r.r.} = (n+1)^{1/2}\left[\exp\left(-\frac{nu}{2}\right)\right](\varepsilon_{0\to 1})_{s.r.r.},$$

$$\sum_{n=0}^{\infty}(\varepsilon_{n\to n+1})_{\ell.r.} = (\varepsilon_{0\to 1})_{\ell.r.}\,(1-e^{-u})^{2},$$

and

$$(\varepsilon_{0\to 2})_{\ell.r.} = 8\left[\exp(-u)\right]\frac{a_O}{a_F}(\varepsilon_{0\to 1})_{\ell.r.} = 0.1564\times 10^{-3}\,p_T L_{HC\ell},$$

$$(\ell\varepsilon_{0\to 2})_{s.r_{\ell}.r.} = 8\left[\exp(-u)\right]\left[1-\exp(-u)\right]^{-1/2}\left(\frac{a_O}{a_F}\right)^{1/2}(\varepsilon_{0\to 1})_{s.r.r.}$$

$$= 0.1115\times 10^{-3}\,p_T\sqrt{L_{HC\ell}},$$

$$(\varepsilon_{n\to n+2})_{\ell.r.} = \left[\frac{(n+2)(n+1)}{2}\right]\left[\exp(-nu)\right](\varepsilon_{0\to 2})_{\ell.r.},$$

and

$$(\varepsilon_{n\to n+2})_{s.r.r.} = \left[\frac{(n+2)(n+1)}{2}\right]^{1/2}\left[\exp\left(-\frac{nu}{2}\right)\right](\varepsilon_{0\to 2})_{s.r.r.}. \qquad (18)$$

Here a_F and a_O are inversely proportional to the temperature and represent, respectively, the integrated intensity of the fundamental band and $\left[1-\exp(-u)\right]\left[1+\exp(-u)\right]^{-1}$ times the integrated intensity of the first overtone band; ω^* (= 2886 cm^{-1}) is the wave number at the band center of the fundamental band; $u = hc\omega^*/kT$ and $\gamma = B_e/\omega_e$ is a known spectroscopic constant; the mole fraction of $HC\ell$ is $\eta_{HC\ell} = 0.2353$

according to Eq. (16). The (collision) half-width of the lines, b, was assumed to be equal to $0.1\,(300/T)^{1/2} p_T$ for both the fundamental and overtone bands. It should be noted that the emissivity in the linear region is independent of b while, in the square root region, it is proportional to the square root of b. Furthermore, the emissivity is independent of b for well-overlapped lines and, therefore, the uncertainties in b will introduce appreciably smaller uncertainties into the emissivity estimates.

For well-overlapped lines, the box model[5] leads to the following relations:

$$\left.\begin{aligned}
(\varepsilon_F)_{box} &= \frac{R^o_{\omega_F}}{\sigma T^4}\,\Delta\omega\left[1-\exp(-\bar{P}_F \eta_{HC\ell}\, p_T L_{HC\ell})\right] \\
&= 0.251\left[1-\exp(-6.37\times 10^{-3}\, p_T L_{HC\ell})\right] \\
\text{and} \\
(\varepsilon_O)_{box} &= \frac{R^o_{\omega_O}}{\sigma T^4}\,\Delta\omega\left[1-\exp(-\bar{P}_O \eta_{HC\ell}\, p_T L_{HC\ell})\right] \\
&= 0.108\left[1-\exp(-1.75\times 10^{-4}\, p_T L_{HC\ell})\right]
\end{aligned}\right\} \qquad (19)$$

where

$$\bar{P}_F = \frac{a_F}{\Delta\omega}$$

and

$$\bar{P}_O = \frac{a_O}{\Delta\omega}\left[\frac{1+\exp(-u)}{1-\exp(-u)}\right] .$$

Here $\Delta\omega$ is the width of the bands; $R^o_{\omega_F}$ and $R^o_{\omega_O}$ are the blackbody radiancies at the centers of the fundamental and first overtone bands,

respectively. The results of emissivity calculations are shown in Fig. 15 for well-overlapped lines. In Figs. 16 to 19 we have utilized the emissivity calculations for nonoverlapped lines and for overlapped lines to estimate the emissivities for the entire range of values of $L_{HC\ell}$ which is of interest in the present analysis. We note the well-known result that, for very small values of $L_{HC\ell}$, both methods of calculation give the same values for the emissivities. For somewhat larger values of $L_{HC\ell}$, we find that the box model yields relatively larger emissivity estimates. Finally, for very large beam lengths, the nonoverlapping line model must become inapplicable and the corresponding emissivities, which exceed $\mathcal{E}_{box}$, are too large.

The regions in which the spectral lines overlap may be ascertained by calculating the absorption coefficient at the centers of the lines and at points midway between adjacent spectral lines. The absorption coefficient of an individual line for the temperature and pressure range of interest is described by the dispersion formula

$$P_\omega \, p_{HC\ell} \, L_{HC\ell} = \frac{S}{\pi} \, \frac{b p_{HC\ell} \, L_{HC\ell}}{(\omega-\omega_o)^2 + b^2} , \qquad (20)$$

where ω_o is the wave number at the line center, b is the line half-width, and S is the integrated intensity of the line. Calculations of this sort have been carried out before for CO.[5] On the basis of known absorption measurements and emissivity calculations,[5] we infer that the true emissivities (for specified half-widths) must be below the emissivities calculated by using either the non-overlapping line model or the box model. This result has been used in Figs. 16 to 19 in order to derive the dotted

curves, which must be considered to be uncertain by perhaps 10 to 20%.

V. EMISSIVITY CALCULATIONS FOR H_2O

Emissivity measurements for H_2O have been made at pressures near 1 atmosphere.[13] To obtain emissivity estimates at higher pressures, a semi-empirical extrapolation of the experimental data will be used. We shall employ an extrapolation described in reference (5) in which the spectral lines of H_2O are assumed to be randomly distributed. The emissivity is given as a sum of emissivities for six spectral regions, viz.,

$$\varepsilon = \Delta\omega \sum_{i=1}^{6} \frac{R^{o}_{\omega_i}}{\sigma T^4} g(\bar{x}_i, b/\delta^*),$$

$$g(\bar{x}_i, b/\delta^*) = 1-\exp\left[-(2\pi b/\delta^*) f(\bar{x}_i)\right], \qquad (21)$$

where

$$f(\bar{x}_i) = \bar{x}_i \left[\exp(-\bar{x}_i)\right]\left[J_0(i\bar{x}_i)-iJ_1(i\bar{x}_i)\right]$$

with J_0 and J_1 representing Bessel functions of order 0 and 1, respectively. Also

$$\bar{x}_i = \frac{a_i \delta^* p_{H_2O} L_{H_2O}}{2\pi b \Delta\omega}$$

where a_i is the integrated intensity of the ith band, b is again the half width of the spectral lines (which is assumed to be the same for all of the lines), δ^* denotes the mean spacing between lines, and $\Delta\omega$ is the width of a band (which is also taken to be uniform for all of the bands).

Numerical values for the required parameters at 1433°K are summarized in Table IV. In Fig. 20 we have plotted the emissivities of

H_2O as a function of optical depth. In the present analysis L_{H_2O} is so small that $f(\bar{x}_i)$ does not differ from $\bar{x}_i$ by more than about 7% for the strongest band and by less for the other bands. Thus $(2\pi b/\delta^*)f(\bar{x}_i)$ is nearly equal to $a_i p_{H_2O} L_{H_2O}/\Delta\omega$ for all of the values of L_{H_2O} which are of interest to us. In other words, ε_{H_2O} should be practically a function only of $p_T L_{H_2O}$, a conclusion which is in agreement with the data plotted in Fig. 20. This result has been employed previously in the suggested application of Fig. 7.

It is apparent that the large extrapolation of available data to very high pressures implicit in the present calculations constitutes the principal uncertainty in our estimates of radiant energy emission. However, in view of the fact that two completely different band models have been shown previously[5] to lead to practically identical emissivity estimates at elevated pressures, we consider it unlikely that the calculated water emissivities are in error by more than 10 to 20%.

VI. CORRECTIONS FOR PARTIAL OVERLAPPING BETWEEN LINES AND BANDS BELONGING TO H_2O AND TO $HC\ell$

For gas mixtures it is inadmissible to add either spectral or total emissivities. However, the products of spectral absorption coefficients and optical depths can be shown to be strictly additive.[5] Using the general expression given in Eq. (13), we may write the following explicit emissivity relation for a mixture of H_2O and $HC\ell$:

$$\varepsilon_{H_2O+HC\ell} = \frac{1}{\sigma T^4} \int_0^\infty R^o_\omega \left\{ 1 - \exp\left[-\left(P_{\omega, H_2O} p_{H_2O} L_{H_2O} + P_{\omega, HC\ell} p_{HC\ell} L_{HC\ell} \right) \right] \right\} d\omega$$

$$= \frac{1}{\sigma T^4} \int_0^\infty R_\omega^o \left[1-\exp(-P_{\omega, H_2O} P_{H_2O} L_{H_2O})\right] d\omega$$

$$+ \frac{1}{\sigma T^4} \int_0^\infty R_\omega^o \left[\exp(-P_{\omega, H_2O} P_{H_2O} L_{H_2O})\right]\left[1-\exp(-P_{\omega, HCl} P_{HCl} L_{HCl})\right] d\omega$$

$$= \varepsilon_{H_2O} + \frac{1}{\sigma T^4} \int_0^\infty R_\omega^o \left[\exp(-P_{\omega, H_2O} P_{H_2O} L_{H_2O})\right]\left[1-\exp(-P_{\omega, HCl} P_{HCl} L_{HCl})\right] d\omega. \quad (22)$$

The preceding expression shows that the emissivity of a mixture of H_2O and HCl is equal to the emissivity of H_2O plus the integral of the spectral emissivity of HCl modified by the spectral transmissivity of H_2O. From the known positions of the H_2O and HCl bands and our previous estimates for the H_2O band-widths, we conclude that the 2.7μ band of H_2O overlaps the HCl fundamental at wave numbers greater than 3125 cm^{-1} and the 1.87μ band of H_2O overlaps the overtone at wave numbers smaller than 5963 cm^{-1}. Using the average absorption coefficients

$$\overline{P}_i = \frac{a_i}{\Delta\omega}$$

for the 2.7μ and 1.87μ bands of H_2O, we obtain

$$\varepsilon_{H_2O+HCl} = \varepsilon_{H_2O} + \frac{1}{\sigma T^4}\Bigg\{ \int_0^{3125} R_\omega^o \left[1-\exp(-P_{\omega, HCl} P_{HCl} L_{HCl})\right] d\omega$$

$$+ \left[\exp(-\overline{P}_{2.7\mu, H_2O} P_{H_2O} L_{H_2O})\right] \int_{3125}^\infty R_\omega^o \left[1-\exp(-P_{\omega, HCl} P_{HCl} L_{HCl})\right] d\omega \Bigg\}$$

HCl fundamental

$$+\frac{1}{\sigma T^4}\left\{\left[\exp(-\bar{P}_{1.87\mu,\,H_2O}P_{H_2O}L_{H_2O})\right]\int_0^{5963} R^o_\omega\left[1-\exp(-P_{\omega,\,HCl}P_{HCl}L_{HCl})\right]d\omega\right.$$

$$\left.+\int_{5963}^{\infty} R^o_\omega\left[1-\exp(-P_{\omega,\,HCl}P_{HCl}L_{HCl})\right]d\omega\right\}_{HCl\ \text{first overtone}} . \qquad (23)$$

It is now convenient to introduce the definitions

$$f \equiv 2\,\frac{R^o_{\omega,\,F}}{\sigma T^4}\int_{2886}^{3125}\frac{\varepsilon_\omega}{\varepsilon_{F,\,HCl}}\,d\omega \qquad (24a)$$

and

$$g \equiv 2\,\frac{R^o_{\omega,\,O}}{\sigma T^4}\int_{5720}^{5963}\frac{\varepsilon_\omega}{\varepsilon_{O,\,HCl}}\,d\omega \qquad (24b)$$

where $R^o_{\omega,\,F}$ and $R^o_{\omega,\,O}$ are evaluated at 2886 cm^{-1} and 5720 cm^{-1}, respectively, i.e., at the wave numbers of the centers of the fundamental (F) and overtone bands (O). Equation (23) becomes, approximately,

$$\varepsilon_{H_2O+HCl} = \varepsilon_{H_2O} + \left[(1+f) + \left[\exp(-\bar{P}_{2.7\mu,\,H_2O}P_{H_2O}L_{H_2O})\right](1-f)\right]\frac{\varepsilon_{F,\,HCl}}{2}$$

$$+\left[\left[\exp(-\bar{P}_{1.87\mu,\,H_2O}P_{H_2O}L_{H_2O})\right](1+g) + (1-g)\right]\frac{\varepsilon_{O,\,HCl}}{2} \qquad (25)$$

if we assume that the emissivity contributions of the P- and R-branches of HCl are equivalent.

We may obtain estimates for the parameters f and g as functions of $L_{HC\ell}$ and p_T by computing f and g for three ranges of values of $L_{HC\ell}$ and p_T and then performing appropriate interpolations. Thus it is a simple matter to compute f and g for the linear and square root regions for nonoverlapping lines and also for the box model (which is applicable to well overlapped lines). For well overlapped lines,

$$\left.\begin{aligned} \varepsilon_{F,\,HC\ell} &= \frac{R^{o}_{\omega,\,F}}{\sigma T^4}\,\bar{\varepsilon}_{\omega}\,\Delta\omega_{F,\,HC\ell} \\ \text{and} \\ \varepsilon_{O,\,HC\ell} &= \frac{R^{o}_{\omega,\,O}}{\sigma T^4}\,\bar{\varepsilon}_{\omega}\,\Delta\omega_{O,\,HC\ell} \end{aligned}\right\} \qquad (26)$$

whence

$$f = \frac{2 \times (3125-2886)}{\Delta\omega_{F,\,HC\ell}} = \frac{2 \times 239}{1147} = 0.417$$

and

$$g = \frac{2 \times (5963 - 5720)}{1147} = 0.424.$$

For nonoverlapped lines in the linear region, the emissivity of a single line is directly proportional to the integrated intensity of the line. Therefore, for the purposes of the present calculation, we may consider the spectral emissivity of $HC\ell$ to be proportional to the integrated intensity of the nearest spectral line. The intensity of a line in a vibration-rotation band varies with rotational quantum number j according to the relation[5]

$$S_j \sim (2j+1)\exp\left[-\sigma' j(j+1)\right] = \frac{2\left[\exp(\sigma'/4)\right]}{\sqrt{\sigma'}}\left[\sqrt{\sigma'}\left(j+\tfrac{1}{2}\right)\right]\exp-\left[\sqrt{\sigma'}\left(j+\tfrac{1}{2}\right)\right]^2 \qquad (27)$$

where $\sigma' = hcB_e/kT$ with B_e representing a spectroscopic constant. The spacing $(\omega-\omega_o)$ between the band center and the jth line is

$$\omega-\omega_o = 2B_e j$$

whence it follows that

$$\varepsilon_\omega \sim S(\omega) \sim \xi \exp(-\xi^2)$$

where

$$\xi \equiv \frac{\sqrt{\sigma'}}{2}\left(\frac{\omega-\omega_o}{B_e} + 1\right) .$$

For the fundamental band at $\omega = \omega_o = 2886\ cm^{-1}$, $\xi = .0515$; for $\omega = 3125\ cm^{-1}$, $\xi = 1.215$. Therefore,

$$f = \frac{\int_{.0515}^{1.215} \xi\left[\exp(-\xi^2)\right] d\xi}{\int_{.0515}^{\infty} \xi\left[\exp-(\xi^2)\right] d\xi} = 0.771.$$

Similarly, for the first overtone,

$$g = \frac{\int_{.0515}^{1.234} \xi\left[\exp-(\xi^2)\right] d\xi}{\int_{.0515}^{\infty} \xi\left[\exp(-\xi^2)\right] d\xi} = 0.782$$

in the linear region.

In the square-root region, the emissivity of a line is proportional to the square root of the integrated intensity of the line. Using the same analysis as before, we find that

$$f = \frac{\int_{\frac{.0515}{\sqrt{2}}}^{\frac{1.215}{\sqrt{2}}} \sqrt{y}\left[\exp(-y^2)\right] dy}{\int_{\frac{.0515}{\sqrt{2}}}^{\infty} \sqrt{y}\left[\exp(-y^2)\right] dy} \simeq \frac{\int_{0}^{.859} \sqrt{y}\left[\exp(-y^2)\right] dy}{\int_{0}^{\infty} \sqrt{y}\left[\exp(-y^2)\right] dy}$$

$$= \frac{\int_{0}^{(.859)^2} e^{-V} V^{-1/4} dV}{\int_{0}^{\infty} e^{-V} V^{-1/4} dV} = \frac{1}{\Gamma\left(\frac{3}{4}\right)} \int_{0}^{.853\sqrt{-\frac{1}{4}+1}} e^{-V} V^{-1/4} dV.$$

The incomplete gamma function $I(u,p)$ is defined by[14]

$$I(u, p) \equiv \frac{1}{\Gamma(p+1)} \int_{0}^{u\sqrt{p+1}} e^{-V} V^{p} dV$$

so that

$$f = I(.853, -\tfrac{1}{4}) = 0.647.$$

Similarly,

$$g = I(.879, -\tfrac{1}{4}) = 0.655$$

in the square-root region.

To find f and g as a function of the mean beam length of HCl, L_{HCl}, for various values of the total pressure p_T, we must examine the detailed emissivity calculations in order to determine at what values of L_{HCl} and p_T the spectral lines fall effectively into the linear or square-

root regions or under what conditions the box model becomes applicable. We may then interpolate to obtain f and g for intermediate cases. The result of this analysis for one case is shown in Fig. 21.

Once f and g have been determined, it is a simple matter to compute $\varepsilon_{H_2O+HC\ell}$ from Eq. (25) by using the following expressions for the average absorption coefficients:

$$\overline{P}_{2.7\mu} = \frac{29.2}{1262} = 2.31 \times 10^{-2} \text{ cm}^{-1}\text{- atmos}^{-1}$$

and

$$\overline{P}_{1.87\mu} = \frac{2.34}{1262} = 1.85 \times 10^{-3} \text{ cm}^{-1}\text{-atmos}^{-1}.$$

Using Figs. 6 and 7 to compute the mean beam lengths, it is now possible to compute the radiation to a face of the parallelepiped. This problem will be examined in the following Section VII.

VII. REPRESENTATIVE ESTIMATES OF RADIANT ENERGY LOSS FROM THE COMBUSTION PRODUCTS AND OF RADIANT HEAT TRANSFER TO THE BURNING PROPELLANT SURFACE

The total radiant energy emission from the combustion products and to the propellant surface may be calculated easily by utilizing the tabulated and plotted results. Representative calculations have been carried out for h/r = 5 with r = 0.2, 2, and 20 cm for p_T = 25 and 300 atmos.

Figures 6 and 7 were used to obtain the mean beam lengths L_{H_2O} and $L_{HC\ell}$. The quantities ε_{H_2O} and $\varepsilon_{HC\ell}$ were then obtained by utilizing Figs. 15 to 20. At p_T = 25 atmos, Fig. 21 was used to obtain f whereas g was set equal to 0.782 since reference to Figs. 10 and 17 shows

that the first overtone consists of non-overlapping lines in the linear region for the mean beam lengths applicable to the present calculations. At 300 atmos, the spectral lines are well overlapped and, therefore, $f = 0.417$ and $g = 0.424$ (compare Section VI). Equation (25) may then be used in order to obtain the emissivities. The results of the calculations are summarized in Table V.

In order to obtain the radiant energy flux to the propellant surface from the combustion products, we utilize the defining relation for emissivity to obtain the total heat transfer to the propellant surface:

$$Q_S = \varepsilon_{\text{to base}} A_{\text{base}} \sigma T^4 ;$$

also, the total heat loss from the combustion products is

$$Q_T = (4\varepsilon_{\text{to face}} A_{\text{face}} + 2\varepsilon_{\text{to base}} A_{\text{base}}) \sigma T^4$$

where A denotes the area and σ is the Stefan-Boltzmann constant ($\sigma = 0.1713 \times 10^{-8}$ btu/(ft)^2-(hr)-(deg R)^4). The results are given in Table VI. Reference to the data listed in Table VI shows that the heat transfer to the propellant surface does not exceed 27,800/400 = 69.5 btu/hr-cm^2 even for the largest rectangular parallelepiped considered at p_T = 300 atmos. The total radiant energy loss to the outside for this extreme case amounts to 612,000 - 27,800 = 584,200 btu/hr.

Evaluation of the significance of the results derived in the present study, in so far as flammability limits for pure ammonium perchlorate are concerned, requires independent study.

Table II. The mean beam length L^o for $p_g L \longrightarrow 0$ for various values of h/r.

$\frac{h}{r}$	for radiation to the base or top face.	for radiation to a side face.
$\rightarrow 0$	2h	--
1	2/3r	2/3r
4	0.86r	0.90r
$\rightarrow \infty$	0.94r	r

Table III. Integrated intensities of the fundamental vibration-rotation bands of NH_3 at T = 300°K.[5]

Band center (cm^{-1})	Integrated intensity (cm^{-2}-atmos^{-1})
950	600
1627	110
3337	20
3448	13

Table IV. Parameters required for emissivity calculations on H_2O at 1433°K.[5]

Band center (cm^{-1})	a_i (cm^{-2}-atmos^{-1})	$\Delta\omega$ (cm^{-1})	$\frac{2\pi b}{\delta^* p_T}$
500	13.55	1262	.685
1595	40.6	↓	↓
3756	29.2	↓	↓
5332	2.34	↓	↓
7251	1.93	↓	↓
8807	.0742	↓	↓

Table V. Emissivities for radiation to a side face and for radiation to the base or top face of a rectangular parallelepiped with $h/r = 5$ at $T = 1433^{\circ}K$.

r (cm)	0.2	2	20
Emissivity for radiation to the side faces: $p_T = 25$ atmos	.0273	.217	.652
Emissivity for radiation to the base or top face:	.0259	.203	.645
Emissivity for radiation to the side faces: $p_T = 300$ atmos	.251	.681	.850
Emissivity for radiation to the base or top face:	.240	.674	.849

Table VI. Radiant energy flux (btu/hr) to the propellant and from the combustion products in all directions (including the heat transfer to the propellant surface) for $h/r = 5$ at $1433^{\circ}K$.

r (cm)	0.2	2	20
Radiant energy flux to the propellant surface (btu/hr): $p_T = 25$ atmos	.0848	66.4	21,000
Radiant energy flux from the combustion products in all directions (btu/hr):	1.96	1550	469,000
Radiant energy flux to propellant surface (btu/hr): $p_T = 300$ atmos	.785	221	27,800
Radiant energy flux from the combustion products in all directions (btu/hr):	18.0	4910	612,000

CHAPTER 3

RADIANT ENERGY TRANSFER FROM NONISOTHERMAL MOLECULAR EMITTERS WITH NON-OVERLAPPING DISPERSION LINES

I. INTRODUCTION

The total radiant energy flux received by the center of the base of a hemisphere of radiators is

$$W = \int_0^Y \int_0^\infty R_\omega^o(X) P_\omega(X) \exp\left[- \int_0^X P_\omega(y)dy \right] d\omega dX \qquad (1)$$

where ω denotes wave number (in cm^{-1}), X denotes optical depth (in cm-atmos), P_ω is the spectral absorption coefficient (in cm^{-1}-$atmos^{-1}$), and R_ω^o is the Planck radiation function (in erg-cm^{-1}-sec^{-1}). The hemisphere is of radius Y, and is made up of radiators whose density varies only radially. For geometric arrangements other than a hemisphere, it is convenient to replace Y by an appropriate effective beam length. This geometrical problem will not be considered further.

Studies have been made on overlapped spectral lines[5,15] and on randomly distributed lines.[16] However, we shall specialize to the case of molecular emitters with non-overlapping lines of Lorentz (dispersion) contour, for which

$$W_{line} = \int_0^Y \int_0^\infty R_\omega^o(X) \frac{S_j(X)}{\pi} \frac{b(X)}{(\omega-\omega_j)^2+b^2(X)} \exp\left[- \int_0^X \frac{S_j(y)}{\pi} \frac{b(y)dy}{(\omega-\omega_j)^2+b^2(y)} \right] d\omega dX. \qquad (2)$$

where S_j is the integrated intensity of the line (in cm^{-2}-$atmos^{-1}$) and b

is the line half-width (in cm^{-1}). The integrals in Eq. (2) cannot be evaluated until S and b are given as functions of the optical depth, i.e., for a gas the temperature and pressure must be given explicitly as a function of optical depth before the integrals can be evaluated for arbitrary Y. We may, however, obtain explicit results for two limiting cases.

II. THE TRANSPARENT GAS APPROXIMATION

The transparent gas approximation corresponds to optical depths which are sufficiently small so that the exponential in Eq. (2) has very nearly the value unity. For this approximation, W_{line} becomes

$$W_{line} = \int_0^Y R^o_{\omega_j}(X) S_j(X) dX \ . \tag{3}$$

To obtain the radiant energy flux for a band we must sum over the individual lines which correspond to the transitions j-1→j and j→j-1. Therefore

$$W_{band} = \sum_j \int_0^Y R^o_{\omega_j}(X) S_j(X) dX = \int_0^Y \overline{R^o_\omega}(X) \sum_j S_j(X) dX \tag{4}$$

where $\overline{R^o_\omega}(X)$ is the Planck radiation function evaluated at the band center, and $\sum_j$ represents the summation over the lines of the band. Now considering the vibration-rotation bands of a diatomic molecule,

$$\left[\sum_j S_j(X) \right]_F = a_F(T) = a_F(T_o) \frac{T_o}{T} \ , \tag{5}$$

$$\left[\sum_j S_j(X)\right]_O = a_O(T)\,\frac{\left[1+\exp\left(-\frac{hc\omega^*}{kT}\right)\right]}{\left[1-\exp\left(-\frac{hc\omega^*}{kT}\right)\right]} = a_O(T_o)\frac{T_o}{T}\,\frac{\left[1+\exp\left(-\frac{hc\omega^*}{kT}\right)\right]}{\left[1-\exp\left(-\frac{hc\omega^*}{kT}\right)\right]}, \qquad (6)$$

for the fundamental and first overtone bands respectively. Here ω^* is the wave number at which the fundamental band center occurs. The values of the Planck radiation function at the centers of the fundamental and first overtone bands, respectively, are

$$\overline{R^o_{\omega_F}} = \frac{2\pi hc^2\,\omega^{*3}}{\exp\left(\frac{hc\omega^*}{kT}\right)-1} \qquad (7)$$

and

$$\overline{R^o_{\omega_O}} \simeq \frac{16\pi hc^2\omega^{*3}}{\exp\left(\frac{2hc\omega^*}{kT}\right)-1} \qquad (8)$$

where h is Planck's constant, c is the velocity of light, and k is the Boltzmann constant. Thus the radiant energy flux contribution of the fundamental band is

$$W_F = 2\pi hc^2\omega^{*3}\,a_F(T_o)T_o\int_0^Y \frac{dX}{\left[\exp\left(\frac{hc\omega^*}{kT(X)}\right)-1\right]T(X)}$$

$$= 2\pi hc^2\omega^{*3}\,a_F(T_o)T_o\int_{T(0)}^{T(Y)} \frac{X'(T)dT}{\left[\exp\left(\frac{hc\omega^*}{kT}\right)-1\right]T} \qquad (9)$$

while, for the first overtone,

$$W_O = 16\pi hc^2\omega^{*3}\,a_O(T_o)T_o\int_0^Y \frac{dX}{\left[\exp\left(\frac{hc\omega^*}{kT(X)}\right)-1\right]^2 T(X)}$$

$$= 16\pi hc^2 \omega^* a_o(T_o) T_o \int_{T(0)}^{T(Y)} \frac{X'(T)dT}{\left[\exp\left(\frac{hc\omega^*}{kT}\right)-1\right]^2 T} \qquad (10)$$

where $X'(T) = dX/dT$. These expressions are also valid when the lines overlap.

III. THE "SQUARE ROOT" APPROXIMATION

For an isothermal gas Eq. (2) becomes

$$W_{line} = R^o_{\omega_j} \int_{-\infty}^{\infty} \left[1-\exp\left(-\frac{S}{\pi}\frac{bY}{(\omega-\omega_j)^2+b^2}\right)\right] d(\omega-\omega_j), \qquad (11)$$

which may be approximated by[5]

$$W_{line} \simeq R^o_{\omega_j} SY \qquad \text{for } \frac{SY}{2\pi b} \lesssim 0.3 \qquad (12)$$

and

$$W_{line} \simeq 2R^o_{\omega_j} \sqrt{SbY} \qquad \text{for } \frac{SY}{2\pi b} \gtrsim 2 \; . \qquad (13)$$

The first of these approximations corresponds to the transparent gas approximation. The second (square root) approximation arises from the fact that for an isothermal gas at sufficiently large optical depths, the exponential in Eq. (11) is very nearly zero for small values of $(\omega-\omega_j)$. We obtain Eq. (13) formally from Eq. (11) by replacing the Lorentz contour $P_\omega = \frac{S}{\pi}\frac{b}{(\omega-\omega_j)^2+b^2}$ by the simpler contour $P_\omega = \frac{S}{\pi}\frac{b}{(\omega-\omega_j)^2}$, which is a good approximation for large values of $(\omega-\omega_j)$.

The square root approximation, i.e., replacing the Lorentz expression for the spectral absorption coefficient by $\frac{S}{\pi}\frac{b}{(\omega-\omega_j)^2}$, may be

used also for a nonisothermal gas provided the temperature is nearly constant in the region X = 0 to X = Y_1, where Y_1 is sufficiently large. This result may be derived by considering the temperature profile

$$T = T_1 \quad \text{for} \quad 0 < X < Y_1$$

and

$$T \text{ arbitrary for } Y_1 < X < Y.$$

Equation (2) becomes now

$$W_{line} \simeq \sum_{i=1}^{N} R^{o}_{\omega_j, i} \int_{-\infty}^{\infty} \left[\exp\left(- \sum_{k=1}^{i-1} \frac{S_{j,k}}{\pi} \frac{b_k (Y_k - Y_{k-1})}{(\omega-\omega_j)^2 + b_k^2} \right) \right]$$

$$\left[1-\exp\left(- \frac{S_{j,i}}{\pi} \frac{b_i (Y_i - Y_{i-1})}{(\omega-\omega_j) + b_i^2} \right) \right] d(\omega-\omega_j)$$

$$= \sum_{i=1}^{N} R^{o}_{\omega_j, i} \left\{ \int_{-\infty}^{\infty} \left[1-\exp\left(- \sum_{k=1}^{i} \frac{S_{j,k}}{\pi} \frac{b_k (Y_k - Y_{k-1})}{(\omega-\omega_j)^2 + b_k^2} \right) \right] d(\omega-\omega_j) \right.$$

$$\left. - \int_{-\infty}^{\infty} \left[1-\exp\left(- \sum_{k=1}^{i-1} \frac{S_{j,i}}{\pi} \frac{b_k (Y_k - Y_{k-1})}{(\omega-\omega_j)^2 + b_k^2} \right) \right] d(\omega-\omega_j) \right\}, \qquad (14)$$

where we have assumed the half-widths in a given vibration-rotation band to be equal and have approximated the actual temperature profile by a "step" profile, which may be made as close to the actual profile as desired by making the number of steps N sufficiently large. The gas in the region $(Y_k - Y_{k-1})$ is at the temperature T_k, with the quantities $S_{j,k}$ and b_k

evaluated at T_k; similarly, the gas in the region $Y_i - Y_{i-1}$ is at the temperature T_i etc.; $R^o_{\omega_j, i}$ is evaluated at the temperature T_i, and Y_o is identically equal to zero. Now comparison with Eq. (11) shows that for $S_{j,1}Y_1/2\pi b_1 \gtrsim 2$, we can replace $S_{j,1}/\pi\left[b_1/(\omega-\omega_j)^2+b_1^2\right]$ in Eq. (14) by either $S_{j,1}/\pi\left[b_1/(\omega-\omega_j)^2\right]$ or $S_{j,1}/\pi\left[b_1/(\omega-\omega_j)^2+b_2^2\right]$ provided b_2 is not much greater than b_1 ($b_2 \gg b_1$ when $T_1 \gg T_2$; this case is not of interest in most practical applications). But

$$\frac{1}{\pi}\,\frac{S_{j,1}b_1Y_1 + S_{j,2}b_2(Y_2-Y_1)}{(\omega-\omega_j)^2 + b_2^2}$$

may be replaced by

$$\frac{1}{\pi}\,\frac{S_{j,1}b_1Y_1 + S_{j,2}b_2(Y_2-Y_1)}{(\omega-\omega_j)^2}$$

or by

$$\frac{1}{\pi}\,\frac{S_{j,1}b_1Y_1 + S_{j,2}b_2(Y_2-Y)}{(\omega-\omega_j)^2 + b_3^2}$$

if

$$\frac{S_{j,2}\left[\dfrac{S_{j,1}b_1Y_1 + S_{j,2}b_2(Y_2-Y_1)}{S_{j,2}b_2}\right]}{2\pi b_2} = \frac{S_{j,1}Y_1}{2\pi b_1}\left(\frac{T_2}{T_1}\right) + \frac{S_{j,2}(Y_2-Y_1)}{2\pi b_2} \gtrsim 2 \tag{15}$$

and if T_2 is not much greater than T_3. In Eq. (15) we have used the relation

$$b = \text{constant} \times \frac{p}{\sqrt{T}} \tag{16}$$

where p represents the total pressure of the gas. Therefore, by induction,

if $\frac{S_{j,1}Y_1}{2\pi b_1} \gtrsim 2\left(\frac{T_1}{T_{min}}\right)$, where T_{min} is minimum temperature of the gas, the following approximation is valid:

$$\sum_{k=1}^{n} \frac{S_{j,k}}{\pi} \frac{b_k(Y_k - Y_{k-1})}{(\omega-\omega_j)^2+b_k^2} \simeq \frac{1}{(\omega-\omega_j)^2} \sum_{k=1}^{n} \frac{S_{j,k}}{\pi} b_k(Y_k - Y_{k-1}).$$

Thus the following expression which is similar to Eq. (2) except that b^2 has been neglected relative to $(\omega-\omega_j)^2$, is obtained:

$$W_{line} \simeq \int_0^Y R^o_{\omega_j}(X) \int_{-\infty}^{\infty} \frac{S_j(X)b(X)}{\pi(\omega-\omega_j)^2} \exp\left[-\frac{1}{\pi(\omega-\omega_j)^2}\int_0^X S_j(y)b(y)dy\right] d(\omega-\omega_j)dX$$

$$\simeq \int_0^Y R^o_{\omega_j}(X) \frac{S_j(X)b(X)}{\pi} 2\int_0^{\infty} \exp\left[-\left(\frac{1}{\pi}\int_0^Y S_j(y)b(y)dy\right)z^2\right] d\,zdX$$

$$\simeq \int_0^Y R^o_{\omega_j}(X) \sqrt{S_j(X)b(X)}\left[\int_0^X \frac{S_j(y)b(y)}{S_j(X)b(X)}\,dy\right]^{-1/2} dX, \qquad (17)$$

when

$$\frac{S_{j,1}Y_1}{2\pi b_1} \gtrsim 2\left(\frac{T_1}{T_{min}}\right).$$

For diatomic molecules at low and moderate temperatures ($e^{-u} << 1$), the integrated intensity S_j for the transition $j \rightarrow j-1$ or $j-1 \rightarrow j$ may be approximated by

$$S_j \simeq a\gamma uj \exp(-u\gamma j^2), \qquad (18)$$

where $u = hc\omega^*/kT$, a is the band integrated intensity, and $\gamma = B_e/\omega_e$ where B_e and ω_e are tabulated spectroscopic constants and $\omega_e \simeq \omega^*$.

Also

$$dy = \eta\, p(y)\, d\ell \tag{19}$$

where p is the total pressure, ℓ is the geometric length, and η is the mole fraction of the absorbing gas. Thus, if we approximate $R^{o}_{\omega_j}$ by R^{o}_{ω} at the band center and assume that the half-widths of the rotational lines are equal, we obtain the following expression for the radiant energy flux of the fundamental vibration-rotation band:

$$W_F \simeq 4\pi hc^2 \omega^{*3} \eta \left[\gamma a_F(T_o) u(T_o) b(T_o, p_o) \frac{\left(T_o\right)^{5/2}}{p_o} \right]^{1/2}$$

$$\sum_{j=1}^{\infty} \int_{T(0)}^{T(Y)} \frac{\left[p(\gamma)\right]^{3/2}}{\left[\exp\left(\frac{hc\omega^*}{k\gamma}\right) - 1\right] \gamma^{5/4}}\, j^{1/2}$$

$$\exp\left(- \frac{hcB_e j^2}{2k} \right) \left\{ \left[\int_{T(0)}^{\gamma} \eta \frac{p'^2(t)}{p(\gamma)} \left(\frac{\gamma}{t}\right)^{5/2} \right.\right.$$

$$\left.\left. \exp\left[- \frac{hcB_e j^2}{k} \left(\frac{1}{t} - \frac{1}{\gamma} \right) \right] \ell'(t)\, dt \right]^{-1/2} \right\} \ell'(\gamma)\, d\gamma \tag{20}$$

where $\ell'(t) = \frac{d\ell}{dt}$. A more accurate relation may be obtained by using more accurate expressions for $R^{o}_{\omega_j}$, $S_{j \to j-1}$, and $S_{j-1 \to j}$.

If instead of the actual temperature profile we use an approximating step function in Eq. (16) the following result is obtained:

$$W_{line} \simeq \sum_{i=1}^{N} 2R^{o}_{\omega_j, i}\left[\sqrt{\sum_{k=1}^{i} S_{j,k} b_k (Y_k - Y_{k-1})} - \sqrt{\sum_{k=1}^{i-1} S_{j,k} b_k (Y_k - Y_{k-1})}\right]. \tag{21}$$

On the other hand for a transparent gas the radiant energy flux is

$$W_{line} \simeq \sum_{i=1}^{N} R^{o}_{\omega_j, i} S_{j,i} (Y_i - Y_{i-1}). \tag{22}$$

Therefore, if the first p-1 regions are transparent $\left(\sum_{k=1}^{p-1} \frac{S_{j,k}(Y_k - Y_{k-1})}{2\pi b_k} \lesssim 0.3\right)$, and if $\frac{S_{j,p}(Y_p - Y_{p-1})}{2\pi b_p} \gtrsim 2$, then

$$W_{line} \simeq \sum_{i=1}^{p+1} R^{o}_{\omega_j, i} S_{j,i} (Y_i - Y_{i-1}) + \sum_{i=p}^{N} 2R^{o}_{\omega_j, i}\left[\sqrt{\sum_{k=1}^{i} S_{j,k} b_k (Y_k - Y_{k-1})} - \sqrt{\sum_{k=1}^{i-1} S_{j,k} b_k (Y_k - Y_{k-1})}\right]. \tag{23}$$

IV. RADIANT ENERGY EMISSION FROM TWO (ADJACENT) ISOTHERMAL REGIONS AT DIFFERENT TEMPERATURES

The preceding results will be applied to the following simple temperature profile:

$$T = T_1 \quad \text{for} \quad 0 < X < Y_1$$

and

$$T = T_2 \quad \text{for} \quad Y_1 < X < Y_2$$

where $T_2 \gtrsim 2T_1$. For the case $p = p_1$, $\eta = \eta_1$ for $0 < X < Y_1$ and $p = p_2$, $\eta = \eta_2$ for $Y_1 < X < Y_2$, appropriate formulas will now be derived, where it is understood that $b_1 = b(T_1, p_1)$, $b_2 = b(T_2, p_2)$, $Y_1 = \eta_1 p_1 \ell_1$, and $(Y_2 - Y_1) = \eta_2 p_2 (\ell_2 - \ell_1)$.

If $S_{j,1} Y_1 / 2\pi b_1 \lesssim 0.3$ for each line, the transparent gas approximation may be used; the following relation for the total radiant energy flux is obtained:

$$W = \sigma T_1^4 \, \varepsilon_{\ell.r.}\left[T_1, Y_1\right] + \sigma T_2^4 \, \varepsilon\left[T_2, Y_2 - Y_1\right]. \tag{24}$$

Here σ is the Stefan-Boltzmann constant, $\varepsilon\left[T, Y\right]$ is the emissivity of a gas at temperature T and optical depth Y, and the subscript $\ell.r.$ shows that the gas is in the "linear region", e.g., the gas in the spacial region $0 < X < Y_1$ is transparent (see reference (5) for explicit relations of emissivities for isothermal gases with non-overlapping dispersion lines).

If $S_{j,1} Y_1 / 2\pi b_1 \gtrsim 2$ and $T_2 > T_1$, Eq. (21) may be used to give

$$W_{\text{line}} \simeq 2R^{o}_{\omega_j,1} \sqrt{S_{j,1} b_1 Y_1} + 2R^{o}_{\omega_j,2} \left[\sqrt{S_{j,1} b_1 Y_1 + S_{j,2} b_2 (Y_2 - Y_1)} - \sqrt{S_{j,1} b_1 Y_1} \right]. \tag{25}$$

Let $W_{0 \to 1}$ denote the total radiant energy flux for all lines of a diatomic molecule having the vibrational transition $0 \to 1$ when $T_2 \gtrsim 2T_1$ and $S_{j,1} Y_1 / 2\pi b_1 \gtrsim 2$ for most of the important lines. Expressions for S(j) and $R^{o}_{\omega}(j)$ to the first order in γj are[5]

$$S_{j \to j-1} \simeq a_F (\gamma u)(1 - e^{-u})^2 \left[1 - h(u)\right] j e^{-u\gamma j^2} \left\{1 + \gamma j \left[6 - u - 2(e^u - 1)^{-1}\right]\right\} \tag{26}$$

where $\gamma = B_e/\omega_e$, $h(u) \equiv \gamma\left(\frac{u}{3} + \frac{8}{u}\right) + \delta(e^u-1)^{-1} + 2x_e u(e^u-1)^2$, δ and x_e are tabulated spectroscopic constants, and

$$\frac{1}{\sigma T^4} R^o_{\omega_{j\to j-1}} \simeq 15\left(\frac{u}{\pi}\right)^4 \frac{1}{\omega^*}(e^u-1)^{-1}\left\{1 + \gamma j\left[2u(1-e^{-u})^{-1}-6\right]\right\}. \qquad (27)$$

The expressions for $S_{j-1\to j}$ and $\frac{1}{\sigma T^4} R^o_{\omega_{j-1\to j}}$ are the same as those given above except that j is replaced by -j. Thus

$$W_{0\to 1} \simeq \left(1 - \frac{R^o_{\omega^*,2}}{R^o_{\omega^*,1}}\right)\sum_{j=1}^{\infty} 4R^o_{\omega^*,1}\sqrt{a_{F,1}(\gamma u_1)(1-e^{-u_1})^2\left[1-h(u_1)\right] j e^{-u_1\gamma j^2} b_1 Y_1}$$

$$+ \sum_{j=1}^{\infty} 4R^o_{\omega^*,2}\sqrt{a_{F,2}(\gamma u_2)(1-e^{-u_2})^2\left[1-h(u_2)\right] j e^{-u_2\gamma j^2} b_2(Y_2-Y_1)}$$

$$\left[1 + \eta e^{-(u_2-u_1)\gamma j^2}\right]^{1/2}$$

$$\simeq \left(1 - \frac{R^o_{\omega^*,2}}{R^o_{\omega^*,1}}\right)\sigma_1 T_1^4 \varepsilon^{0\to 1}_{s.r.r.}\left[T_1, Y_1\right] + \sigma T_2^4 \varepsilon^{0\to 1}_{s.r.r.}\left[T_2, Y_2-Y_1\right] \qquad (28)$$

to the first order in γj, where

$$\eta \equiv \left(\frac{Y_1}{Y_2-Y_1}\right)\left(\frac{T_2}{T_1}\right)^{\frac{5}{2}}\left(\frac{1-e^{-u_1}}{1-e^{-u_2}}\right)^2\left(\frac{1-h(u_1)}{1-h(u_2)}\right), \qquad (29)$$

$$\xi \equiv \frac{\int_0^\infty j^{1/2}\, e^{-\frac{u_2}{2}\gamma j^2}\left[1+\eta e^{-(u_1-u_2)\gamma j^2}\right]^{1/2} dj}{\int_0^\infty j^{1/2}\, e^{-\frac{u_2}{2}\gamma j^2}\, dj}, \tag{30}$$

and $\mathcal{E}^{0\to 1}_{s.r.r}[T,X]$ is the emissivity for the $0\to 1$ transition for a gas in the "square root region" at temperature T and optical depth X, namely,[5]

$$\mathcal{E}^{0\to 1}_{s.r.r.}[T,X] = \frac{0.6345}{(\gamma)^{1/4}\omega^*}\left(\frac{a F^b}{u^{3/2}}\right)^{1/2} u^{9/2}\, e^{-u}\, X^{1/2}. \tag{31}$$

Now

$$\int_0^\infty j^{1/2}\, e^{-aj^2}\, dj = \frac{1}{2}\,\Gamma(3/4)\left(\frac{1}{a}\right)^{3/4} \tag{32}$$

where Γ is the gamma function. Since $T_2 \gtrsim 2T_1$, the term $\eta e^{-(u_1-u_2)\gamma j^2}$ decreases rapidly with j over the interval in which the integral in the numerator of the relation for ξ has an appreciable contribution. Therefore ξ may be approximated by

$$\xi \simeq \frac{2}{(\frac{3}{4})\left(\frac{2}{\gamma u_2}\right)^{3/4}}\left\{(1+\eta)^{\frac{1}{2}}\int_0^{j'} j^{\frac{1}{2}}\, e^{-\frac{u_1}{2}\gamma j^2}\, dj + \int_{j'}^\infty j^{\frac{1}{2}}\, e^{-\frac{u_2}{2}\gamma j^2}\, dj\right\} \tag{33}$$

where j' is given by

$$\eta e^{-(u_1-u_2)\, j'^2} = 1$$

or

$$j' = \left[\frac{1}{\gamma(u_1-u_2)}\, \ell n\eta\right]^{\frac{1}{2}} \tag{34}$$

for $\eta > 1$; if $\eta < 1$, $\xi \simeq 1$. Now

$$\int_{j'}^{\infty} j^{\frac{1}{2}} e^{-\frac{u_2}{2}\gamma j^2} dj = \frac{1}{2}\Gamma\left(\frac{3}{4}\right)\left(\frac{2}{\gamma u_2}\right)^{\frac{3}{4}} - \int_{0}^{j'} j^{\frac{1}{2}} e^{-\frac{u_2}{2}\gamma j^2} dj \tag{35}$$

and

$$\int_{0}^{j'} j^{\frac{1}{2}} e^{-bj^2} dj = \frac{1}{2}\left(\frac{1}{b}\right)^{\frac{3}{4}} \int_{0}^{bj'^2} e^{-v} v^{-1/4} dv. \tag{36}$$

But the function I(u, p) is defined by[14]

$$I(u, p) \equiv \frac{1}{\Gamma(p+1)} \int_{0}^{u\sqrt{p+1}} e^{-v} v^{p} dv, \tag{37}$$

so that

$$\xi \simeq 1 + (1+\eta)^{\frac{1}{2}}\left(\frac{T_1}{T_2}\right)^{\frac{3}{4}} I\left(\frac{\ell n\eta}{\sqrt{3}\left(1-\frac{T_1}{T_2}\right)}, -\frac{1}{4}\right) - I\left(\frac{\ell n\eta}{\sqrt{3}\left(\frac{T_2}{T_1}-1\right)}, -\frac{1}{4}\right) \tag{38}$$

for $\eta > 1$. Graphs of $I(u, -\frac{1}{4})$ as a function of u are given in Figures 22 and 23. Since

$$\frac{R^{o}_{\omega^*, 2}}{R^{o}_{\omega^*, 1}} = \frac{e^{u_1}-1}{e^{u_2}-1}, \tag{39}$$

Eqs. (28) and Eq. (31) lead to

$$W_{0-1} \simeq \sigma T_2^{\,4}\, \varepsilon^{0\to 1}_{s.r.r.}\left[T_2, Y_2-Y_1\right]\gamma + \sigma T_1^{\,4}\, \varepsilon^{0\to 1}_{s.r.r.}\left[T_1, Y_1\right] \tag{40}$$

where

$$\tau = \xi - \left(\frac{1-e^{-u_1}}{1-e^{-u_2}} \right) \left(\frac{T_2}{T_1} \right)^{\frac{1}{2}} \left(\frac{Y_1}{Y_2 - Y_1} \right)^{\frac{1}{2}} . \qquad (41)$$

Equations (40) and (41) may be used conveniently for heat transfer calculations for two adjacent isothermal regions. The result is seen to be given explicitly in terms of tabulated engineering emissivities and the parameter τ defined by Eq. (41) with ξ given through Eq. (38).

CHAPTER 4

EMISSIVITY CALCULATIONS FOR A HYDROGEN PLASMA AT TEMPERATURES BELOW 10,000°K

I. INTRODUCTION

Radiant-heat transfer from a hydrogen plasma is of considerable interest in a number of engineering applications, e.g., power plants utilizing hydrogen as a driving fluid. For these applications it is necessary to consider pressures up to several hundred atmospheres and temperatures from several hundred °K to many thousands of °K. Accordingly, the emission for temperatures between 300°K and 10,000°K at high as well as low pressures is considered here (see reference (17) for a calculation of the continuous emission above 10,000°K). Above 10,000°K the emissivity will be essentially unity for high pressures and moderate or large mean beam lengths, [cf. Fig. 41 and reference (17)].

Only equilibrium radiation from a pure hydrogen plasma is considered. However, this work may be adapted easily to the case where other constituents are present.

II. EQUILIBRIUM COMPOSITION

For the calculation of the equilibrium composition it is sufficient to consider the species H_2, H, H^+, e, H^-, and H_2^+. The defining relations for the equilibrium constants are

$$K_1 = \frac{p_H}{\left(p_{H_2}\right)^{\frac{1}{2}}} \quad , \tag{1}$$

$$K_2 = \left(\frac{p_{H^+} \cdot p_e}{p_H}\right)^{\frac{1}{2}} \quad , \tag{2}$$

$$K_3 = \left(\frac{p_H\, p_e}{p_{H^-}}\right)^{\frac{1}{2}} \quad , \tag{3}$$

$$K_4 = \left[\frac{p_{H_2^+} \cdot p_e}{p_{H_2}}\right]^{\frac{1}{2}} \quad ; \tag{4}$$

the definition of total pressure is

$$p_T = p_{H_2} + p_H + p_{H^+} + p_e + p_{H^-} + p_{H_2^+} \tag{5}$$

and the conservation of charge may be expressed through the relation

$$p_e + p_{H^-} = p_{H^+} + p_{H_2^+} \quad . \tag{6}$$

Equations (1) to (6) constitute 6 equations for the 6 partial pressures. For example, these equations may be combined to yield

$$p_T = p_H + \frac{p_H^{\,2}}{K_1^{\,2}} + 2\left[\left(\frac{K_4^{\,2}}{K_1^{\,2}}\, p_H^{\,2} + K_2^{\,2}\, p_H\right)\left(1 + \frac{p_H}{K_3^{\,2}}\right)\right]^{\frac{1}{2}} \tag{7}$$

which may be solved for p_H by a trial-and-error procedure for a given

total pressure p_T provided the equilibrium constants are known. The remaining partial pressures may then be obtained by employing equations (1) to (4) and (6) to give

$$p_{H_2} = \frac{p_H^2}{K_1^2} \quad , \tag{8}$$

$$p_e = \left[\frac{\frac{K_4^2}{K_1^2} p_H^2 + K_2^2 p_H}{1 + \frac{p_H}{K_3^2}} \right]^{\frac{1}{2}} \quad , \tag{9}$$

$$p_{H^-} = \frac{p_H p_e}{K_3^2} \quad , \tag{10}$$

$$p_{H^+} = K_2^2 \frac{p_H}{p_e} \quad , \tag{11}$$

$$p_{H_2^+} = K_4^2 \frac{p_{H_2}}{p_e} \quad . \tag{12}$$

For low ion densities, the equilibrium constants may be determined by application of the dissociation and ionization (Saha) equations but for high ion densities the effective lowering of the ionization potentials by the ions and electrons must be investigated.

A. Equilibrium Composition for Low Ion Densities

Application of the dissociation equation yields K_1 directly,

$$K_1 = \frac{p_H}{(p_{H_2})^{\frac{1}{2}}} = \left[\frac{4\left(\frac{\pi m_H}{h^2} \right)^{3/2} (kT)^{5/2}}{Q_{H_2}} e^{-D/kT} \right]^{\frac{1}{2}} \qquad (13)$$

where the partition function Q_{H_2} is given by [18]

$$Q_{H_2} = \frac{1}{2\sigma (1-e^{-u})} \left[1 + \frac{\sigma}{3} + \frac{8\gamma^2}{\sigma} + \frac{\delta}{e^u - 1} + \frac{2xu}{(e^u-1)^2} \right] . \qquad (14)$$

In equation (13), D = dissociation energy, m_H = mass of the hydrogen atom, h = Planck's constant, k = Boltzmann's constant, and T = temperature. The terms in equation (14) are given by

$$\sigma = \frac{hcB_o}{kT} = \frac{hcB_e}{kT} \left(1 - \frac{1}{2}\delta\right) \quad , \quad \delta = \frac{a_e}{B_e} \quad ,$$

and

$$u = \frac{hc\omega^*}{kT} = \frac{hc}{kT} \left(\omega_e - 2\omega_e x_e\right) \quad , \quad \gamma = \frac{B_e}{\omega_e} \quad , \quad x \simeq x_e \quad ,$$

where B_e, a_e, ω_e, and x_e are tabulated spectroscopic constants [see, for example, reference 19] and c is the velocity of light. The values of K_1 calculated from equation (13) agree within better than one percent with the values tabulated in reference 20 for temperatures below 5000°K.

For low ion densities, application of the ionization equation yields

$$K_2 = \left[\frac{(2\pi m_e)^{3/2} (kT)^{5/2}}{h^3} e^{-I_2/kT} \right]^{\frac{1}{2}}, \quad (15)$$

$$K_3 = \left[\frac{4(2\pi m_e)^{3/2} (kT)^{5/2}}{h^3} e^{-I_3/kT} \right]^{\frac{1}{2}}, \quad (16)$$

and

$$K_4 = \left[2 \frac{Q_{H_2^+}}{Q_{H_2}} \frac{(2\pi m_e)^{3/2} (kT)^{5/2}}{h^3} e^{-I_4/kT} \right]^{\frac{1}{2}}, \quad (17)$$

where m_e is the mass of the electron, I_2, I_3, and I_4 are the ionization potentials for the respective reactions, and $Q_{H_2^+}$ is the partition function for H_2^+, which is given by equation (14) if the spectroscopic constants for H_2^+ are used.

Using the equilibrium constants calculated by use of equations (13) to (17), the equilibrium compositions given in Figures 24 to 26 were calculated for total pressures of 1, 10, and 100 atmos.

B. Lowering of the Ionization Potential at High Ion Densities

In the above relations for low ion densities it was assumed that a bound electron moves in a potential determined only by the core of

the given particle (atom, ion, or molecule), which is true only for an isolated particle. As the ion density is increased, some of the bound electrons become free to pass over to nearby ions because the potential barrier is lowered by the fields of the ions (cf. Fig. 27). Therefore, in addition to the electrons which would be free in a dilute plasma, there exist electrons with a degree of "freedom" that depends on their energy and the surrounding ion density. These electrons wander around in the potential troughs between close ions.

In order to retain the concept of regarding any electron as being either bound or free, various simple models have been proposed for the plasma from which a lowering of the ionization potential due to the ion and electron densities may be calculated. Unsöld[21] considers the model of an electron passing from the particle to a single perturbing ion, situated at a distance equal to the mean distance between the particle and the perturbing ions. For this model, the lowering of the hydrogen atom ionization potential is

$$\Delta I = 7 \times 10^{-7} (N_i)^{\frac{1}{3}} \text{ ev} \qquad (18)$$

where N_i is the number of ions per cm^3. In the treatments by Ecker and Weizel[22] and by Margenau and Lewis[23] the electron is considered to be moving in a Debye field with the lowering of the ionization potential obtained by solving the Schrödinger equation.

In addition to the change in equilibrium composition, emissivity calculations will be directly affected by the ion density since the transition

probabilities depend on the potential curves for an electron. This direct effect is proportional to the change in the square of the matrix element, which should not be much larger than the change in equilibrium composition since the electron and ion densities depend exponentially on the ionization potentials. The simple formula of Unsöld may therefore be used to determine under what conditions the effects of ion fields become important.

Since the electron density is determined primarily by the ionization of the hydrogen atom and because the lower effective core charge of the H^- ion produces a smaller change in ionization potential, the change in the ionization potential of H^- may be neglected (cf. Ref. 17). The change in ionization potential of H_2 is taken to be the same as that of H. In the temperature range of interest, viz., 5000°K to 10,000°K, p_e, p_{H^+}, p_{H^-}, and $p_{H_2^+}$ are all much smaller than p_T and $p_e \simeq p_{H^+}$. Therefore,

$$\frac{p_e}{(p_e)_0} \simeq \frac{p_{H^+}}{(p_{H^+})_0} \simeq \frac{p_{H^-}}{(p_{H^-})_0} \simeq \frac{p_{H_2^+}}{(p_{H_2^+})_0} \simeq \exp\left(\frac{\Delta I}{2kT}\right) \qquad (19)$$

where the subscript zero denotes the partial pressure for no lowering of the ionization potential. Using equation (18) for ΔI, the calculated values of $\exp(\frac{\Delta I}{2kT})$ are given in Table VII and the resulting partial pressures are given by the dashed curves in Figures 24 to 26. Reference to Table VII shows that the ion densities increase by less than 15%

Table VII. The quantity $\exp\left(\frac{\Delta I}{2kT}\right)$ for various total pressures and temperatures.

T, °K	p_T=1 atmos	p_T=10 atmos	p_T=100 atmos
5000	1.01	1.02	1.03
6000	1.03	1.04	1.06
7000	1.05	1.07	1.10
8000	1.07	1.10	1.15
9000	1.09	1.13	1.21
10,000	1.11	1.16	1.27

except near the highest temperatures and pressures considered. However, for mean beam lengths of several centimeters or larger, the emissivity is near unity at these high pressures and temperatures (cf. Fig. 41) and therefore, the emission is not strongly dependent on the partial pressures. Hence serious errors in the emissivity estimates will be introduced only for very small mean beam lengths and at the highest temperatures and pressures considered.

III. EMISSIVITY CONTRIBUTIONS FROM THE HYDROGEN MOLECULE

For a gas at constant temperature and pressure, the total emissivity is given by[5]

$$\mathcal{E} = \frac{1}{\sigma T^4} \int_0^\infty R_\omega^o \, [1 - \exp(-k_\omega \ell)] d\omega \qquad (20)$$

where σ is the Stefan-Boltzmann constant, R_ω^o is the spectral blackbody radiancy at the wavenumber ω, ℓ is the mean beam length, and k_ω is the spectral absorption coefficient (in cm^{-1} for ℓ in cm).

For low temperatures, the blackbody radiancy is large only at small wavenumbers where the vibration-rotation bands and rotational lines occur. The H_2 molecule is homonuclear, however, so that ordinary vibrational and rotational transitions are forbidden. Investigation of other emission processes shows that the so-called "pressure-induced" spectrum will give the dominant contribution to the emissivity at low temperatures.

A. The Pressure-Induced Spectrum

The pressure-induced spectrum consists of vibration-rotation bands and rotational lines resulting from transitions which occur during collisions when dipole moments are induced in the colliding molecules. Since the integrated intensities of the overtone bands are much smaller than those of the fundamental[24], and because the blackbody radiancy at the fundamental band is not appreciably less than any of the values at the overtone bands for the temperatures of interest, only the fundamental vibration-rotation band and the pure rotational lines need to be considered for emissivity calculations.

(1). Fundamental Vibration-Rotation Band

Considerable experimental work has been done on the absorption of the fundamental band at temperatures near 300°K and at lower temperatures[25-27]. The theoretical equations of Van Kranendonk[28-30] may be used to extend the experimental results to higher temperatures.

For his theoretical model, Van Kranendonk considers the induced dipole moment to be made up of two parts: a short-range part produced by the overlapping charge clouds of the molecules producing exchange and deformation dipole moments and a long-range part produced by quadrupolar induction. The short-range overlap moment is angle-independent, decreasing exponentially with the intermolecular separation R, and may be determined by two parameters ξ (or λ) and ρ which measure, respectively, the magnitude and the range of the moment. The values of the parameters ξ (or λ) and ρ can be obtained from measurements of the total absorption coefficient and its temperature dependence. The long-range moment is proportional to R^{-4} with an angular dependence characteristic for quadrupolar induction. The magnitude of the long-range induced moment is determined from the known values of the quadrupole moment and average polarizability of the H_2 molecule and their derivatives with respect to internuclear distance in the molecule.

Using the Lennard-Jones 6-12 intermolecular potential, Van Kranendonk obtains

$$\tilde{\alpha}_1 \equiv \frac{c}{\rho^2} \int_{\substack{\text{fund.} \\ \text{band}}} \frac{k_\omega}{\omega} \, d\omega = \lambda^2 I \tilde{\gamma} + (\mu_1^2 + \mu_2^2) J \tilde{\gamma} \tag{21}$$

where ρ is the density and, for the hydrogen molecule,

$$\lambda = 9.04 \times 10^{-3}$$

$$\mu_1^2 + \mu_2^2 = 7.55 \times 10^{-6}$$

$$\gamma = 5.80 \times 10^{-32} \text{ sec}^{-1}\text{cm}^6 .$$

The functions I and J are given by the integrals

$$I = 4\pi \int_0^\infty e^{-2(x-1)\frac{\sigma}{\rho}} g_o(x) \, dx \tag{22}$$

and

$$J = 12\pi \int_0^\infty x^{-8} g_o(x) \, x^2 \, dx \tag{23}$$

where $x = \frac{R}{\sigma}$ with σ being the molecular diameter in the Lennard-Jones 6-12 intermolecular potential:

$$V(R) = 4 \left[\left(\frac{\sigma}{R}\right)^{12} - \left(\frac{\sigma}{R}\right)^6 \right] . \tag{24}$$

For hydrogen, $\sigma = 2.928$ A and $\rho = 0.145\sigma$. At high temperatures, the quantum effects in the translational motion of the molecules may be neglected and the distribution function $g_o(x)$ is then given by

$$g_o(x) = \exp \left[- \frac{V(x)}{kT} \right] \tag{25}$$

with $V(x)$ obtained from equation (24). Equation (25) may be used to extend the tabulated[28] classical values of the integrals I and J, denoted by $I_{c\ell}$ and $J_{c\ell}$, to temperatures of several thousand °K (see Fig. 28). At temperatures above 600°K, $I_{c\ell}$ and $J_{c\ell}$ are essentially equal to I and J.

Since the mean wave number $\bar{\omega}$, defined by

$$\tilde{a}_1 = \frac{c}{\rho^2} \int \frac{k_\omega}{\omega} d\omega = \frac{c}{\rho^2} \frac{1}{\bar{\omega}} \int k_\omega \, d\omega \quad , \tag{26}$$

is nearly constant for the temperatures considered, the following relation is obtained for the integrated intensity of the fundamental band:

$$a \equiv \int k_\omega d\omega = (37.2\, I + 3.43\, J) \left(\frac{p_{H_2}}{T} \right)^2 \text{ cm}^{-1} \tag{27}$$

for p_{H_2} in atmos and T in °K. In equation (27) the perfect gas relation, which is good to a few percent for pressures up to 100 atmos, has been used, (compare Ref. 31).

From Figure 29 it is evident that the fundamental band may be approximated by the box model,[5] i.e., by an average absorption coefficient acting over an effective band width $\Delta\omega$ which is proportional to the square root of the temperature. Using this model, the emissivity of the fundamental band may be calculated from the relation

$$\mathcal{E} = \int_{\Delta\omega} R^o_\omega \, d\omega \left[1 - \exp\left(- \frac{a}{\Delta\omega}\right) \right] . \tag{28}$$

In the temperature region in which the fundamental band is important, viz., $1000°K \lesssim T \lesssim 4500°K$, the gas is essentially transparent for values of $p_{H_2}^2 \ell$ less than about 10^6 cm atmos^2. For the case of a transparent gas, equation (28) constitutes an approximation only in the averaging of the blackbody function over the band.

(2). Pure Rotation Spectrum

Several papers on the pressure-induced rotational spectrum have been published recently[32-35]. In addition to the rotational spectrum, one should also consider the collision-induced translational spectrum corresponding to transitions with no change in the internal quantum numbers. However, the integrated intensity of the translational spectrum amounts to only about 15% of that for the rotational spectrum and occurs primarily at smaller wavenumbers[35], corresponding to smaller blackbody radiances for $T \gtrsim 300°K$; thus the emissivity contribution of the translational spectrum is small. Accordingly, a pure rotational model is used for extrapolation of the experimental integrated intensity to higher temperatures and for determination of the spectral dependence of the absorption coefficient.

In an analysis similar to that used for the fundamental band, Van Kranendonk and Kiss show that the integrated intensity of the rotational line for the $j \rightarrow j + 2$ transition may be approximated by[34]

$$\tilde{\alpha}_1(j) \equiv \frac{c}{\rho^2} \int_{j\to j+2 \text{ line}} \frac{k_\omega}{\omega}\, d\omega = L(j)\Big[(\lambda_o^2 + 2\lambda_1) I + \bar{\mu}^2 J + \bar{\mu}\left(\lambda_o - \frac{2}{3}\lambda_1\right)K\Big]\, \gamma' + L(j)L'\bar{\mu}'^2 J \gamma' \tag{29}$$

where I and J are again defined by equations (22) and (23); now $\rho = 0.126\sigma$ and K is defined by the relation

$$K = \frac{2\pi}{5} \int_o^\infty x^{-4}\, e^{-(x-1)\sigma/\rho}\, g_o(x)\, x^2\, dx \; ; \tag{30}$$

$L(j)$ and L' are given by

$$L(j) = \frac{3(j+1)(j+2)}{2(2j+3)} \left[p(j) - p(j+2) \right] \tag{31}$$

and

$$L' = \sum_{j=0}^{\infty} \frac{3(j+1)(j+2)}{2(2j+3)}\, p(j) \; , \tag{32}$$

respectively, where $p(j)$ is the normalized Boltzmann factor for the rotational state j. The quantities λ and μ are constants describing the overlap and quadrupolar induced moments, respectively, while $\gamma' = (4\pi^2 e^2 \sigma^5 / 3\hbar)$.

In equation (29) the first term on the right-hand side is the intensity due to the overlap moment alone, the second and fourth terms are produced by the quadrupolar induction effect, while the third term

represents the interference effect between quadrupolar and overlap moments. For pure hydrogen the second term contributes about 90% of the total intensity; hence the approximation

$$\tilde{a}_1(j) \equiv \frac{c}{\rho^2} \int_{j\rightarrow j+2 \text{ line}} \frac{k_\omega}{\omega}\, d\omega = \bar{\mu}^2 \gamma^4 \, L(j)\, J \tag{33}$$

may be used.

Kiss and Welsh have shown in reference (35) that the absorption coefficient $\tilde{k}_\omega \equiv \frac{1}{\omega} k_\omega$ for a rotational line may be represented by a dispersion contour modified on the low-frequency side by a Boltzmann factor and with a half-width proportional to the square root of the temperature. For the temperatures considered here, $T \geq 300°K$, the Boltzmann factor in the line contour is nearly unity over most of the line and the absorption coefficient may, therefore, be represented by

$$k_\omega = \sum_j \frac{a_1(j)}{\pi} \frac{\delta\omega}{(\omega-\omega_j)^2 + \delta^2} \rho_{H_2}^2$$

$$= \sum_j \frac{a_1(j)}{\pi} \frac{\delta\omega}{(\omega-\omega_j)^2 + \delta^2} \left(\frac{273}{T} p_{H_2}\right)^2 \tag{34}$$

with ω_j denoting the wavenumber at the center of the jth line and δ the half-width. For $a_1(j)$ in cm^{-1} amagat^{-2}, p_{H_2} should be expressed in atmos to give k_ω in cm^{-1}. Equation (34) was used to calculate the points shown in Figure 30 which are compared with the experimental

absorption coefficients of Kiss et al.[33] Figures 31 and 32 show the computed absorption coefficients using equation (34) at 600°K and 1000°K, respectively. These absorption coefficients may be used directly in equation (20) in order to estimate the emissivity contribution of the rotational spectrum.

In the above analysis, the plasma was assumed to be pure H_2. This assumption will not introduce a serious error because emission processes involving only atoms and ions (Sections IV to VI) make the dominant contributions to the total emissivity at temperatures high enough for an appreciable fraction of H_2 to be dissociated. It should be noted in this connection that collisions of an H_2 molecule with molecules of other gases, including monatomic gases, produce absorption coefficients that are of the same order of magnitude as the absorption coefficients resulting from collisions with other H_2 molecules[25-27,33]. Therefore H_2- H_2 collisions will contribute most of the pressure-induced emission up to temperatures where atomic and ionic emission processes take over as the dominant contributions to the total emissivity.

B. Electronic Transitions

In this section it is shown that the band and continuum spectra resulting from electronic transitions in the hydrogen molecule for $p_T \geq \frac{1}{10}$ atmos make a much smaller contribution to the total emissivity than the pressure-induced spectrum in the low-temperature range where

the molecular emissivity contributions are important. Reference to the energy level diagram for H_2 in Figure 10 and consideration of selection rules show that there will be one strong transition to the low-lying continuum state, viz., the transition $2s\sigma\,^3\sum_g^+ \longrightarrow 2p\sigma\,^3\sum_u^+$, and two strong transitions to the ground state, viz., the Lyman and Werner band systems corresponding to the transitions $2p\sigma\,^1\sum_u^+ \longrightarrow 1s\sigma\,^1\sum_g^+$ and $2p\pi\,^1\Pi_u \longrightarrow 1s\sigma\,^1\sum_g^+$, respectively. Accordingly, these transitions are considered in detail and the emissivity contribution from all other electronic transitions is shown to be less than that from the Lyman bands.

(1). The Continuum Transition $2s\sigma\,^3\sum_g^+ \longrightarrow 2p\sigma\,^3\sum_u^+$

Using the known potential curves and electronic wave functions, James and Coolidge[36] calculated dipole moments from which they obtained values for the mean lifetimes for transitions from the first four vibrational levels of the upper electronic state. They also present curves of the spectral intensities I_λ, normalized to equal integrated intensities from the different vibrational levels.

Considering equation (20) for the case of a transparent gas, which gives an upper limit for the emissivity,

$$\mathcal{E} \leq \mathcal{E}_L = \int_0^\infty \frac{R_\omega^o}{\sigma T^4} k_\omega \, d\omega \, \ell \qquad (35)$$

where the subscript L stands for the "linear region," i.e., the linear dependence of $\mathcal{E}$ on ℓ for a transparent gas. The blackbody function

$R^{o}_{\omega} / \sigma T^{4}$ is given by

$$\frac{R^{o}_{\omega}}{\sigma T^{4}} = \left(\frac{15}{\pi^{4}} \right) \frac{\left(\frac{hc\omega}{kT} \right)^{4} \frac{1}{\omega}}{e^{\frac{hc\omega}{kT}} - 1} \tag{36}$$

and k_{ω} by[5]

$$k_{\omega} = \left(\frac{1}{8\pi c\omega^{2}} \right) \sum_{v'} \left(N_{v'} e^{\frac{hc\omega}{kT}} \right) A_{\omega} \left(1 - e^{-\frac{hc\omega}{kT}} \right) . \tag{37}$$

In equation (37), $N_{v'}$ is the number of molecules per unit volume in the vibrational state with quantum number v' of the upper electronic level; the sum extends over all of the vibrational states in the upper electronic level; A_{ω} is the transition probability per unit wavenumber, which may be obtained from the calculation of James and Coolidge of the mean lifetimes $\tau_{v'}$ and the relative spectral intensity I_{λ} by use of the following relations:

$$\left(\int_{o}^{\infty} A_{\omega} \, d\omega \right)_{v'} = \frac{1}{\tau_{v'}} \tag{38}$$

and

$$(A_{\omega})_{v'} \propto \frac{1}{\omega^{3}} (I_{\lambda})_{v'} . \tag{39}$$

Since $(N_{T})_{H_2} = \frac{p_{H_2}}{kT}$, equations (35) to (37) yield

$$\mathcal{E}_L = \frac{15}{8\pi^5 hc^2} \left(\frac{hc}{kT}\right)^5 \left[\sum_{v'} \left(\frac{N_{v'}}{N_T}\right) \left(\int_0^\infty \omega A_\omega d\omega \right)_{v'} \right] p_{H_2} \ell \qquad (40)$$

where[18]

$$\frac{N_{v'}}{N_T} = e^{\frac{-hcT_e}{kT}} \frac{\sigma}{\sigma'} (1 - e^{-u}) \frac{e^{-\frac{hc\omega_e'}{2kT}(1 - \frac{1}{2}x_e')}}{e^{-\frac{hc\omega_e}{2kT}(1 - \frac{1}{2}x_e)}} e^{-u'\left[v' - x'v'(v'-1)\right]}$$

$$\times \frac{\left[1 + \frac{\sigma'}{3} + \frac{8\gamma'^2}{\sigma'} + \delta' v'\right]}{\left[1 + \frac{\sigma}{3} + \frac{8\gamma^2}{\sigma} + \frac{\delta}{e^u - 1} + \frac{2x_e u}{(e^u - 1)^2}\right]} . \qquad (41)$$

In equation (41), quantities for the upper state are primed whereas those for the lower state are unprimed; T_e is the energy of the upper electronic state which is listed in reference (19); the quantities u, σ, ω_e, x_e, γ, and δ are the same as those given in Section II-A.

Calculations of $\mathcal{E}_L$ were carried out using equations (40) and (41) with $(A_\omega)_{v'}$ for the first four vibrational levels determined from equations (38) and (39) on the basis of the calculations made by James and Coolidge[36] for $\gamma_{v'}$ and $(I_\lambda)_{v'}$. For the higher vibrational states, the values of $\left(\int_0^\infty \omega A_\omega d\omega \right)_{v'}$ were obtained by extrapolation; these contributed very little to the emissivity at temperatures below about 5000°K. These calculated values of $\frac{\mathcal{E}_L}{p_{H_2} \ell}$ are given in Table VIII.

Table VIII. The emissivity term $\frac{\varepsilon_L}{p_{H_2}\,\ell}$ for the continuum transition $2s\sigma\,{}^3\Sigma_g^+ \longrightarrow 2p\sigma\,{}^3\Sigma_u^+$ for the temperature range between 1000°K and 6000°K.

T, °K	1000	2000	3000	4000	5000
$\frac{\varepsilon_L}{p_{H_2}\,\ell}$	1.3×10^{-51}	2.6×10^{-24}	3.1×10^{-15}	4.2×10^{-11}	2.7×10^{-8}

(2). The Lyman and Werner Bands

Several calculations of the electronic f-numbers for the Lyman and Werner bands have been made. For the emissivity calculation, the discrepancies between the calculated f-numbers are unimportant. The values[37] $f_{Lyman} \equiv f = 0.18$ and $f_{Werner} \equiv f' = 0.42$ have been chosen. Since the lower electronic state involved in the Lyman and Werner transitions is the ground state, the sums of the integrated intensities of all the lines belonging to the Lyman and Werner band systems, a and a' respectively, are[5]

$$a \equiv \sum_{\substack{\text{all Lyman}\\ \text{lines}}} \left(\int k_\omega \, d\omega \right) = \frac{\pi e^2}{m_e c} (N_T)_{H_2} f \qquad (42)$$

$$= \left(\frac{6.50\times10^9}{T} \right) f p_{H_2} = \frac{1.17\times10^9}{T} p_{H_2} \ (cm^{-1})$$

and

$$\alpha' = \left(\frac{6.50 \times 10^9}{T} \right) f' p_{H_2} = \frac{2.73 \times 10^9}{T} p_{H_2} \ (cm^{-1}) \qquad (43)$$

where e denotes the electronic charge. In equations (42) and (43) the number of molecules in the ground state was set equal to the total number of molecules and the induced emission factor $(1 - e^{-\frac{hc\omega}{kT}})$ was set equal to unity since both of these approximations are valid for the temperature range of interest.

To obtain an upper limit for the emissivity, the form for a transparent gas is used, viz.,

$$\varepsilon \leq \varepsilon_L = \int_0^\infty \frac{R^o_\omega}{\sigma T^4} k_\omega \, d\omega \, \ell \, . \qquad (44)$$

To obtain an approximate expression for k_ω, the simple treatment in reference (38) is followed. In this treatment, all of the upper vibrational levels are approximated by the lowest vibrational level of the upper electronic state. The absorption coefficient is then roughly proportional to the number of molecules in the lower vibrational state, i.e.,

$$k_\omega \simeq \alpha \left(\frac{hc}{kT} \right) e^{-\frac{hc}{kT}(\omega_1 - \omega)} \qquad (45)$$

since $e^{-\frac{hc}{kT}(\omega_1 - \omega_2)} \ll 1$ for the specified temperature range; ω_1 and ω_2 are the maximum and minimum wavenumbers for the band system (cf. Fig. 34). Introduction of equations (36) and (45) into equation (44) yields for the Lyman and Werner bands

$$\mathcal{E}_L \simeq \left(\frac{15}{\pi^4}\right)\left(\frac{hc}{kT}\right)\left[a\ell\, e^{-u_1}\int_{u_2}^{u_1} u^3\, du + a'\ell\, e^{-u_1'}\int_{u_2'}^{u_1'} u'^3\, du'\right]$$

$$= \frac{1}{4}\left(\frac{15}{\pi^4}\right)\left(\frac{hc}{kT}\right)\ell\left[a\, e^{-u_1}(u_1^4 - u_2^4) + a' e^{-u_1'}(u_1'^4 - u_2'^4)\right] \qquad (46)$$

since $e^{\frac{hc\omega}{kT}} - 1 \quad e^{\frac{hc\omega}{kT}}$; $u = \frac{hc\omega}{kT}$; the quantities for the Lyman band system are again unprimed while those for the Werner system are primed.

The preceding analysis tends to give excessively large values for the emissivity contribution of the Lyman and Werner bands because the transparent gas relation was used and because replacing the upper levels by the lowest vibrational level in the upper electronic state means that the actual emission occurs at larger wavenumbers than calculated, i.e., the blackbody radiancy has been overestimated.

The emissivity term $\frac{\mathcal{E}_L}{p_{H_2}\ell}$ calculated from equation (46) is given in Table IX. Comparison of Table IX with Table VIII and Figure 37 shows that, although the emissivity contribution of the Lyman and Werner bands is greater than that of the H_2 continuum considered in the previous section, it will generally be small compared to the emissivity contribution of the pressure-induced spectrum for the temperature and pressure range in which H_2 emission is important. For example, the emissivity contribution of the Lyman and Werner bands is small compared to that of the pressure-induced spectrum for $p_{H_2} \gtrsim \frac{1}{10}$ atmos

Table IX. The emissivity term $\frac{\varepsilon_L}{p_{H_2}\,\ell}$ for the Lyman and Werner bands.

T, °K	2000	3000	4000	5000
$\frac{\varepsilon_L}{p_{H_2}\,\ell}$	1.6×10^{-20}	3.6×10^{-12}	3.5×10^{-8}	6.9×10^{-6}

and $T \lesssim 3500°K$; $p_{H_2} \gtrsim 1$ atmos, $T \lesssim 3700°K$; $p_{H_2} \gtrsim 10$ atmos, $T \lesssim 4000°K$; and $p_{H_2} \gtrsim 100$ atmos, $T \lesssim 4300°K$.

(3). The Other Electronic Transitions

In order to obtain an upper limit for the intensity of all the transitions other than the $2s\sigma\,{}^3\Sigma_g^+ \longrightarrow 2p\sigma\,{}^3\Sigma_u^+$ continuum and the Lyman and Werner bands, the intensities of various transitions may be compared with that of the Lyman bands. Since the transparent gas approximation was used in the preceding section, the intensity of the Lyman bands may be represented by the simple relation

$$I_{Lyman} = \left(\frac{\pi^2 e^2 h}{m_e}\right) N_u\, \bar{\omega}^{-3}\, f_{Lyman} \qquad (47)$$

where N_u is the total number of molecules in the upper $(2p\sigma\,{}^1\Sigma_u^+)$ state and $\bar{\omega}$ is a mean wavenumber for the transition. Considering the intensity $I_{kk'}$ of the transition $k' \rightarrow k$,

$$\frac{I_{kk'}}{I_{Lyman}} = \frac{(N_u)_{k'}}{(N_u)_{Lyman}} \left(\frac{\bar{\omega}_{kk'}}{\bar{\omega}_{Lyman}}\right)^3 \frac{f_{kk'}}{f_{Lyman}} \qquad (48)$$

and inserting $f_{Lyman} = 0.18$ and $\bar{\omega}_{Lyman} > \omega_{min} \simeq 54,000\ cm^{-1}$, the following inequality is obtained:

$$\frac{I_{kk'}}{I_{Lyman}} < 10\, e^{-\frac{hc\,\Delta\omega_{k'}}{kT}} \left(\frac{\omega_{kk'}}{54,000}\right)^3 f_{kk'} . \qquad (49)$$

Here $hc\Delta\omega_{k'}$ is the energy difference between the $2p\sigma\,{}^1\Sigma_u^+$ state and the upper state of the $k' \rightarrow k$ transition.

All transitions to the ground state, other than the Lyman and Werner transitions, will be considered for temperatures less than 5000°K. For these transitions, $\omega_{k'} \geq 22,198\ cm^{-1}$ and $\omega_k < 124,429$ so that

$$\frac{\sum_{k'} I_{kk'}}{I_{Lyman}} < 0.21 \times \sum_{k'} f_{kk'} . \qquad (50)$$

But the sum rule for $f_{kk'}$ requires that $\sum_{k'} f_{kk'} = 1 - f_{Lyman} - f_{Werner} = 0.4$. Therefore these transitions contribute less than one tenth of the intensity of the Lyman bands for $T \leq 5000°K$.

This procedure may be applied to the other transitions since the sum rule[19]

$$\sum_{\text{all } k'} f_{kk'} = 1 \qquad (51)$$

exists for a single emission electron.

In equation (51) the f-numbers for transitions from the state k to lower states k' are included as negative quantities so that the sum of f-numbers from states higher than k may be somewhat greater than unity.

The continuum transitions may be included in this analysis if the mean f-number, $\bar{f}$, and mean wavenumber, $\bar{\omega}$, are defined by

$$\int \omega^3 \left(\frac{df_{k',\omega}}{d\omega} \right) d\omega \equiv \bar{\omega}^3_{ck'} \bar{f}_{ck'} \tag{52}$$

for a transition from the bound upper state k'. Applying this relation to all transitions in the continuum state $2p\sigma^3 \sum_u^+$, other than the $2s\sigma^3 \sum_g^+ \rightarrow 2p\sigma^3 \sum_u^+$ transition considered in Section III B-(1), the following inequality is obtained:

$$\frac{\sum_{k'} I_{ck'}}{I_{Lyman}} < \frac{\sum_{k'} \left[(N_u)_{k'} \cdot \bar{\omega}^3_{ck'} \cdot f_{ck'} \right]}{(N_u)_{Lyman} \times (5400)^3 \times 0.18} < .04. \tag{53}$$

Direct application of equation (49) to the individual transitions for which n = 2 in both the upper and lower states shows that these may also be neglected.

Thus all possible transitions between singly excited levels for which the lower state is below $E(cm^{-1}) = 107,770\ cm^{-1}$ have been considered (cf. Fig. 33). Application of equations (49) and (51) shows that

$\frac{\sum_{k'} I_{kk'}}{I_{Lyman}} < 2 \times 10^{-3}$ for any lower state with $E > 107,770\ cm^{-1}$. Since there are fewer than about 50 states with $107,770\ cm^{-1} \leq E \leq 120,000\ cm^{-1}$, it may be concluded that the emission for which these states are the lower state may be neglected. Finally, all lower states with energies between $120,000\ cm^{-1}$ and the ionization energy ($124,429\ cm^{-1}$) will be considered. For any of these states, $\sum_{k'} I_{kk'} / I_{Lyman} < 10^{-6}$. But there will be fewer than 10^5 states in this region whence these transitions may also be neglected.

Since it may be shown that the emission involving doubly excited levels is very weak, it is concluded that the emissivities for the Lyman and Werner bands computed in the preceding section constitute approximate upper limits for all electronic transitions at temperatures below 5000°K.

C. Quadrupole and HD Radiation

In addition to the pressure-induced vibration-rotation spectrum, there will be a quadrupole vibration-rotation spectrum for H_2 and an ordinary dipole vibration-rotation spectrum of the isotopic species HD, where D is the deuterium atom.

(1). Quadrupole Spectrum

Calculations[39-40] show that the integrated intensity of the fundamental quadrupole vibration-rotation band is about 8×10^{-9} times

that of the ordinary fundamental of HCl . The first and second overtone quadrupole bands are about 0.9 and 0.2 times as strong as the fundamental. Accordingly, $\frac{\mathcal{E}_{\text{quadrupole}}}{p_{H_2}\,\ell}$ will have a value of about 5×10^{-11} cm^{-1} atm^{-1} at 1000°K . Since the temperature dependence of the emissivity will be roughly the same as that for the pressure-induced spectrum, it may be concluded that the emissivity contribution of the quadrupole spectrum will be small compared to that of the pressure-induced spectrum for pressures greater than about 1/100 atmos.

(2). HD Vibration-Rotation Spectrum

The calculated ratio of the integrated intensities[39, 41] for the fundamental bands of HD and HCl is about $1:7 \times 10^{5}$. Using an abundance ratio of $3.1 \times 10^{-4}:1$, the integrated intensity of the HD fundamental in natural hydrogen is about 4×10^{-10} times that of the HCl fundamental. Therefore the HD emissivity contribution may be neglected.

IV. EMISSIVITY CONTRIBUTIONS FROM THE H^- ION

Considerable work has been done on the calculation of the absorption coefficient for the H^- ion for use in astrophysical applications.[42-45] The two processes contributing to the absorption coefficient are the bound-free (photodetachment) transitions represented by the reaction

$$H^- + h\nu \longrightarrow H + e^-$$

and the free-free transitions represented by

$$H + e^- + h\nu \longrightarrow H + e^- ,$$

where e^- represents an electron and $h\nu$ is the absorbed photon.

A. Bound-Free Transitions

Chandrasekhar[42-44] has evaluated the absorption coefficient for bound-free transitions directly by evaluating the matrix element. In the latest calculations[43, 44], the 20-parameter wave function of Hart and Herzberg[46] was used for the bound state. The wave function for the continuous state was first approximated by a plane wave representation of the outgoing electron, then more accurately by the wave function of an electron moving in the static field of a hydrogen atom (Hartree approximation). The accuracy of the calculation was improved by use of the dipole-velocity form of the matrix element[44].

Direct measurements of the bound-free cross section by Branscomb and Fite[47] agree reasonably well with Chandrasekhar's calculations. In a note added to reference 42, Chandrasekhar uses the calculations of Bransden et al.[48] for p-waves in the field of a neutral hydrogen atom, which allow for exchange and polarization. This sample calculation indicates that his earlier estimates of the bound-free absorption coefficients should be decreased by about 20%.

B. Free-Free Transitions

In the earliest evaluations of the free-free absorption coefficient the Born approximation was used to describe the motion of an electron

in the field of a hydrogen atom. However, Chandrasekhar[45] showed that the electron velocities in the temperature range considered are too low for a valid application of the Born approximation. For this reason, he calculated the free-free absorption coefficients using the Hartree approximation described above[45].

A calculation of the free-free absorption coefficient using the computations of Bransden et al.[48] is being performed by T. Ohmura[49]. Preliminary estimates for the absorption coefficient are 40 to 50% smaller than those of Chandrasekhar and Breen[45].

The values of the absorption coefficient calculated by Chandrasekhar et al. are used in the present emissivity calculation. Since the bound-free contribution to the total emissivity is appreciably greater than that of the free-free transitions, the results should be accurate to better than about 25%.

V. EMISSIVITY CONTRIBUTIONS FROM THE H_2^+ ION

The absorption coefficient of H_2^+ arises from the bound-free transition

$$H_2^+ + h\nu \rightarrow H + H^+$$

and from the free-free transition

$$H + H^+ + h\nu \rightarrow H + H^+ .$$

By first evaluating the exact two-center wave functions[50] and the dipole moments[51], Bates calculated the H_2^+ absorption coefficient[52].

Using the absorption coefficients given by Bates, it is found that the H_2^+ contribution to the total emissivity is less than about 5% of the H^- contribution for temperatures less than 10,000°K.

VI. EMISSIVITY CONTRIBUTIONS FROM THE HYDROGEN ATOM

In addition to the line spectrum of the hydrogen atom, there exists a continuum spectrum consisting of the bound-free transitions

$$H + h\nu \rightarrow H^+ + e^-$$

and the free-free transitions (Bremsstrahlung)

$$H^+ + e^- + h\nu \rightarrow H^+ + e^- .$$

A. The Continuum Spectrum

An expression for the free-free absorption coefficient was first derived by Kramers[53] by utilizing the correspondence principle. Subsequent derivations[54-56] have shown that the quantum-mechanical expression may be written as Kramer's expression times the quantity g_{ff}, called the Gaunt factor, which is of the order of unity, viz.,

$$\frac{k_\omega^{ff}}{p_H} = \frac{32}{3\sqrt{3}} \frac{\pi^2 e^6 R_y}{m_H h^3 c^3 kT} \frac{e^{-x_1}}{\omega^3} \left(\frac{1}{2x_1}\right)\left(1 - e^{-\frac{hc\omega}{kT}}\right) \cdot g_{ff}(\omega) \quad (54)$$

where R_y is the Rydberg constant and $x_1 = \frac{hcR_y}{kT}$. Extrapolation of

the results given in reference (57) for $T > 11,605°K$ shows that, for the temperatures of interest in our calculation, $g_{ff}(\omega)$ may be replaced by the mean value $\bar{g}_{ff} \simeq 1.24$.

The bound-free absorption coefficient may similarly be written in terms of a simple expression, obtainable from the equation derived from the correspondence principle but multiplied by the Gaunt factor $g_{bf,n}$ [58], viz.,

$$\frac{k_{\omega}^{bf}}{p_H} = \frac{32}{3\sqrt{3}} \frac{\pi^2 e^6 R_y}{m_H h^3 c^3 kT} \frac{e^{-x_1}}{\omega^3} \left(\sum_{\omega_n < \omega}^{\infty} \frac{e^{x_n}}{n^3} g_{bf,n}(\omega) \right) (1 - e^{-\frac{hc\omega}{kT}}) \quad (55)$$

where $x_n = \frac{hcR_y}{kTn^2}$ and $\omega_n = R_y/n^2$. The Gaunt factors $g_{bf,n}(\omega)$ vary from about 0.90 to 1.10 [7]; hence the approximation $g_{bf,n}(\omega) \simeq 1.00$ may be used.

Using the mean values for the Gaunt factors, the total continuum absorption coefficient for the hydrogen atom becomes

$$\frac{k_{c,\omega}}{p_H} = \frac{32}{3\sqrt{3}} \frac{\pi^2 e^6 R_y}{m_H h^3 c^3 kT} \frac{e^{-x_1}}{\omega^3} \left(\sum_{\omega_n < \omega}^{\infty} \frac{e^{x_n}}{n^3} + \frac{0.62}{x_1} \right) (1 - e^{-\frac{hc\omega}{kT}}). \quad (56)$$

Equation (56) was used directly for the calculation of the continuum absorption coefficient, since the temperatures considered here are not high enough to validate the use of Unsöld's [59] approximation

$$\sum_{n=5}^{\infty} \frac{1}{n^3} \; e^{x_n} \qquad \frac{e^{x_5} - 1}{2x_1} \quad .$$

B. The Line Spectrum

The f-number for an atomic line corresponding to a transition between states with principal quantum numbers n and n' is[60]

$$f_{n\ n'} = \frac{64}{3\sqrt{3}} \frac{1}{\pi 2 n^2} \left(\frac{1}{\frac{1}{n^2} - \frac{1}{n'^2}} \right) \left| \frac{1}{n^3 (n')^3} \right| g \quad . \qquad (57)$$

Except for the Gaunt g-factor, equation (57) may be obtained from the correspondence principle. The f-number values are tabulated in reference (59). For a transparent gas it is sufficient to know only the f-numbers in order to calculate the emissivity contributions of the atomic lines. On the other hand, if there is appreciable self-absorption, it is necessary to know the line contours in order to calculate the line emissivities. Accordingly, except for the transparent gas case, it is necessary to consider collision-broadened and Stark-broadened line contours.

(1). Transparent Gases

For a transparent gas, the total emissivity of a single line is

$$\mathcal{E}_L = \frac{R^o_{\omega_o}}{\sigma T^4} \; S \; p_H \ell \qquad (58)$$

where $R^o_{\omega_o}$ is the blackbody radiancy at the line center and

$S = \frac{1}{p_H} \int k_\omega \, d\omega$ is the line integrated intensity. Here S may be evaluated from the relation[5]

$$S_{nn'} = \frac{\pi e^2}{m_e c^2} f_{n \to n'} n^2 \left(\frac{N_H}{p_H}\right) e^{-(x_1 - x_n)} \left(1 - e^{-\frac{hc\omega_{nn'}}{kT}}\right) \qquad (59)$$

where N_H is the number of hydrogen atoms per unit volume.

(2). Collision-Broadened Lines

For the temperatures considered here, practically all of the hydrogen atoms are in the ground (1s) state. Between these 1s atoms and an atom in an np state there will exist a resonance interaction energy which may be approximated by[61]

$$(\Delta E)_{np,1s} \quad \pm \left(\frac{he^2}{8\pi^2 m_e c} \frac{f_{np,1s}}{\omega_{1,n}} \right) \frac{1}{r^3} \qquad (60)$$

where r is the distance between the two atoms. This resonance interaction will account for the collision broadening since the van der Waals interaction energies are much lower, being proportional to r^{-6}. Using the statistical theory of line broadening, Margenau and Watson[61] show that, in the wings of the spectral line for a 1s-2p transition, equation (60) leads to

$$\frac{k_\omega}{p_H} \simeq \frac{S}{\pi} \frac{b_c}{(\Delta\omega)^2} \qquad (61)$$

where the half-width b_c is

$$b_c = \frac{Ne^2}{12m_e c^2} \left(\frac{f_{2p,1s}}{\omega_{1,2}} \right) \tag{62}$$

and $\Delta\omega = (\omega - \omega_o)$ with ω_o being the wavenumber at the line center. This result agrees well with

$$b_c = \frac{Ne^2}{4\pi m_e c^2} \left(\frac{f_{2p,1s}}{\omega_{1,2}} \right) \tag{63}$$

obtained by Weisskopf[62] using a modification of the Lorentz formula.

In reference (63), equation (63) was incorrectly used for the Balmer and Paschen lines. Recalling that the resonance interaction occurs only when the emitting atom is in an np state, it is possible to add the transitions contributing to a single line and to obtain for the Balmer line $(n \rightarrow 2)$

$$b_c = \left(\frac{Ne^2}{12m_e c^2} \right) \frac{1}{4} \left[f_{np,2s} \left(\frac{f_{np,1s}}{\omega_{1,n}} \right) + 3 \left(f_{ns,2p} + f_{nd,2p} \right) \left(\frac{f_{2p,1s}}{\omega_{1,2}} \right) \right] \frac{1}{f_{n,2}} \tag{64}$$

where

$$f_{n,2} = \frac{1}{4} \left[f_{np,2s} + 3 \left(f_{ns,2p} + f_{nd,2p} \right) \right] . \tag{65}$$

In equation (64) the broadening for a given transition is multiplied by the fraction of the total line intensity contributed by the transition. Similarly,

for the Paschen line $(n \rightarrow 3)$,

$$b_c = \left(\frac{Ne^2}{12m_e c^2}\right) \frac{1}{9}\left[\left(f_{np,3s} + 5f_{np,3d}\right)\left(\frac{f_{np,1s}}{\omega_{1,n}}\right) + 3\left(f_{ns,3p} + f_{nd,3p}\right)\left(\frac{f_{3p,1s}}{\omega_{1,3}}\right)\right] \frac{1}{f_{n,3}} \tag{66}$$

where

$$f_{n,3} = \frac{1}{9}\left[f_{np,3s} + 3\left(f_{ns,3p} + f_{nd,3p}\right) + 5\left(f_{np,3d} + f_{nf,3d}\right)\right] . \tag{67}$$

For the Lyman lines we find

$$b_c = \frac{Ne^2}{12m_e c^2}\left(\frac{f_{np,1s}}{\omega_{1,n}}\right) \tag{68}$$

However, as will be discussed in Section 4, only the very distant parts of the low wavenumber wings of the Lyman lines are of interest here. (Equation (60) is not applicable in this region.)

The values of $b_c \cdot \frac{12m_e c^2}{Ne^2}$, using equation (62), for the Balmer and Paschen lines are given in Table X.

Insertion of the absorption coefficient given by equation (61) into the general expression for the total emissivity, equation (20), yields

$$\mathcal{E} = \frac{R^o_{\omega_o}}{\sigma T^4} 2\sqrt{S\, b_c\, p_H\, \ell} . \tag{69}$$

Table X. The half-width factor $b_c \cdot \frac{12m_e c^2}{Ne^2}$ for the Balmer and Paschen lines computed from equations (62) and (64) to (67).

n	Balmer lines	Paschen lines
3	4.36×10^{-6}	
4	4.05×10^{-6}	1.74×10^{-6}
5	3.89×10^{-6}	3.73×10^{-7}
6	4.05×10^{-6}	1.48×10^{-7}
7	3.85×10^{-6}	7.45×10^{-8}
8	3.89×10^{-6}	4.44×10^{-8}

Since equation (61) describes only the wings of the spectral line, equation (69) applies only when $p_H \ell$ is large enough to lead to blackened line centers. Specifically[5], equation (58) applies for $\frac{Sp_H \ell}{2\pi b_c} \lesssim \frac{2}{\pi}$ and equation (69) for $\frac{Sp_H \ell}{2\pi b_c} \gtrsim \frac{2}{\pi}$, with the actual emissivity never exceeding either expression.

(3). Stark-Broadened Lines

The absorption coefficient in the wings of a line broadened by the Stark effect is[5]

$$\frac{k_\omega}{p_H p_e} = \frac{321\, c_\ell \omega_o^5}{kT^2} n^2 \left(\exp\left[-\frac{R_y hc}{kT} \left(1 - \frac{1}{n^2}\right)\right]\right) \cdot \frac{1}{(\omega - \omega_o)^{5/2}} \qquad (70)$$

where ω_o is the wavenumber at the line center, n is the principal

quantum number of the lower state, and c_ℓ is a constant, which is tabulated in references (5) and (60) .

Using equation (70) to evaluate the total emissivity for the line, one obtains

$$\mathcal{E} = \frac{R^o_{\omega_o}}{\sigma T^4} \, 2\,\Gamma(3/5) \left[\frac{321\, c_\ell\, \omega_o^{\,5}}{kT^2} \; n^2 \left(\exp\left[- \frac{R_y hc}{kT} \left(1 - \frac{1}{n^2}\right)\right]\right) p_H p_{e\ell} \right]^{\frac{2}{5}}$$

$$\equiv \frac{R^o_{\omega_o}}{\sigma T^4} \, A \, (p_H p_{e\ell})^{\frac{2}{5}} \qquad (71)$$

where Γ denotes the Gamma function. For pure Stark broadening, equation (70) is applicable for $\dfrac{p_{H^\ell}}{(p_e)^{2/3}} \gtrsim \left(\dfrac{A}{S}\right)^{5/3}$ while the transparent gas relation, equation (58), is applicable for $\dfrac{p_{H^\ell}}{(p_e)^{2/3}} \lesssim \left(\dfrac{A}{S}\right)^{5/3}$, with the actual emissivity never exceeding either expression.

If desired, the more elaborate Stark broadening theories may be used, rather than the simple Holtsmark formula given in equation (70).

(4). The Lyman α Line

If the simple collision and Stark broadening theories discussed above are used to compute the profile of the Lyman α line, the absorption coefficient far out in the wings will be appreciable because of the large intensity of the Lyman α line. Even though the center of the Lyman α line is at 82,258 cm^{-1}, the absorption coefficient of the low wavenumber wing computed from the simple broadening theories, is

large enough at low wavenumbers, where the blackbody radiancy is large, to account for the major portion of the total emitted intensity of the hydrogen plasma from approximately 4000°K to 8000°K. This is not actually the case, however, because the simple relations for collision and Stark broadening are not applicable very far from the line centers.

First of all, the above Stark broadening theory is not applicable because large displacements require such large electric fields at the atom that the atom is quickly ionized. Therefore, the line wings become quenched. This quenching has been observed and calculated for some of the Balmer lines[64, 65]. For the Lyman α line, one would not expect much intensity farther than about 15,000 cm^{-1} from the line center. Accordingly, the wings of the Stark-broadened Lyman lines will not give an important contribution to the emissivity.

The statistical theory of line broadening, which is applicable far out in the line wings[23], may be used to estimate the collision-broadened profile of the Lyman α line. The r^{-3} resonance interaction considered in Section 2 above is valid only for interatomic distances greater than about 6A, corresponding to absorption less than about 2000 cm^{-1} from the line center. Therefore, the appropriate potentials for the small interatomic distances must be used. Reference to Figure 35 shows that two normal atoms approaching along the $2p\sigma\,^3\Sigma_u^+$ potential curve may undergo a transition to the $2s\sigma\,^3\Sigma_g^+$ curve by the absorption

of a low energy photon, resulting in an absorption coefficient at low wavenumbers. As is illustrated in Figure 35, the absorbed photon has an energy equal to the energy difference between the potential curves (this is the physical principle involved in the statistical theory).

To obtain an approximate upper limit for the absorption coefficient, we use for the f-number the value calculated for an isolated atom and we assume that the transitions between the $2s\sigma\,^3\Sigma_g^+$ and $2p\sigma\,^3\Sigma_u^+$ states account for half of the total integrated intensity. Therefore, use of the statistical theory yields

$$\frac{k_\omega}{p_H} \simeq 2\pi N r^2 S \left(\frac{dr}{d\omega}\right) e^{-\frac{hc\omega_\ell}{kT}} \qquad (72)$$

where the exponential term arises from the contribution of the repulsive potential to the probability that the two atoms are a distance r apart; $\omega_\ell(r)$ is the energy of the repulsive potential (cf. Fig. 35). The energy difference $hc\omega$ between the potential curves is determined as a function of r from Figure 35.

In Table XI, the absorption coefficients $\frac{k_\omega}{p_H}_2$ for the Lyman α line, calculated from equation (72), is given at 4000°K and 8000°K. Comparison of these values with absorption coefficients for the H^- ion indicates that the outer part of the low wavenumber wing of the Lyman α line will not make an important contribution to the emissivity.

Table XI. The absorption coefficient $\frac{k_\omega}{p_H^2}$ for the Lyman α line calculated from equation (72).

$\omega(cm^{-1})$	$\left(k_\omega/p_H^2,\ cm^{-1}atm^{-2}\right)$	
	T = 4000°K	T = 8000°K
12,840	2.9×10^{-13}	1.1×10^{-9}
19,090	2.7×10^{-11}	1.1×10^{-8}
25,760	8.5×10^{-10}	7.3×10^{-8}
31,280	8.9×10^{-9}	2.6×10^{-7}
35,240	4.0×10^{-8}	5.9×10^{-7}
38,730	1.4×10^{-7}	1.2×10^{-6}
44,490	1.2×10^{-6}	4.2×10^{-6}
49,580	4.6×10^{-6}	9.5×10^{-6}
53,970	1.5×10^{-5}	1.9×10^{-5}
57,920	3.9×10^{-5}	3.6×10^{-5}
61,560	9.0×10^{-5}	6.1×10^{-5}
64,710	1.7×10^{-4}	9.3×10^{-5}

The quantity $\frac{1}{p_H^2 \ell} \frac{d\mathcal{E}_L}{d\omega} = \frac{R_\omega^o}{\sigma T^4} \frac{k_\omega}{p_H^2}$, which is proportional to the emitted intensity of a transparent gas, is given in Figure 36 for T = 8000°K. Curve (a) of Figure 36 was computed by using equation (72), curve (b) by using equation (72) with the repulsive (exponential) term omitted, and curve (c) by using equations (61) and (62), which do not include the repulsive term. It is evident from Figure 36 that it is the repulsive term which reduces the absorption coefficient in the outer part of the low wavenumber wing to such an extent that it becomes unimportant in our emissivity calculations.

The above is only a preliminary analysis, but the conclusions should be correct. A similar analysis[67] for the Na doublet shows that the calculated decrease in wing intensity due to the repulsive term is in good agreement with the measured contour.

VII. CALCULATION OF THE TOTAL EMISSIVITY

The results of the preceding sections will now be used to calculate the total emissivity of a hydrogen plasma.

A. Summation of the Emissivity Contributions

To sum emissivity contributions one must add the absorption coefficients for the various processes and use this sum as the total absorption coefficient k_ω in equation (20). For a transparent gas this will be equivalent to adding directly the emissivities of the various emission processes.

At high temperatures, when both continuum and line radiation may be important, it is convenient to utilize the total line emissivities directly since these can be easily calculated from equations (58), (69), and (71). For this purpose, equation (20) can be written in the form

$$\mathcal{E} = \int \frac{R_\omega^o}{\sigma T^4} \left(1 - \exp\left[-\left(k_\omega^c + \sum_i k_\omega^{\text{line } i}\right) \ell\right]\right) d\omega$$

$$= \int \frac{R_\omega^o}{\sigma T^4} \left(1 - \exp\left[- k_\omega^c \ell\right]\right) d\omega \qquad (73)$$

$$+ \int \frac{R_\omega^o}{\sigma T^4} \exp\left[- k_\omega^c \ell\right] \left(1 - \exp\left[- \sum_i k_\omega^{\text{line } i} \ell\right]\right) d\omega$$

where k_ω^c is the spectral absorption coefficient for the continuum spectrum while $k_\omega^{\text{line } i}$ is that for the i^{th} line. Since the continuum absorption coefficient is essentially constant over a line width, and since the important lines do not overlap, equation (73) may be written as

$$\mathcal{E} = \mathcal{E}_c + \sum_i \left(\exp\left[- k_{\omega_i}^c \ell\right]\right) \mathcal{E}^{\text{line } i} \qquad (74)$$

where ω_i is the wavenumber at the center of the i^{th} line. Thus the total emissivity is equal to the continuum emissivity $\mathcal{E}_c$ plus the line emissivities $\mathcal{E}^{\text{line } i}$ decreased by the transmissivity for continuum absorption at the line centers.

B. Representative Calculations

First the component emissivities for a transparent gas, applicable over large ranges of T, p_T, and ℓ, will be considered. The emissivity for p_T = 100 atmos and ℓ = 30 cm has also been calculated.

(1). Transparent Gases

For a transparent gas, the emissivity of a component is given simply by a temperature dependent function times the mean beam length and the particular partial pressure(s) representative of the transitions involved.

The transparent gas emissivity term $\dfrac{(\varepsilon_{H_2})_L}{p_{H_2}^2 \ell}$ for the H_2 molecule is given in Figure 37. This figure supplies the actual H_2 emissivity for values of $p_{H_2}^2 \ell$ for which there is little self-absorption. Since the absorption coefficient for H_2 varies rather gradually and covers a large portion of the blackbody curve, there will be little self-absorption for $(\varepsilon_{H_2})_L \lesssim 10^{-2}$. Thus Figure 37 gives the actual H_2 emissivity down to 300°K for $p_{H_2}^2 \ell \lesssim 10^4$ cm atmos^2, down to 1000°K for $p_{H_2}^2 \ell \lesssim 10^5$ cm atmos^2, etc.

Similarly, for the H^- and H_2^+ ions, Figure 38 presents the emissivity term $\dfrac{(\varepsilon_{H^-} + \varepsilon_{H_2^+})}{p_e p_H \ell} L$ in the temperature range 3000°K to 10,000°K. In this temperature range $(\varepsilon_{H^-})_L$ is more than ten times greater than $(\varepsilon_{H_2^+})_L$. Since the sum of the absorption coefficients

for H^- and H_2^+ varies gradually over a large wavenumber range, the criterion for the gas to be transparent to a mixture of H^- and H_2^+ is

$$(\varepsilon_{H^-} + \varepsilon_{H_2^+})_L \lesssim 10^{-2} \quad . \tag{75}$$

For example, it may be observed from Figure 38 that the sum of the H^- and H_2^+ contributions to the emissivity at 5000°K is $0.144\ p_e p_H \ell$ if $p_e p_H \ell \lesssim 0.1$.

Using equation (56) for the continuum absorption coefficient of the H atom, the expression for the emissivity of a transparent gas, equation (35), may be integrated directly to yield

$$\frac{(\varepsilon_{H,c})_L}{p_H \ell} = \frac{160}{\pi^4\sqrt{3}} \frac{\pi^2 e^6 R_y}{m_H (kT)^4} e^{-x_1} \left(\sum_{n=1}^{\infty} \frac{1}{n^3} + \frac{0.62}{x_1} \right) \tag{76}$$

and

$$\frac{(\varepsilon_{H,c})'_L}{p_H \ell} = \frac{160}{\pi^4\sqrt{3}} \frac{\pi^2 e^6 R_y}{m_H (kT)^4} e^{-x_1} \left(\sum_{n=2}^{\infty} \frac{1}{n^3} + \frac{0.62}{x_1} \right) \quad . \tag{77}$$

where the prime denotes the emissivity exclusive of the Lyman continuum. The value of the sum $\sum_{n=1}^{\infty} \frac{1}{n^3}$ is 1.20206. These emissivity terms are given in Figure 39 along with the maximum absorption coefficient $\frac{k_{B,\omega}}{p_H}$ in the Balmer continuum. When $p_H \ell \lesssim \frac{10^{-2}}{k_{B,\omega}/p_H}$, equation (77) may be used to give the actual emissivity of the H atom continuum, exclusive of the Lyman continuum. For the conditions of interest, the Lyman continuum region is generally far from transparent. In this

connection the maximum emissivity contribution possible from the Lyman continuum, viz.,

$$\mathcal{E}_{max}^{Lyman} = \frac{1}{\sigma T^4} \int_{R_y = 109,678\ cm^{-1}}^{\infty} R_\omega^o \, d\omega \quad , \tag{78}$$

is also given in Figure 39. Considering $T = 6000°K$, for example, it is evident from Figure 39 that equation (77) will give the actual emissivity of the H atom continuum for $10 \lesssim p_H \ell \lesssim 10^6$ cm atmos.

Figure 40 gives the transparent gas emissivity terms for the Balmer and Paschen lines computed from equations (58) and (59). A given line will be approximately transparent if the emissivity computed from equation (58) is less than one or both of the values computed from equations (69) and (71), i.e., when one or both of the inequalities $\frac{S p_H \ell}{2\pi b_c} \lesssim \frac{2}{\pi}$ and $\frac{p_H \ell}{(p_e)^{2/3}} \lesssim \left(\frac{A}{S}\right)^{5/3}$ hold. The lines will be primarily collision-broadened at the higher pressures and Stark-broadened at the lower pressures. The Lyman α line will be far from transparent at most optical depths of interest. The emissivity contribution of the Lyman α line can be estimated from the analysis of Section VI-B-(4), and proves to be negligibly small except for very small optical depths and high temperatures. The emissivity contributions of the Brackett series, Pfund series, etc., are negligibly small.

(2). Calculation for a Total Pressure of 100 atmos and a Mean Beam Length of 30 cm

In Figure 41 the results are shown of an emissivity calculation for p_T = 100 atmos and ℓ = 30 cm for T = 300°K to 10,000°K. At temperatures below about 1200°K, the pressure-induced rotational spectrum of H_2 provides the dominant emissivity contribution. The spectral radiancies at 300°K and 600°K are compared with the black-body radiancies in Figures 42 and 43. The dominate emissivity contribution is provided by the pressure-induced fundamental vibration-rotation band between 1200°K and 4400°K, and by the continuum radiation from 4400°K up to 10,000°K. The continuum radiation is primarily from the H^- bound-free and free-free transitions with the bound-free transitions of the H atom starting to become important at the higher temperatures. In Figures 44 to 48 we show the spectral radiancy of the continuum spectrum. In Figures 44 to 46 the division of the H^- continuum radiation as the sum of a contribution from free-free transitions and from bound-free transitions is evident. In Figures 46 to 48 the Balmer bound-free continuum is observable. The emissivities of the atomic lines, decreased by the transmissivity of the continuum [cf. Eq. (74)], amounted to less than a few percent of the continuum emissivity. At p_T = 100 atmos and T < 10,000°K, collision broadening is more important than Stark broadening.

Since the absorption coefficient for the H^- ion is proportional to $p_e p_H$ and that for the H atom is proportional to p_H, the H atom spectrum will become more important at lower total pressures.

REFERENCES

1. S. S. Penner and A. Thomson, J. Appl. Phys. 28, 614-623 (1957).

2. A. Thomson, Ph. D. Thesis, California Institute of Technology, Pasadena, June 1958.

3. A. Thomson, W. J. Hooker, and S. S. Penner, J. Appl. Phys. 30, 124 (1959).

4. D. Olfe and S. S. Penner, J. Appl. Phys. 30, 125 (1959).

5. S. S. Penner, Quantitative Molecular Spectroscopy and Gas Emissivities, Addison-Wesley Publishing Co., Reading (Mass.), 1959.

6. R. M. Goody, Quart. J. Roy. Met. Soc. 78, 165-169 (1952).

7. H. Mayer, Los Alamos Scientific Laboratory Report LA-647 (1947).

8. H. C. Hottel and H. G. Mangelsdorf, Trans. Am. Inst. Chem. Eng. 31, 517-549 (1935).

9. H. C. Hottel and R. B. Egbert, Trans. Am. Inst. Chem. Eng. 38, 531-568 (1942).

10. U. P. Oppenheim, J. Appl. Phys. 30, 803-807 (1959).

11. D. Weber and S. S. Penner, J. Chem. Phys. 21, 1503-1506 (1953).

12. R. Friedman, J. B. Levy, and K. E. Rumbel, "The Mechanism of Deflagration of Pure Ammonium Perchlorate," Report AFOSR-TN 59-173, AD No. 211-313, Atlantic Research Corporation, Alexandria, Virginia, February 1959.

13. W. H. MacAdams, Heat Transmission, 3rd Edition, Chapter 4 by H. C. Hottel, McGraw-Hill Book Co., New York, 1954.

14. Karl Pearson, Tables of the Incomplete Γ-Function, Cambridge University Press, 1922.

15. J. A. L. Thomson and S. S. Penner, Technical Report No. 30, Contract Nonr-220(03), NR 015-401, California Institute of Technology, Pasadena, California, February 1959.

16. J. A. L. Thomson, Convair, San Diego (personal communication).

17. F. Mastrup, J. Opt. Soc. Am. 50, 32-35 (1960).

18. J. E. Mayer and M. G. Mayer, Statistical Mechanics, John Wiley and Sons, New York, 1940.

19. G. Herzberg, Molecular Spectra and Molecular Structure I. Spectra of Diatomic Molecules, D. Van Nostrand Co., New York, 1953.

20. S. S. Penner, Chemistry Problems in Jet Propulsion, p. 127, Pergamon Press, New York, 1957.

21. A. Unsöld, Z. Astrophys. 24, 355-362 (1948).

22. G. Ecker and W. Weizel, Ann. Physik 17, 126-140 (1956).

23. H. Margenau and M. Lewis, Revs. Mod. Phys. 31, 569-615 (1959).

24. M. Mizushima, Phys. Rev. 77, 150-151 (1950).

25. W. F. J. Hare and H. L. Welsh, Can. J. Phys. 36, 88-103 (1958).

26. H. P. Gush, A. Nanassy, and H. L. Welsh, Can. J. Phys. 35, 712-719 (1957).

27. D. A. Chisholm and H. L. Welsh, Can. J. Phys. 32, 291-312 (1954).

28. J. Van Kranendonk, Physica 24, 347-362 (1958).

29. J. Van Kranendonk, Physica 23, 825-837 (1957).

30. J. Van Kranendonk and R. B. Bird, Physica 17, 953-967, 968-975 (1951).

31. NBS Circular 564, Tables of Thermal Properties of Gases, 1 November 1955.

32. J. P. Colpa and J. A. A. Ketelaar, Molec. Phys. 1, 14-22, 343-357 (1958).

33. Z. J. Kiss, H. P. Gush, and H. L. Welsh, Can. J. Phys. 37, 362-376 (1959).

34. J. Van Kranendonk and Z. J. Kiss, Can. J. Phys. 37, 1187-1198 (1959).

35. Z. J. Kiss and H. L. Welsh, Can. J. Phys. 37, 1249-1259 (1959).

36. H. M. James and A. S. Coolidge, Phys. Rev. 55, 184-190 (1939).

37. Harrison Shull, J. Chem. Phys. 20, 18-21 (1952).

38. B. Kivel, H. Mayer, and H. Bethe, Annals of Physics 2, 57-80 (1957).

39. H. M. James and A. S. Coolidge, Ap. J. 87, 438-459 (1938).

40. G. Herzberg, Ap. J. 87, 428-437 (1938).

41. G. C. Wick, Accad. Lincei Atti, 21, 708-714 (1935).

42. S. Chandrasekhar and D. D. Elbert, Ap. J. 128, 633-635 (1958).

43. S. Chandrasekhar, Ap. J. 128, 114-123 (1958).

44. S. Chandrasekhar, Ap. J. 102, 395-401 (1945).

45. S. Chandrasekhar and F. H. Breen, Ap. J. 104, 430-445 (1946).

46. J. F. Hart and G. Herzberg, Phys. Rev. 106, 79-82 (1957).

47. L. M. Branscomb and W. L. Fite, Phys. Rev. 93, 651 (1954).

48. B. H. Bransden, A. Dalgarno, T. L. John, and M. L. Seaton, Proc. Phys. Soc. 71, 877-892 (1958).

49. T. Ohmura, National Research Council of Canada, Ottawa (personal communication).

50. D. R. Bates, K. Ledsham, and A. L. Stewart, Phil. Trans. Roy. Soc. (London) A246, 215-240 (1953).

51. D. R. Bates, J. Chem. Phys. 19, 1122-1124 (1951).

52. D. R. Bates, M. N. 112, 40-44 (1952); 111, 303-314 (1951).

53. H. A. Kramers, Phil. Mag. 46, 836-871 (1923).

54. J. A. Gaunt, Proc. Roy. Soc. (London), A126, 654-660 (1930).

55. A. W. Maue, Ann. Physik 13, 161-190 (1932).

56. A. Sommerfeld, Atombau und Spektrallinien, F. Vieweg und Sohn, Braunschweig, 1939.

57. J. Greene, Ap. J. 130, 693-701 (1959).

58. D. H. Menzel and C. L. Pekeris, M. N. 96, 77-111 (1935).

59. A. Unsöld, Physik der Sternatmosphären, Julius Springer, Berlin, 1938.

60. L. H. Aller, Astrophysics, p. 133, The Ronald Press Co., New York, 1953.

61. H. Margenau and W. W. Watson, Revs. Mod. Phys. 8, 22-53 (1936).

62. V. Weisskopf, Zeits. f. Physik 75, 287-301 (1932).

63. H. Aroeste and W. C. Benton, J. Appl. Phys. 27, 117-121 (1956).

64. C. Lanczos, Zeits. f. Physik 62, 518-544 (1930); 65, 431-455 (1930); 68, 204-232 (1931).

65. H. A. Bethe and E. E. Salpeter, Quantum Mechanics of One- and Two-Electron Atoms, Academic Press, New York, 1957.

66. A. S. Coolidge and H. M. James, J. Chem. Phys. 6, 730-734 (1938).

67. R. Bergeon and B. Vodar, Comptes Rendus 240, 172-174 (1955).

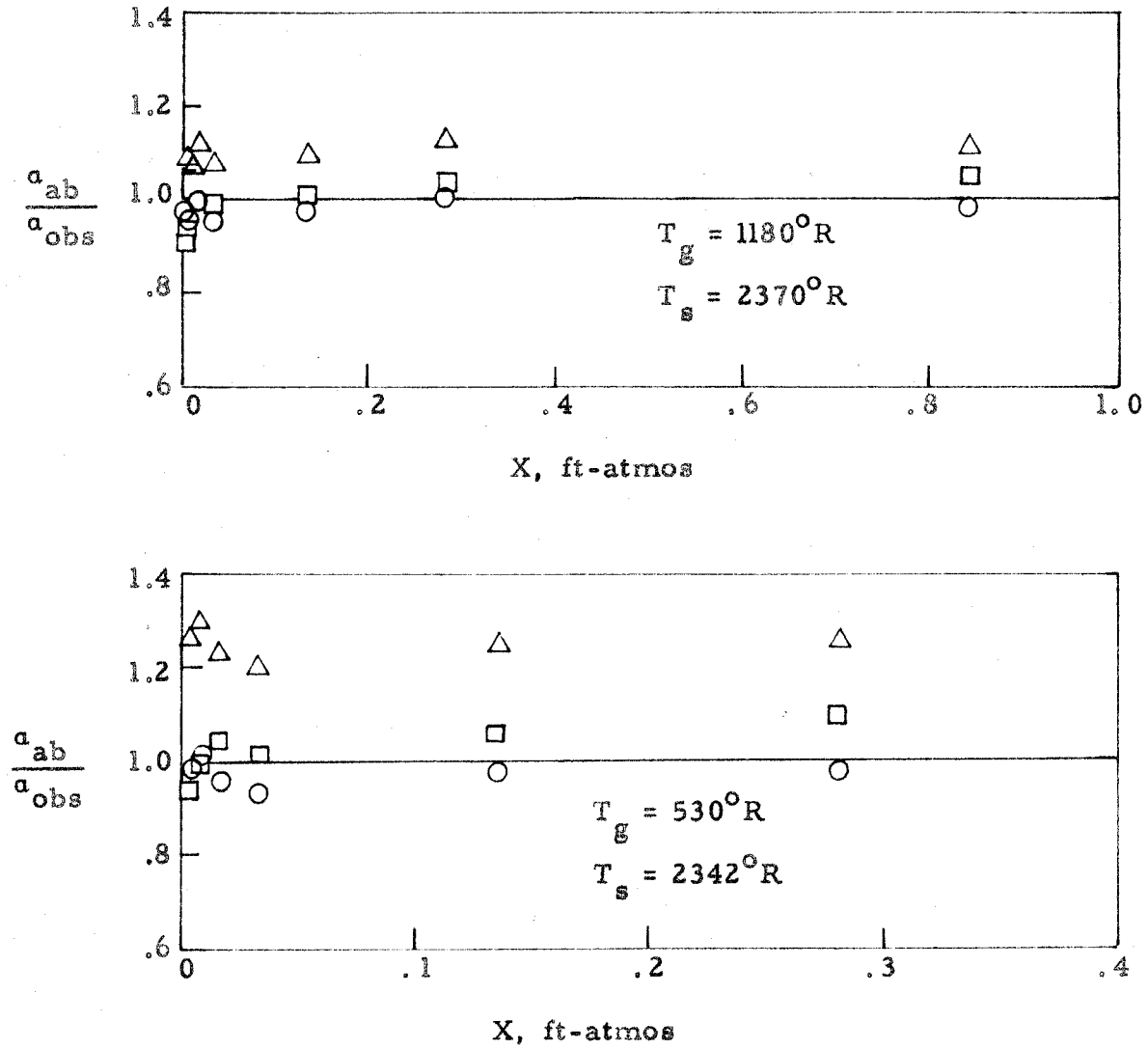

Fig. 1. The ratios of calculated to observed absorptivities for CO_2 as a function of optical depth [calculated using Eq. (49): O; calculated using Eq. (33) with $\eta = 4/3$: □ ; calculated using Eq. (33) with $\eta = 1$: △].

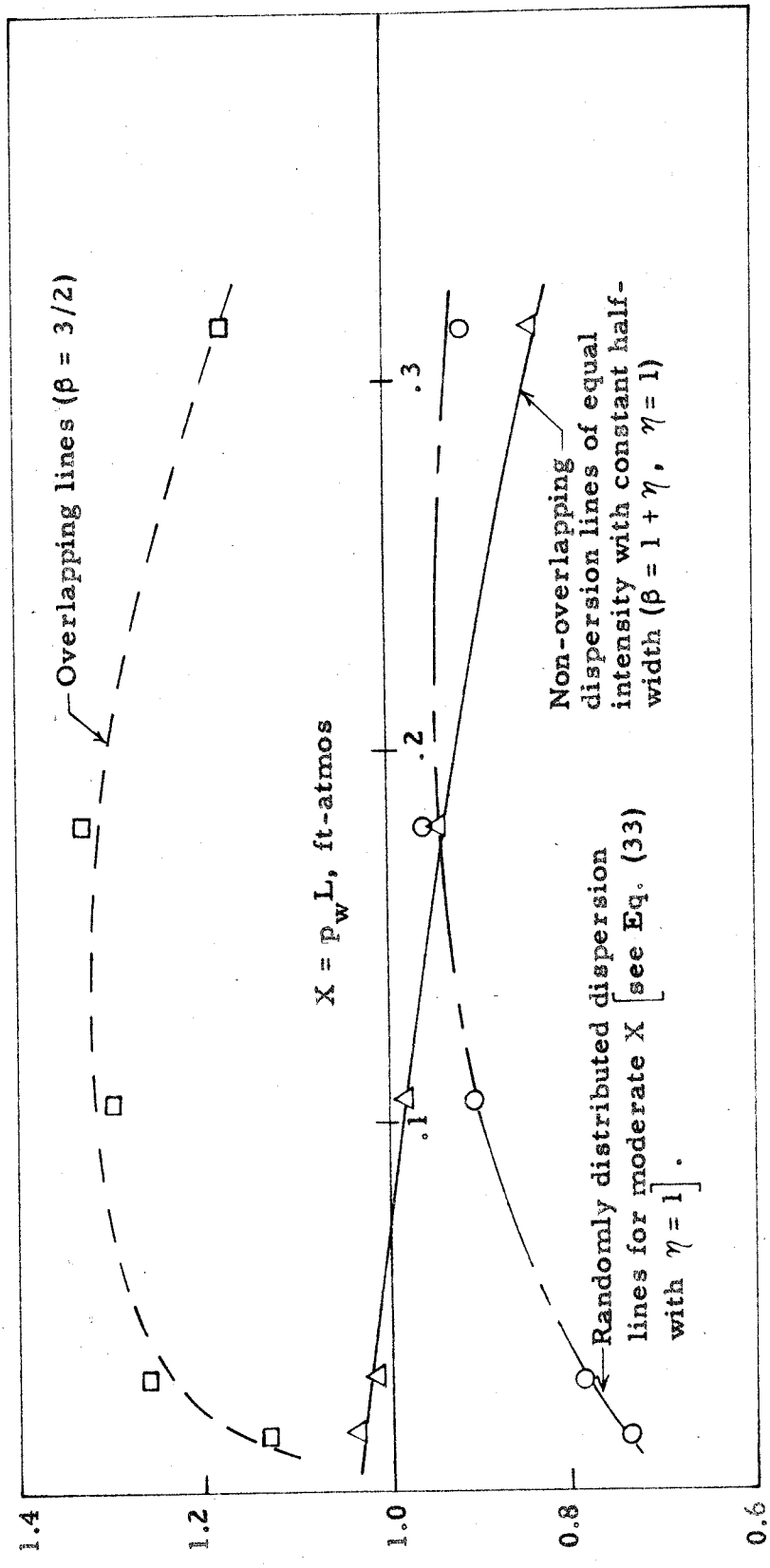

Fig. 2. The ratios of calculated absorptivities α_{ab} to observed absorptivities α_{obs} as a function of optical depth for water vapor using different band models ($T_s = 2500^{\circ}R$, $T_g = 750^{\circ}R$, total pressure p = 1 atmos; from Olfe and Penner[3]).

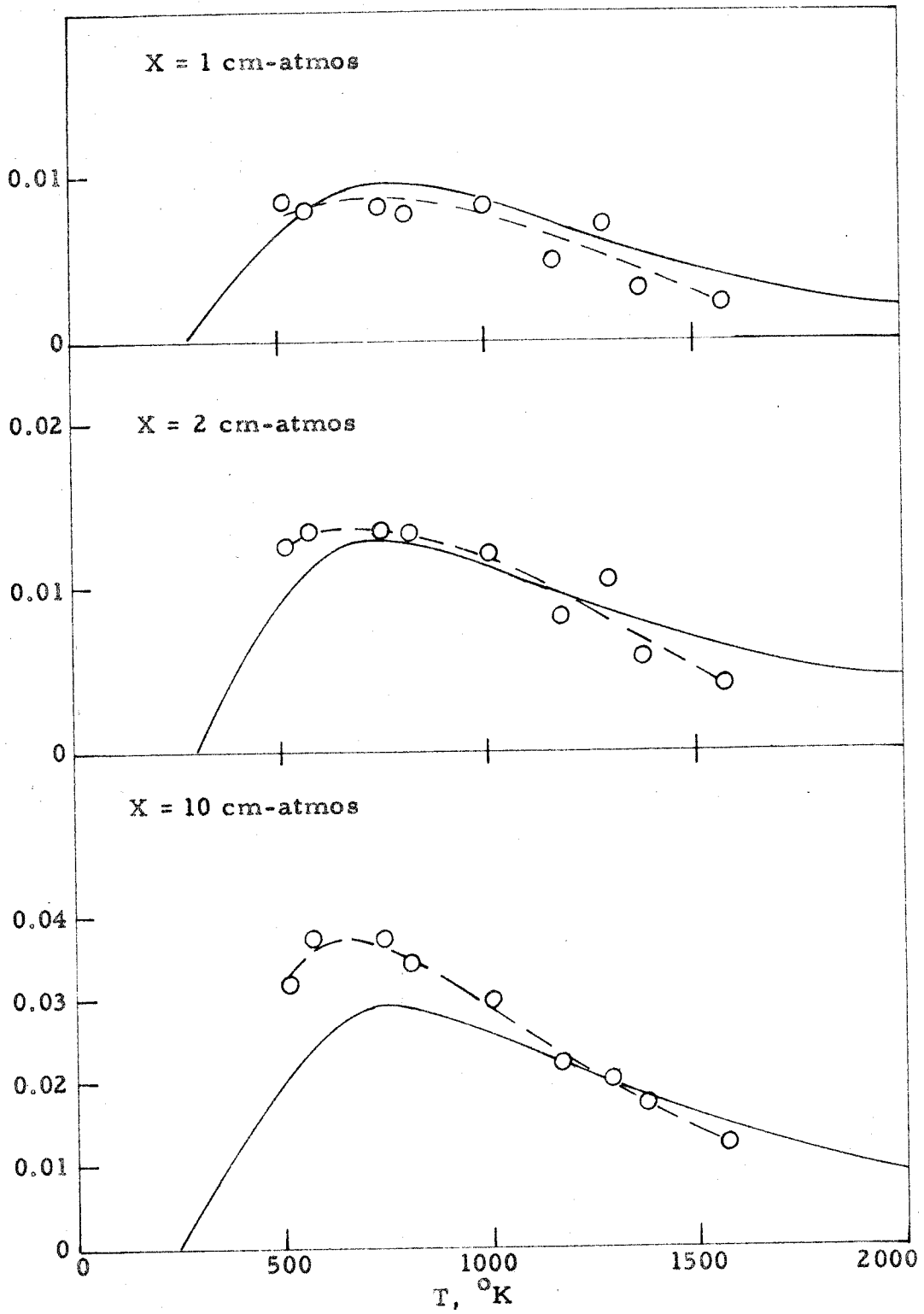

Fig. 3. The total emissivity of CO as a function of temperature for various optical depths and a total pressure of 1 atmos. The solid curve is the emissivity calculated from basic principles using a non-overlapping line theory,[5] while the circles indicate points calculated using Eq.(20) and absorption measurements (from U. P. Oppenheim[10]).

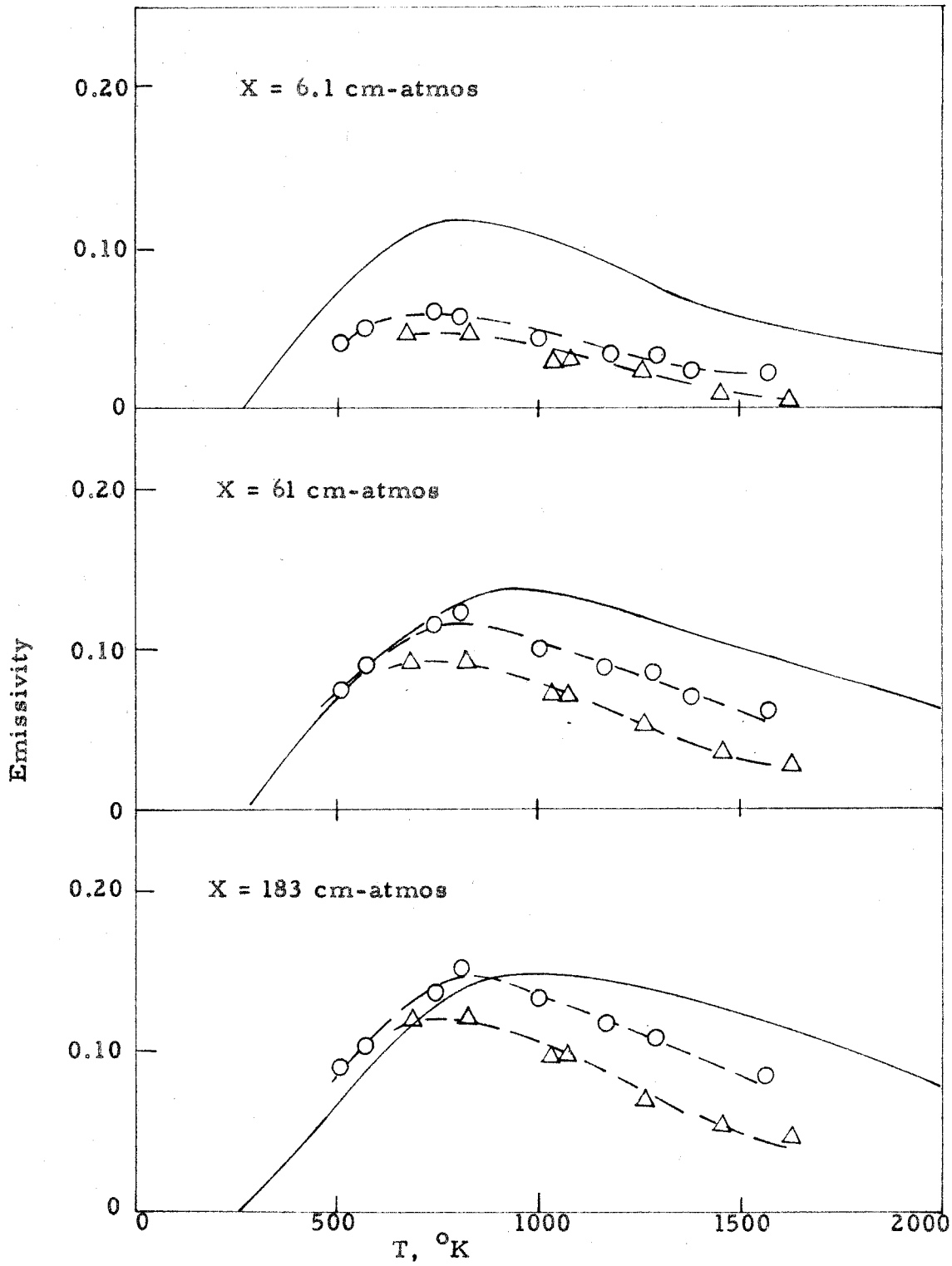

Fig. 4. The total emissivity of CO as a function of temperature for various optical depths. The solid curve is the emissivity calculated from basic principles using an overlapping line theory[5] calculated from Eq. (12) and using absorption measurements of CO-A mixtures at a total pressure of 35 atmos: O; calculated from Eq. (12) and using absorption measurements of CO-He mixtures at a total pressure of 18 atmos: Δ (from U. P. Oppenheim[10])] .

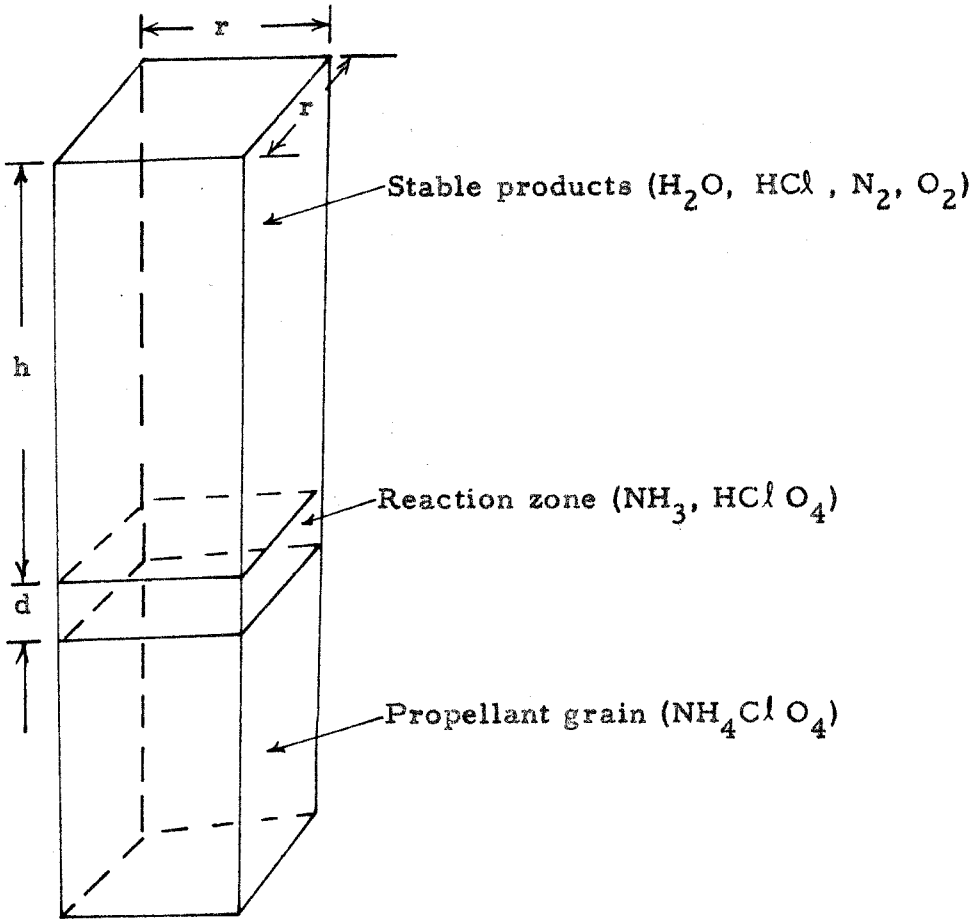

Fig. 5. Schematic diagram of the assumed geometry of the propellant grain and combustion products.

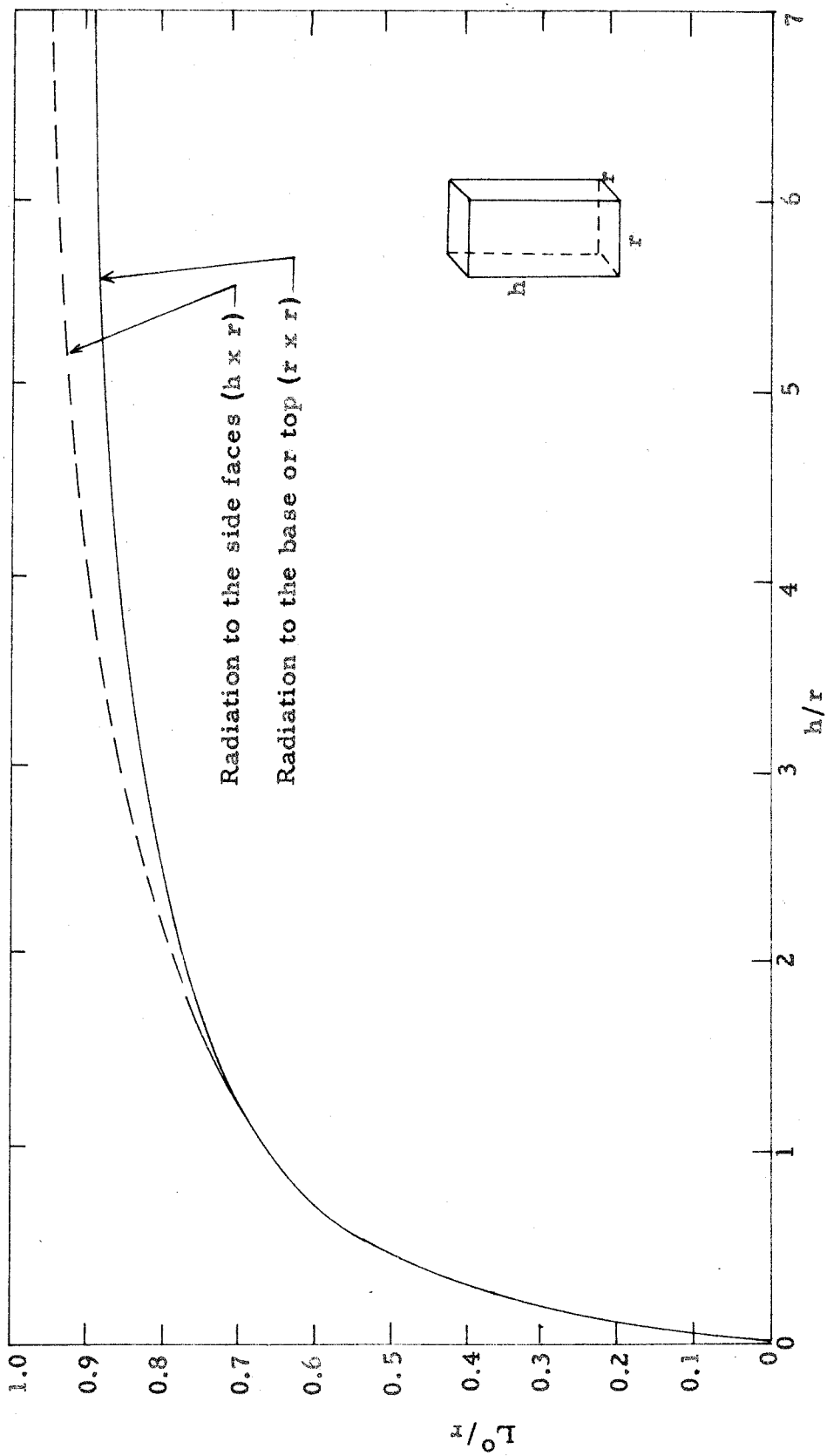

Fig. 6. The ratio of mean beam length L^o to r for $p_g L \to 0$ as a function of h/r.

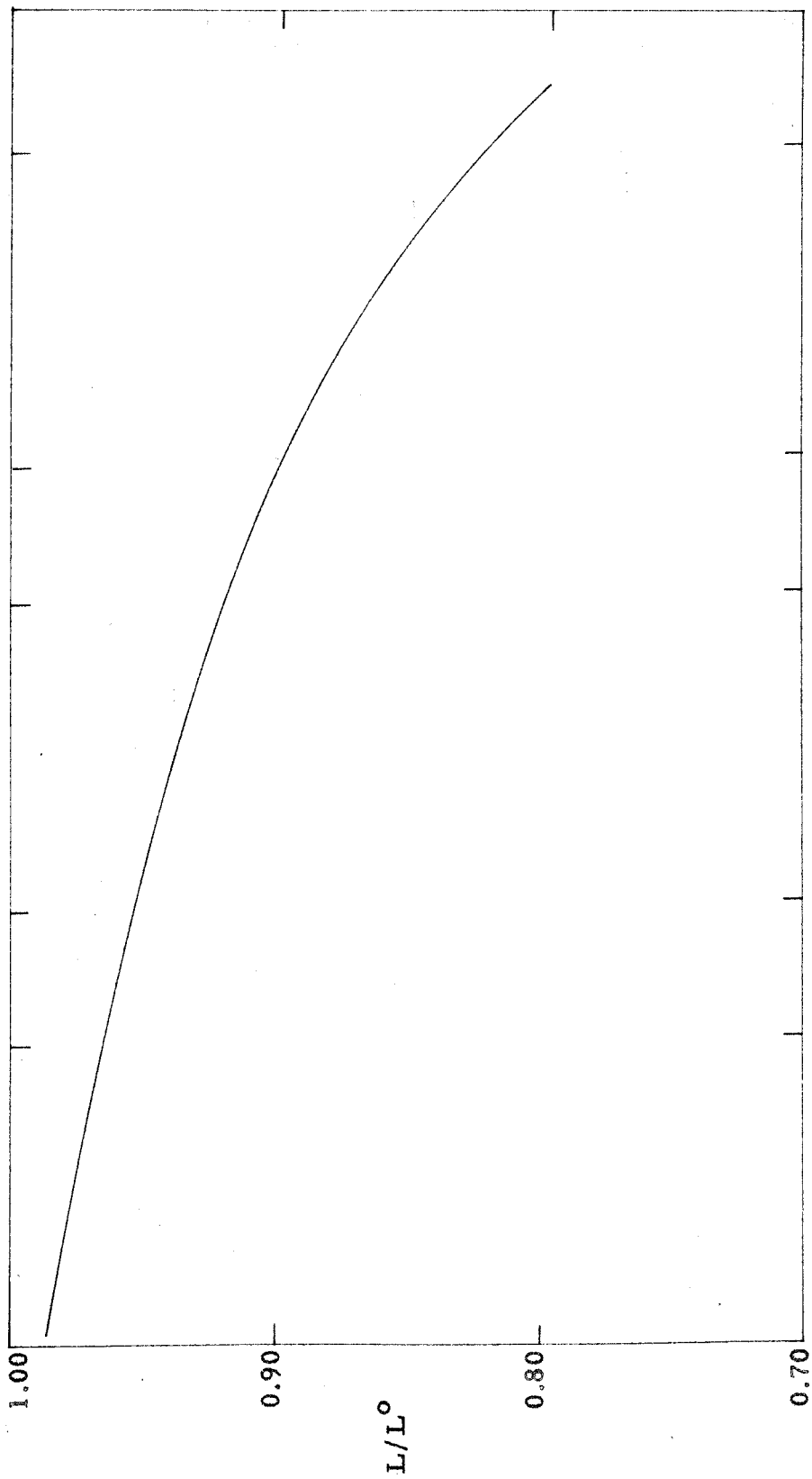

Fig. 7. The ratio L/L° as a function of $p_{H_2O}L_{H_2O}$ (after Hottel[13]).

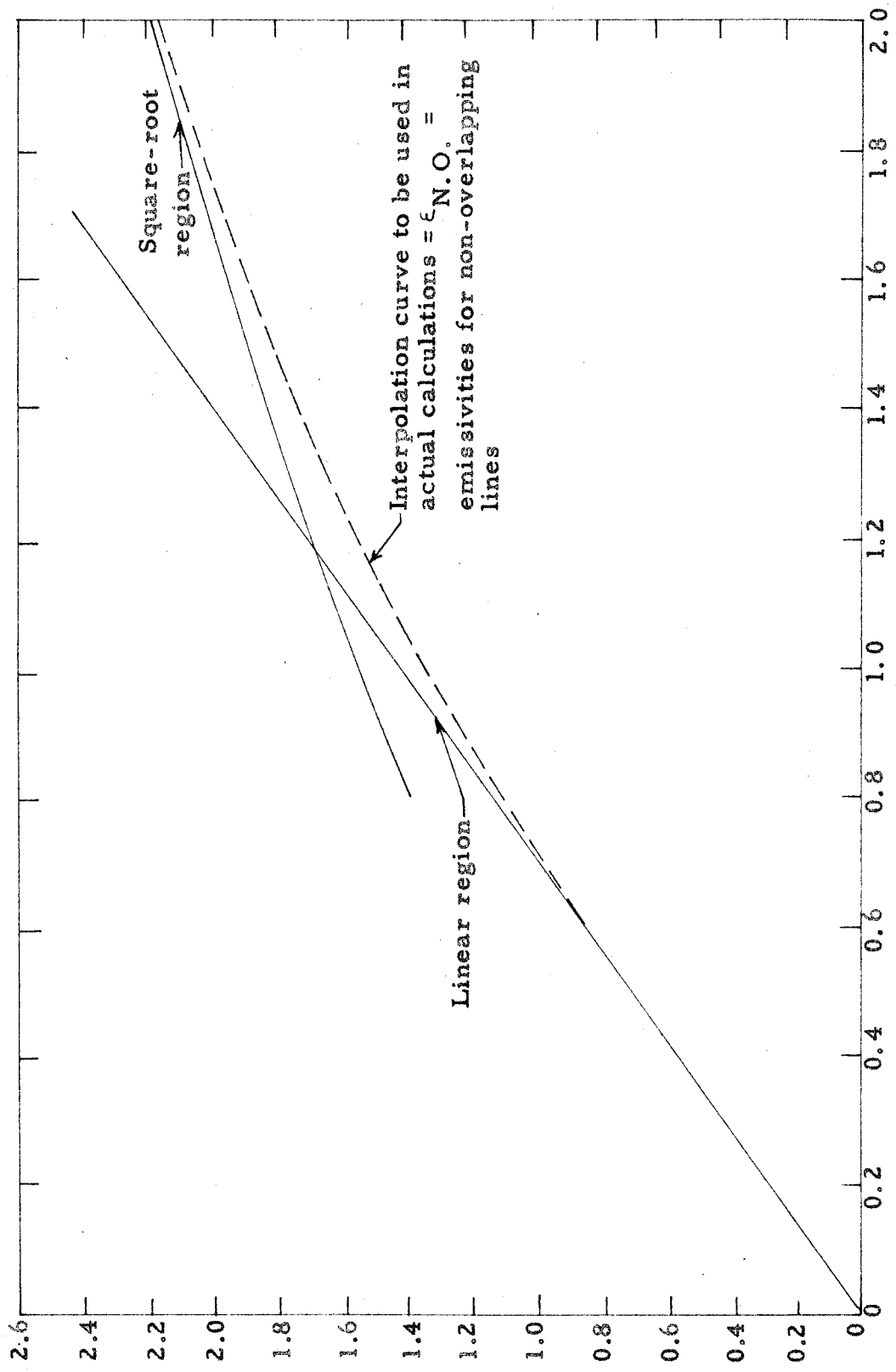

Fig. 8. The ratio $10^3 (\epsilon_{0\rightarrow 1}/p_T)$ as a function of L_{HCl} at 1433° for $\eta_{HCl} = 0.2353$ (non-overlapping lines).

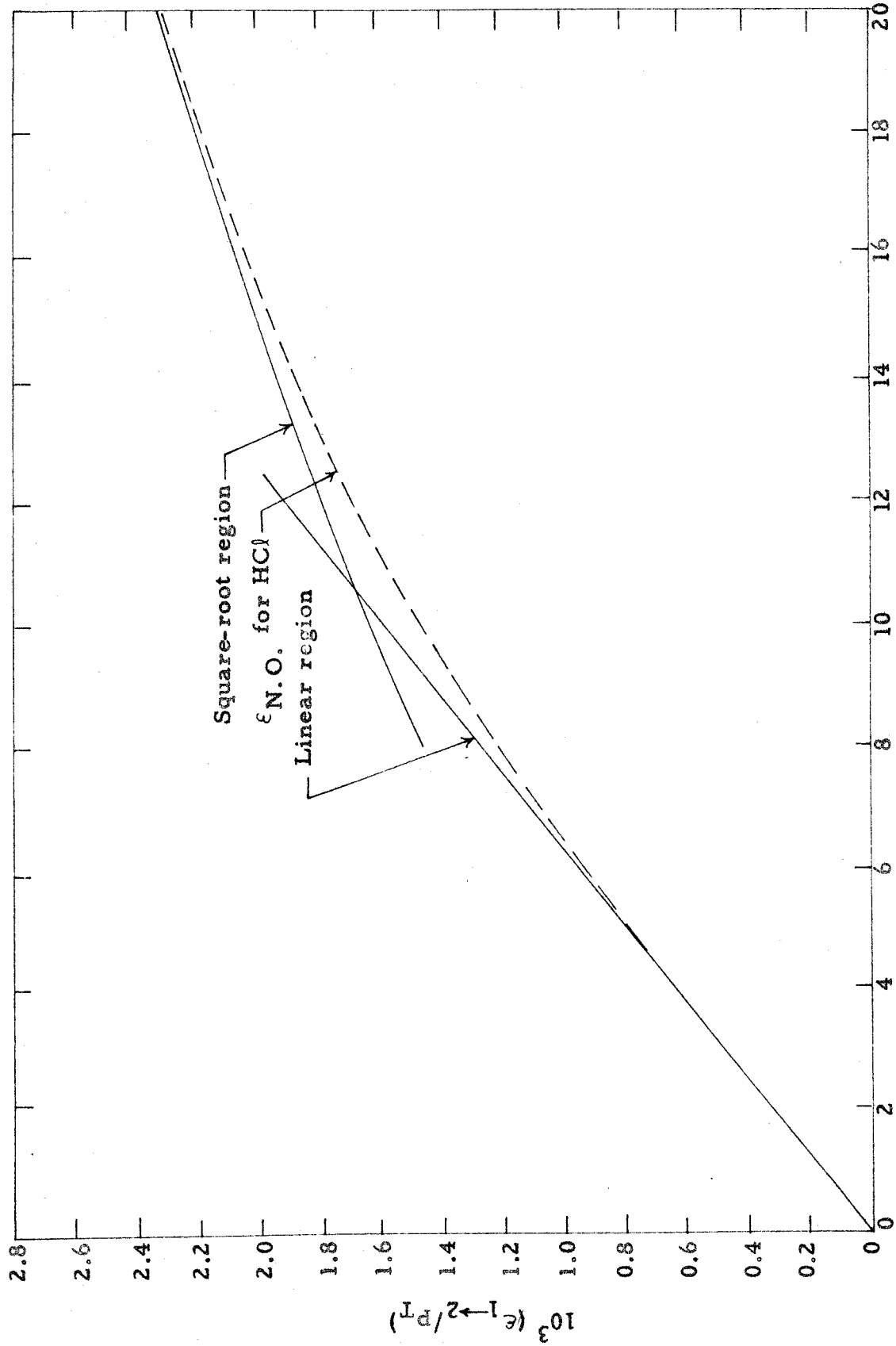

Fig. 9. The ratio $10^3(\epsilon_{1\rightarrow 2}/p_T)$ as a function of L_{HCl} at 1433°K for $\%_{HCl}=0.2353$ (non-overlapping lines).

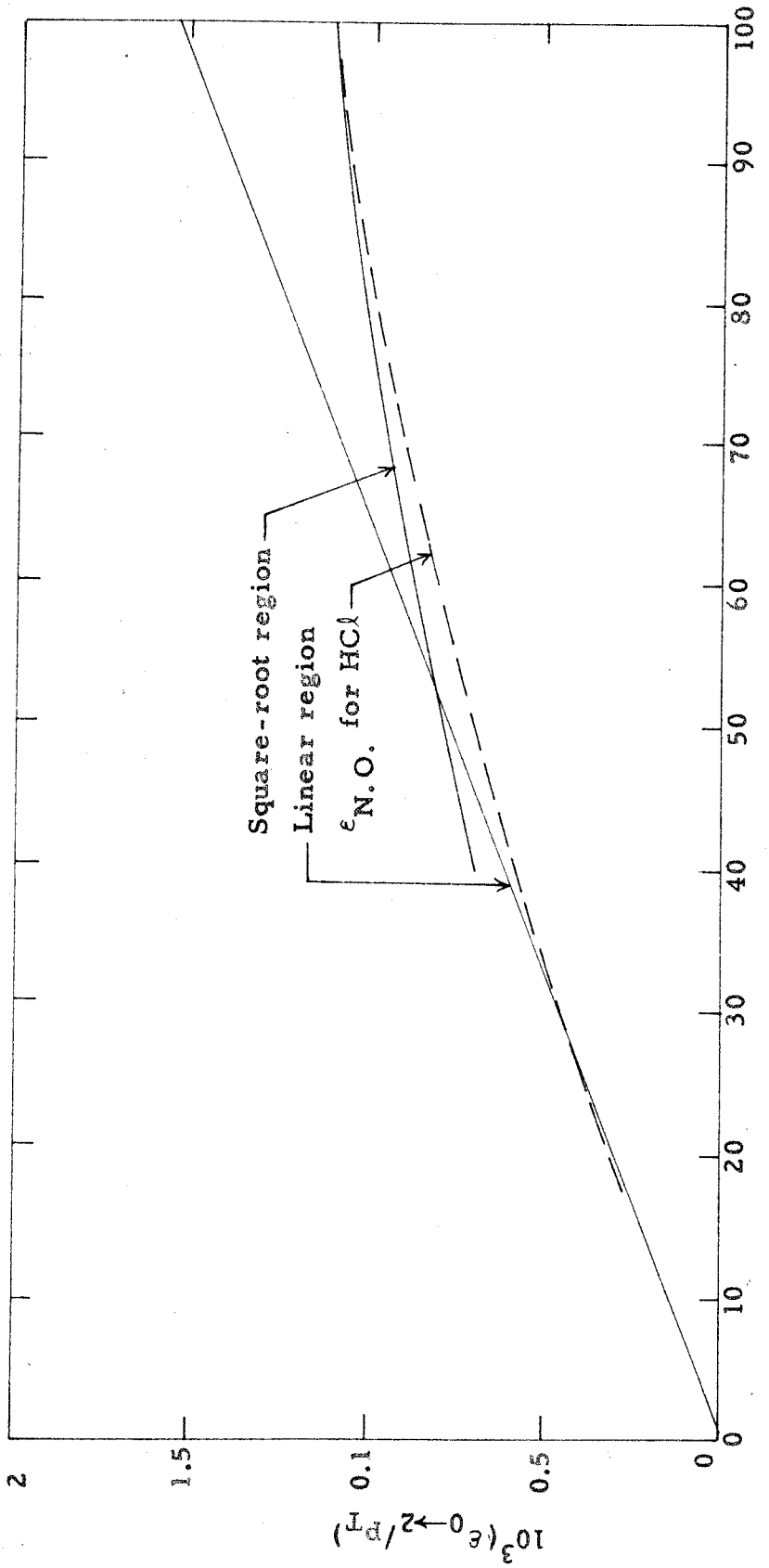

Fig. 10. The ratio $10^3\,(\epsilon_{0\rightarrow 2}/p_T)$ as a function of L_{HCl} at 1433°K for $\gamma_{HCl} = 0.2353$ (non-overlapping lines).

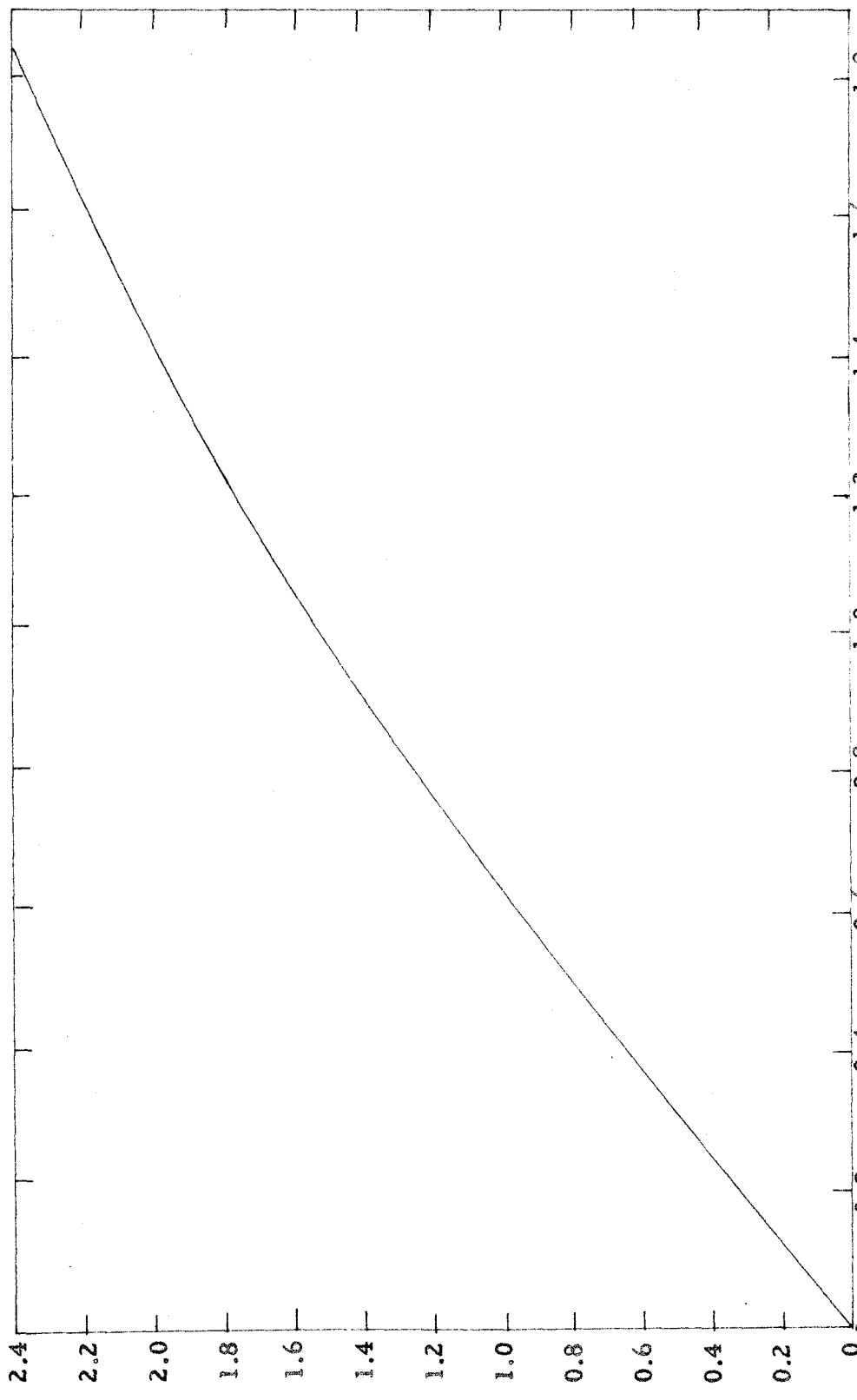

Fig. 11. The ratio $10^3(\epsilon_{F,HC\ell}/p_T)$ as a function of $L_{HC\ell}$ at 1433°K for $\gamma_{HC\ell}$=0.2353 (non-overlapping lines).

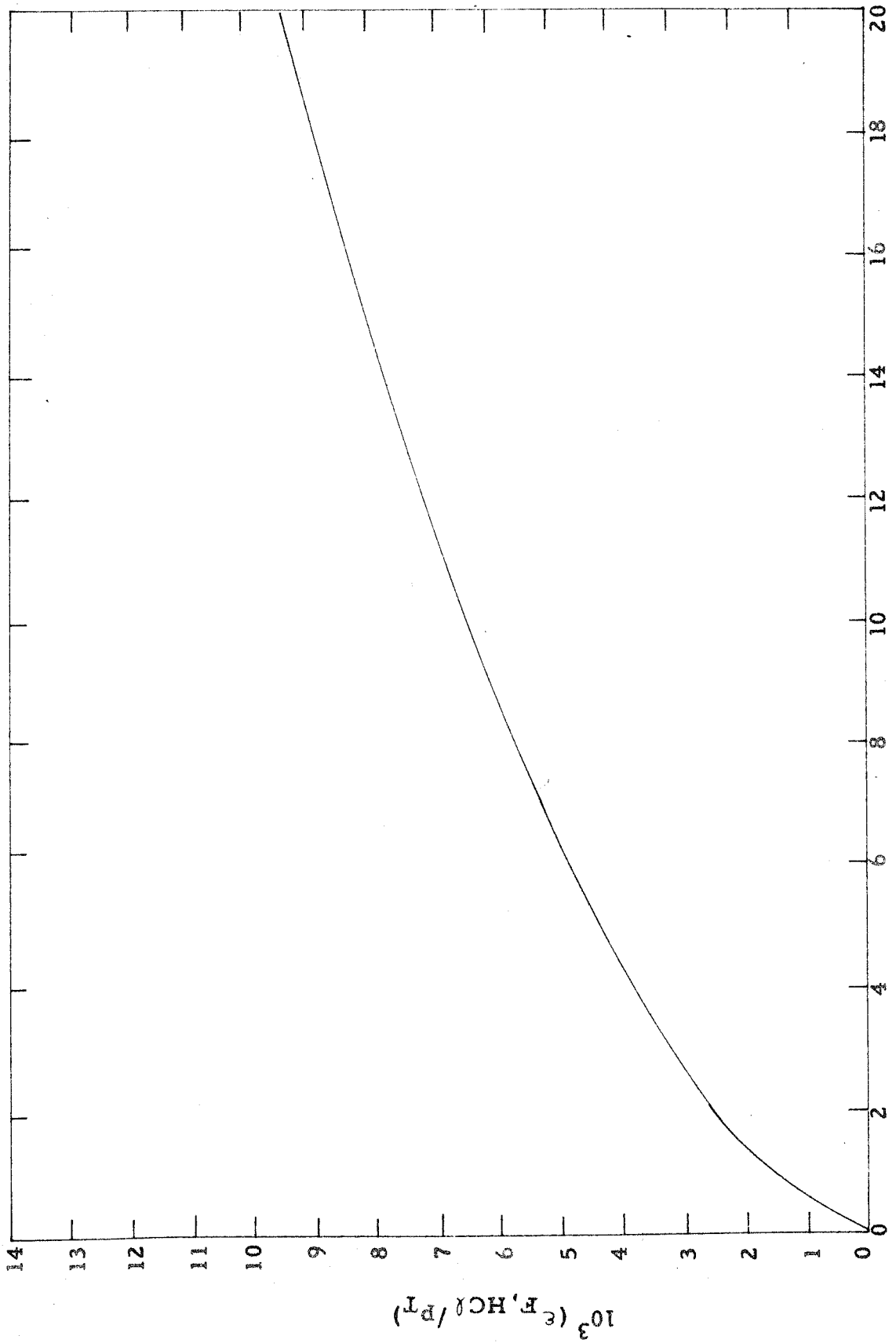

Fig. 12. The ratio $10^3 (\epsilon_{F,HC\ell}/p_T)$ as a function of $L_{HC\ell}$ at 1433°K for $\gamma_{HC\ell}=0.2353$ (non-overlapping lines).

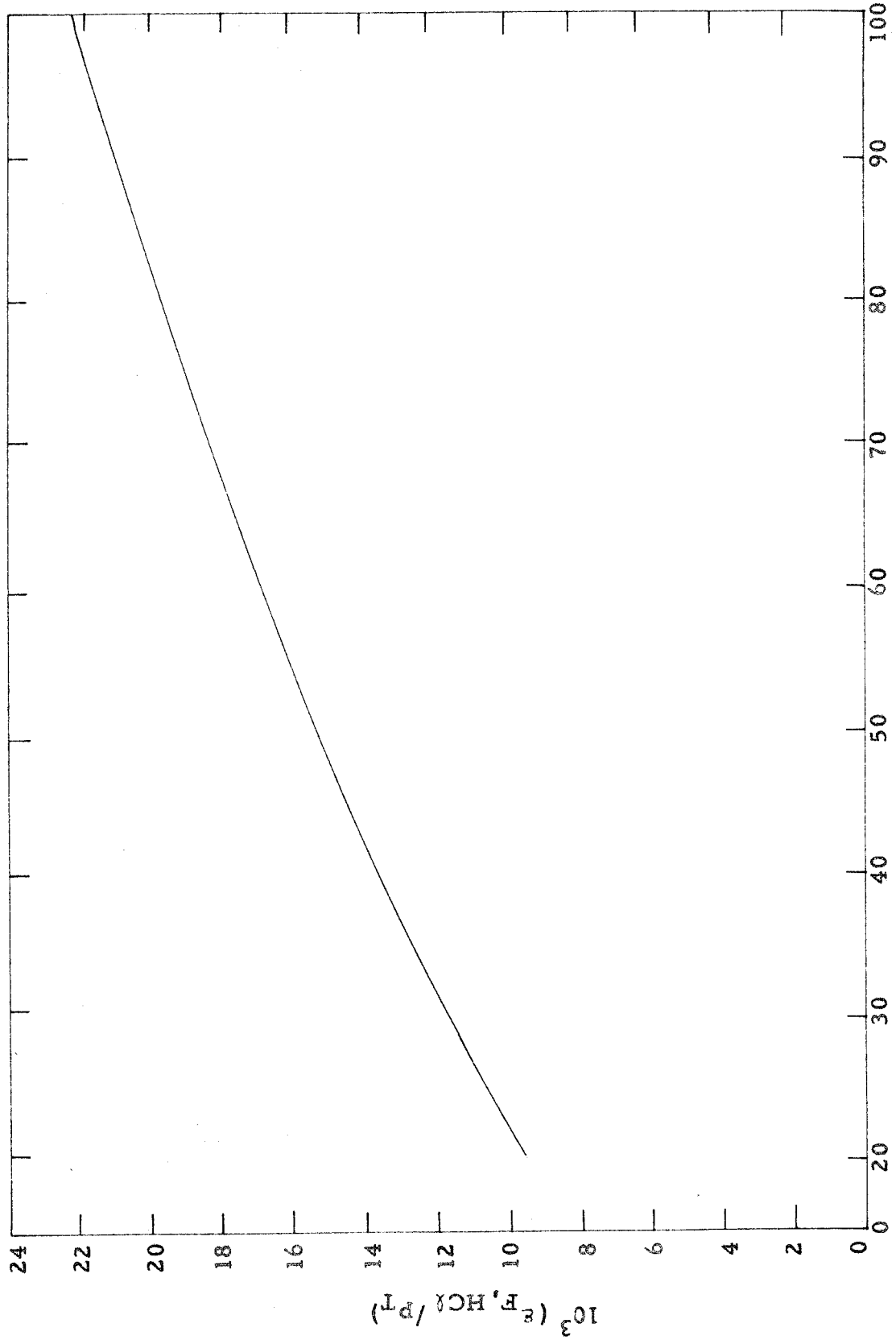

Fig. 13. The ratio 10^3 ($\epsilon_{F,HC\ell}/p_T$) as a function of $L_{HC\ell}$ at 1433°K for $\eta_{HC\ell}$=0.2353 (non-overlapping lines).

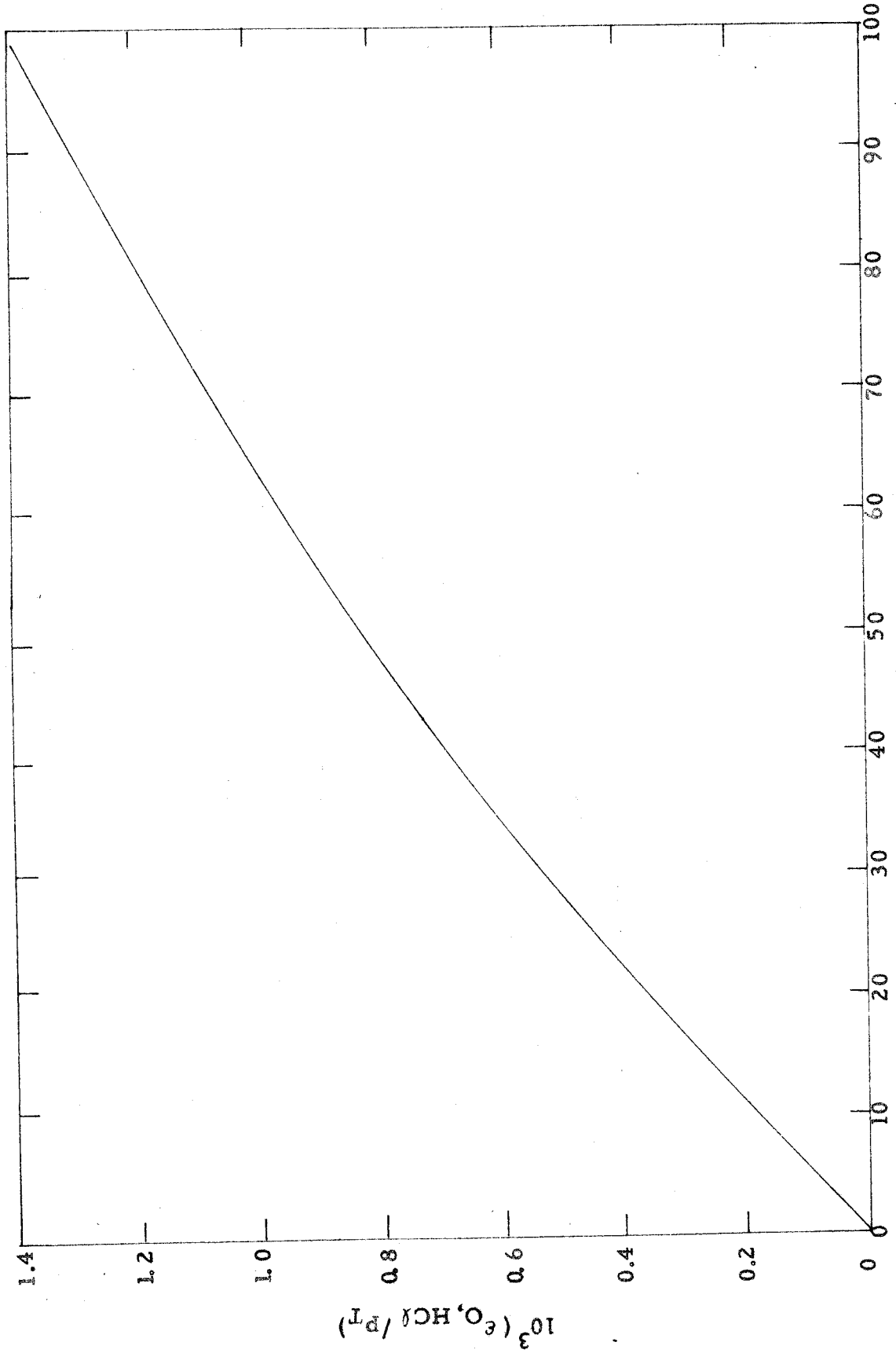

Fig. 14. The ratio $10^3 (\varepsilon_{O,HCl}/p_T)$ as a function of L_{HCl} at 1433°K for $\eta_{HCl} = 0.2353$ (non-overlapping lines).

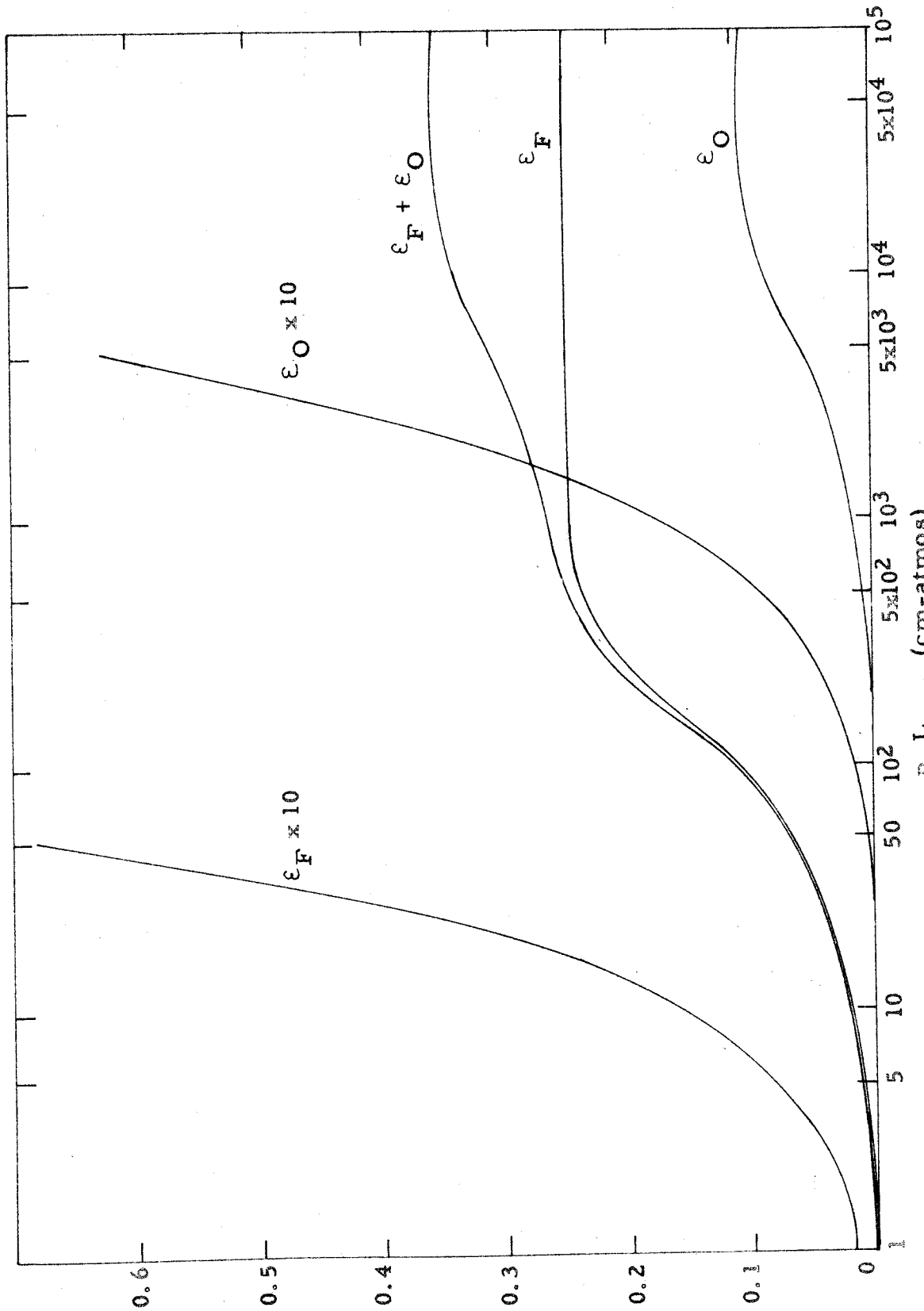

Fig. 15. The emissivities ε_F, ε_O, and $\varepsilon_F + \varepsilon_O$ for HCl at 1433°K as functions of $P_T L_{HCl}$ for the box model.

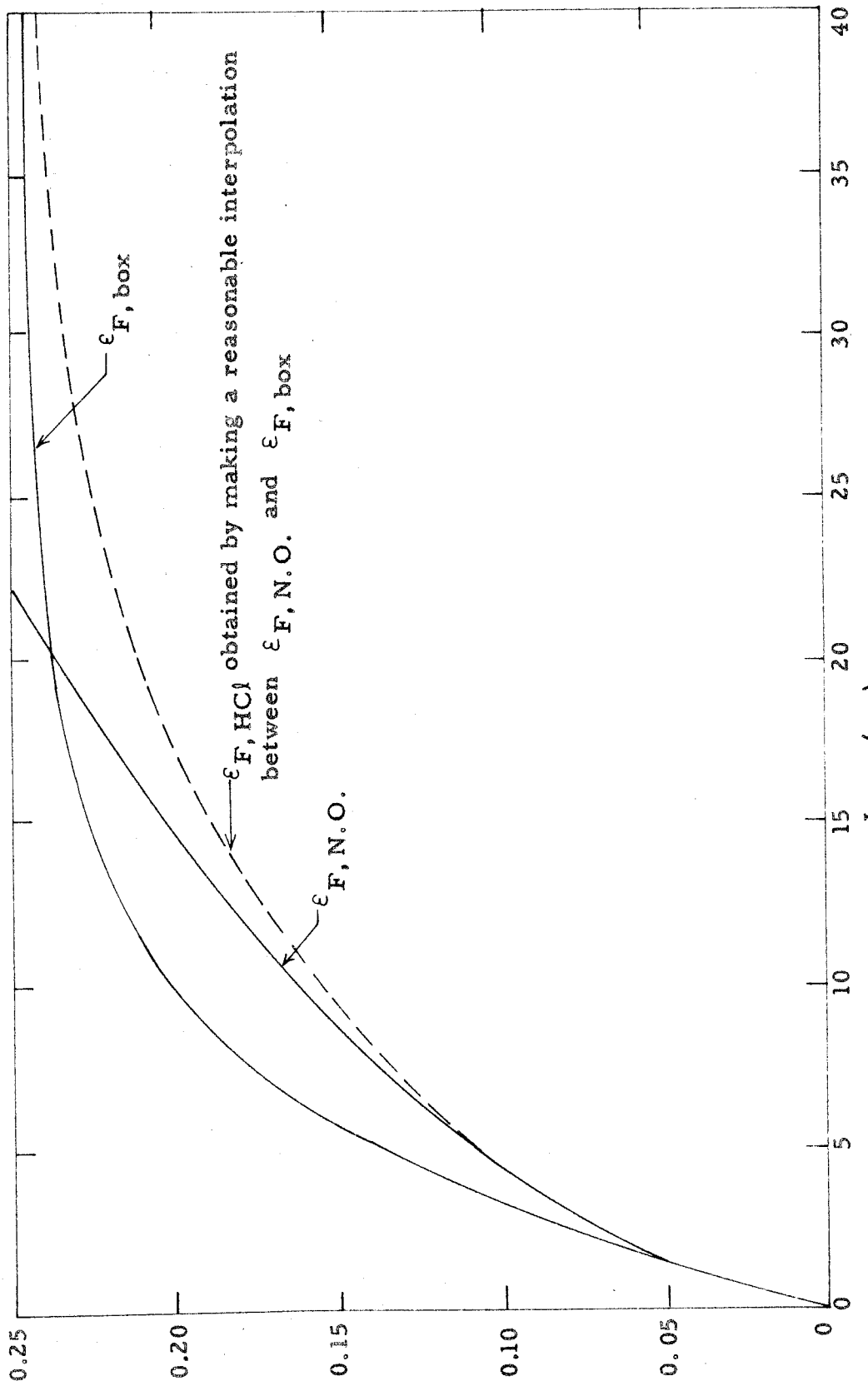

Fig. 16. The emissivities $\varepsilon_{F,N.O.}$, $\varepsilon_{F,box}$ and $\varepsilon_{F,HCl}$ for HCl at 1433°K and p_T = 25 atmos for $\eta_{HCl} = 0.2353$.

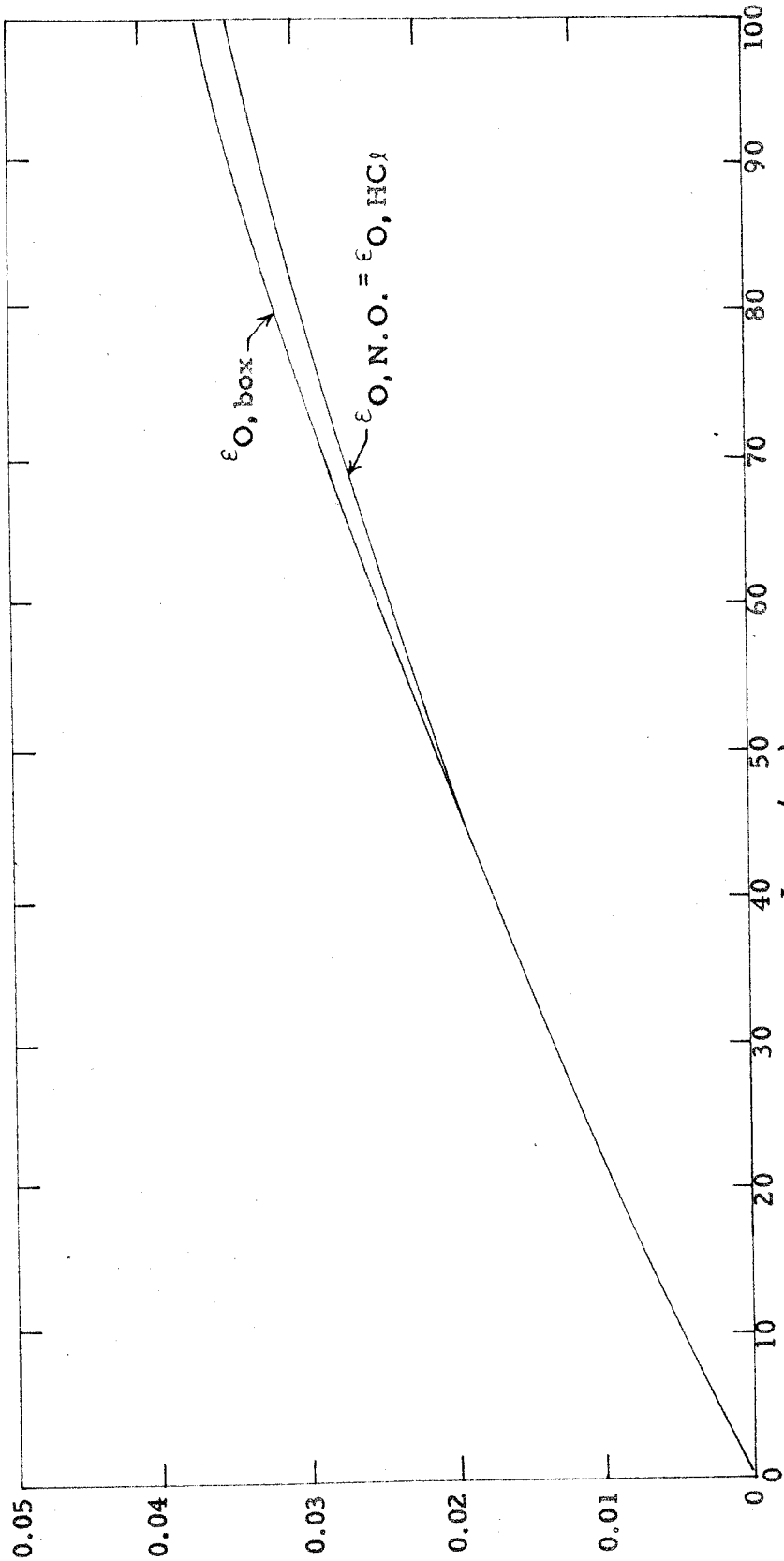

Fig. 17. The emissivities $\varepsilon_{O,box}$ and $\varepsilon_{O,N.O.} = \varepsilon_{O,HC\ell}$ for $HC\ell$ at 1433°K and p_T = 25 atmos for $\eta_{HC\ell} = 0.2353$.

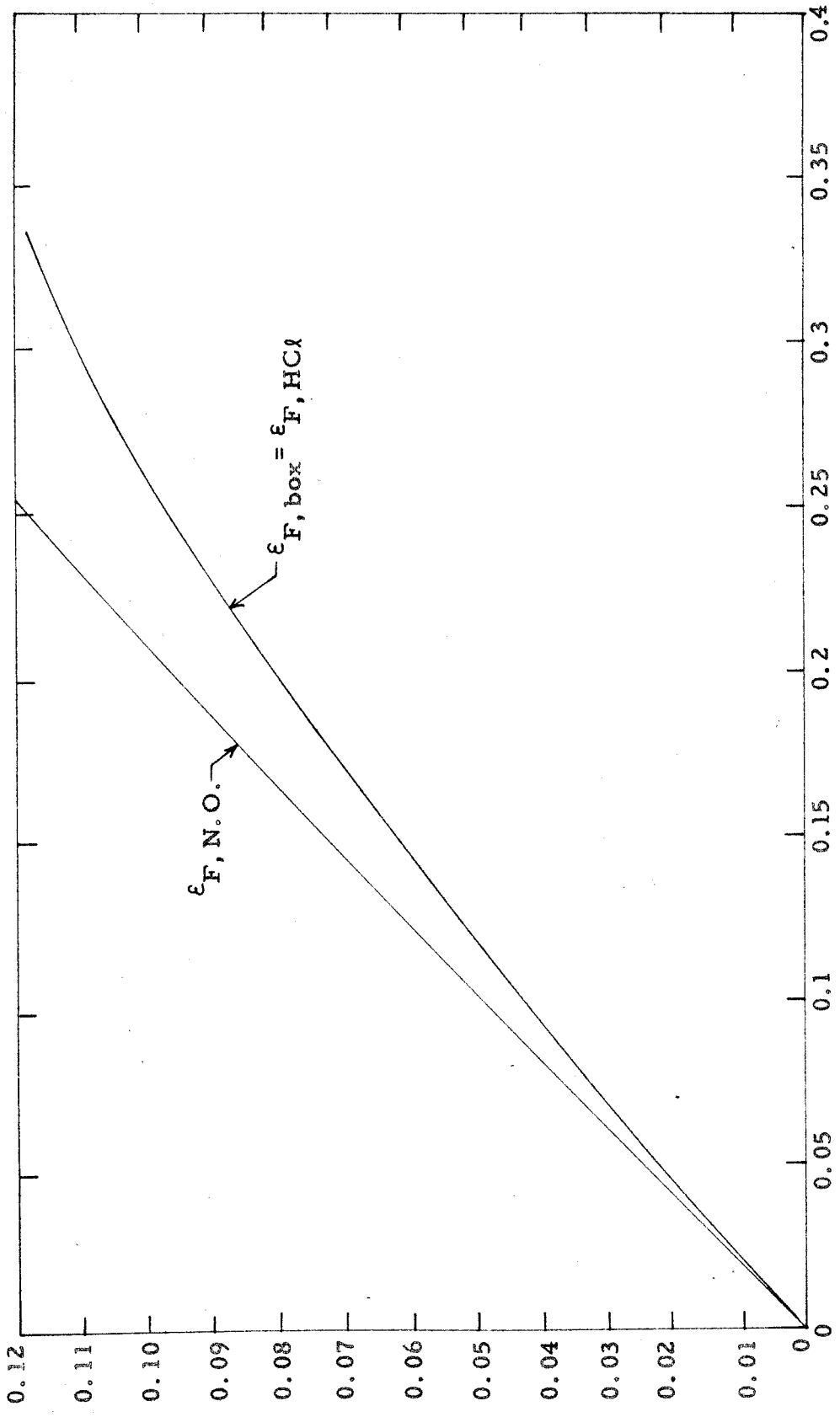

Fig. 18. The emissivities $\varepsilon_{F,N.O.}$ and $\varepsilon_{F,box} = \varepsilon_{F,HCl}$ for HCl at 1433°K and $p_T = 300$ atmos for $\eta_{HCl} = 0.2353$.

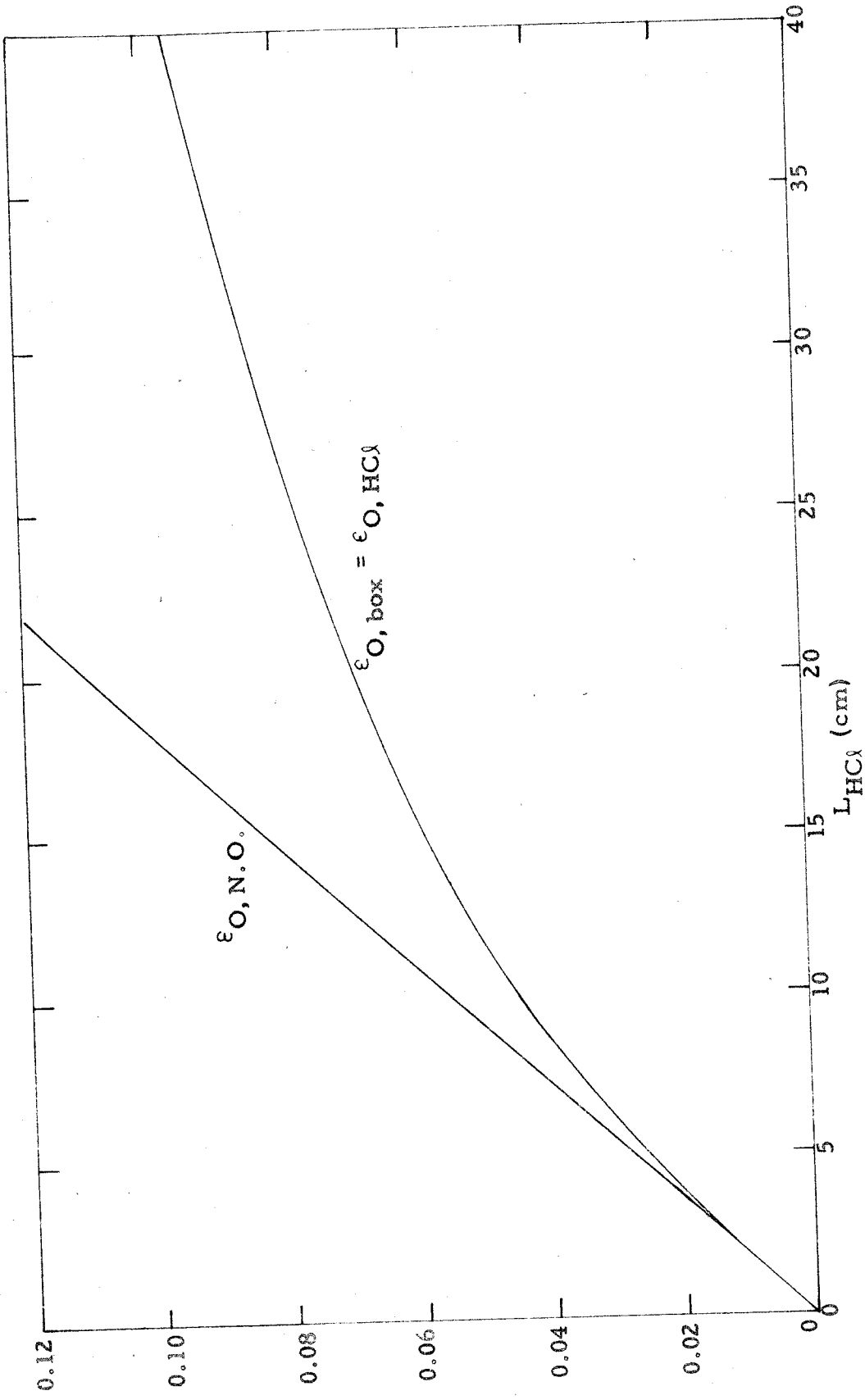

Fig. 19. The emissivities $\varepsilon_{O,\,N.O.}$ and $\varepsilon_{O,\,box} = \varepsilon_{O,\,HC\ell}$ for $HC\ell$ at 1433°K and $p_T = 300$ atmos for $\gamma_{HC\ell} = 0.2353$.

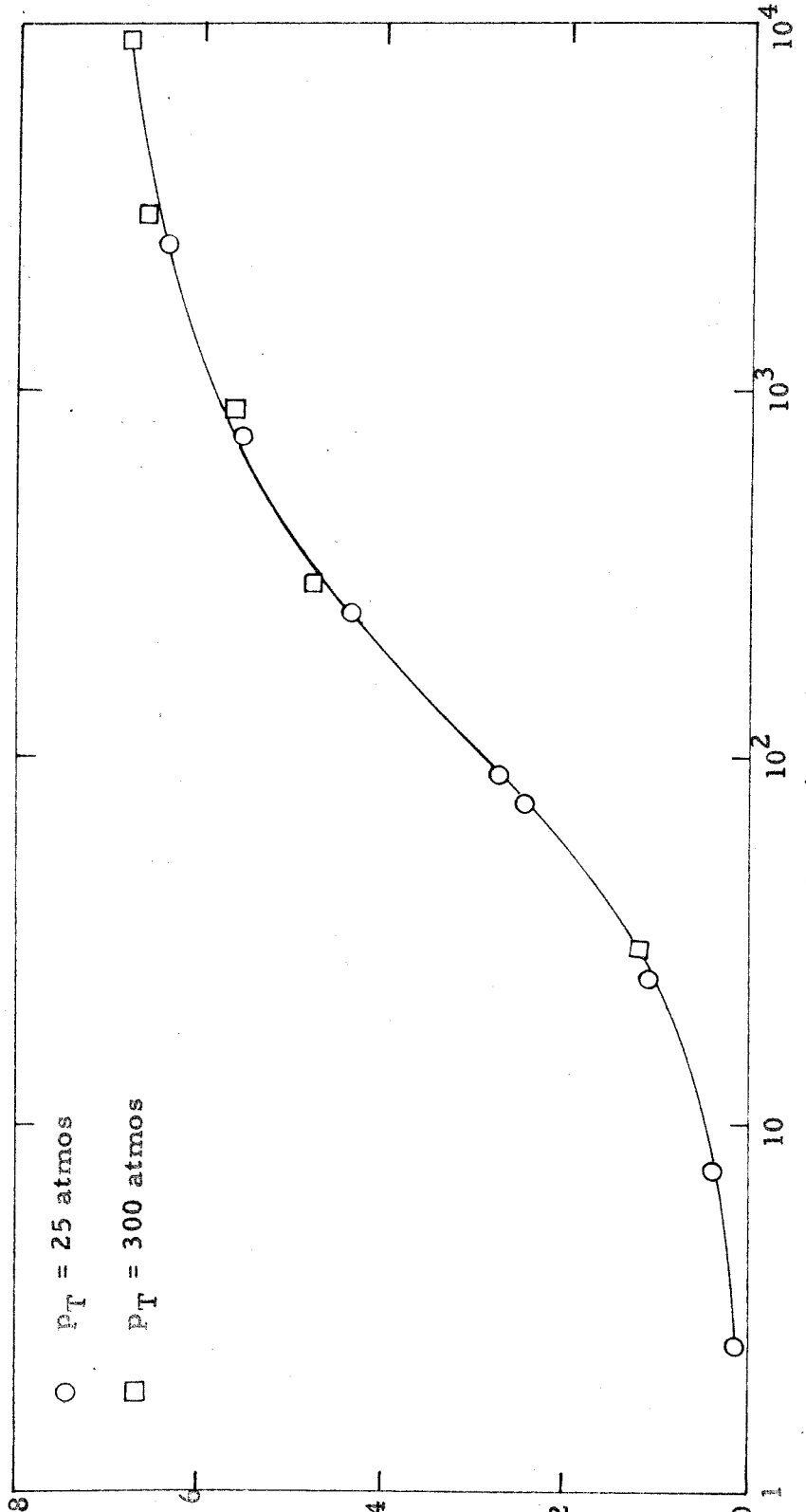

Fig. 20. The emissivities of water vapor (using a statistical model) as a function of optical depth at 1433°K and p_T = 25 atmos or p_T = 300 atmos for $\eta_{H_2O} = 0.2353$.

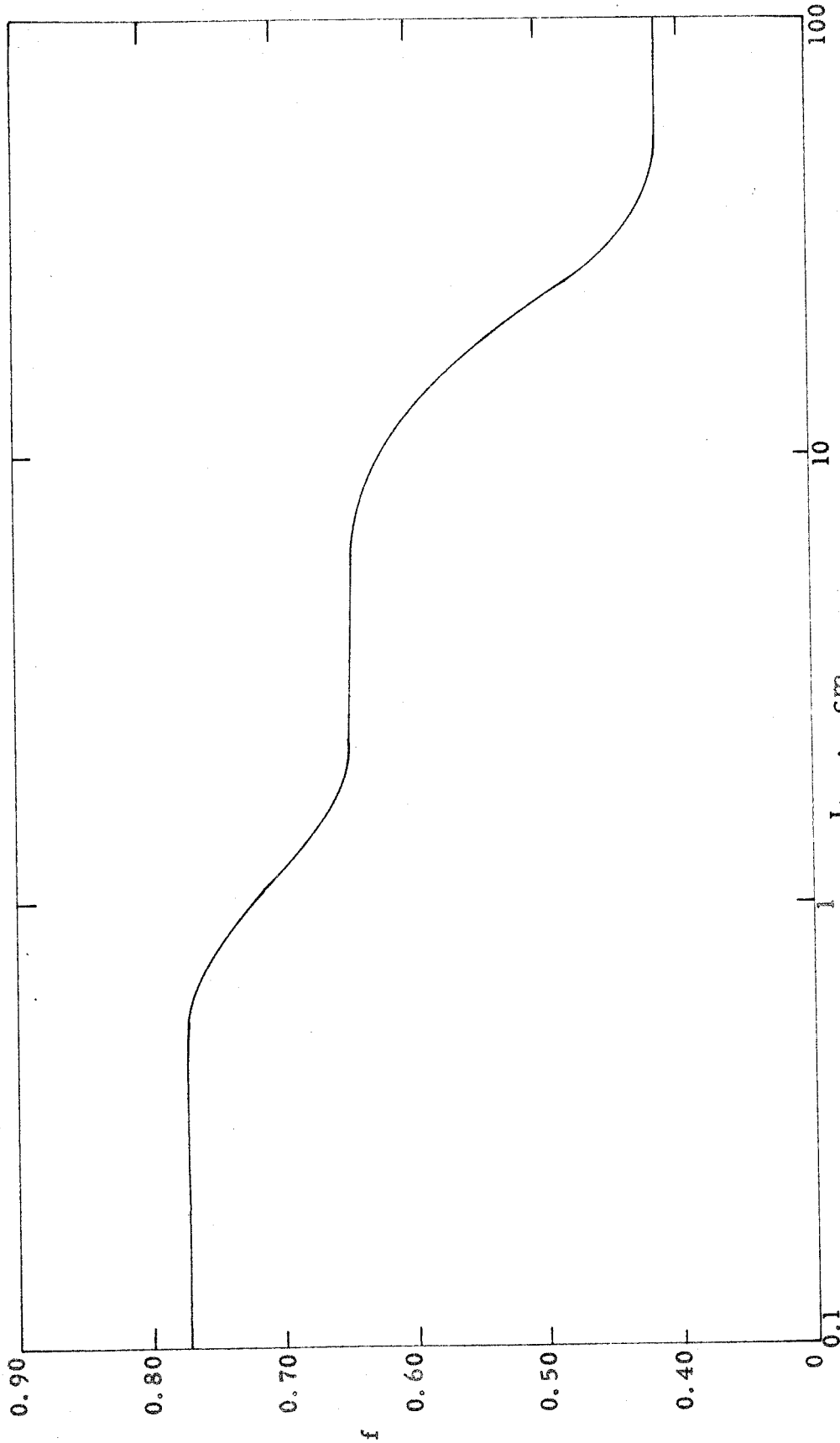

Fig. 21. The parameter f defined in Eq. (24a) as a function of the beam length L_{HCl} at 1433°K and P_T = 25 atmos.

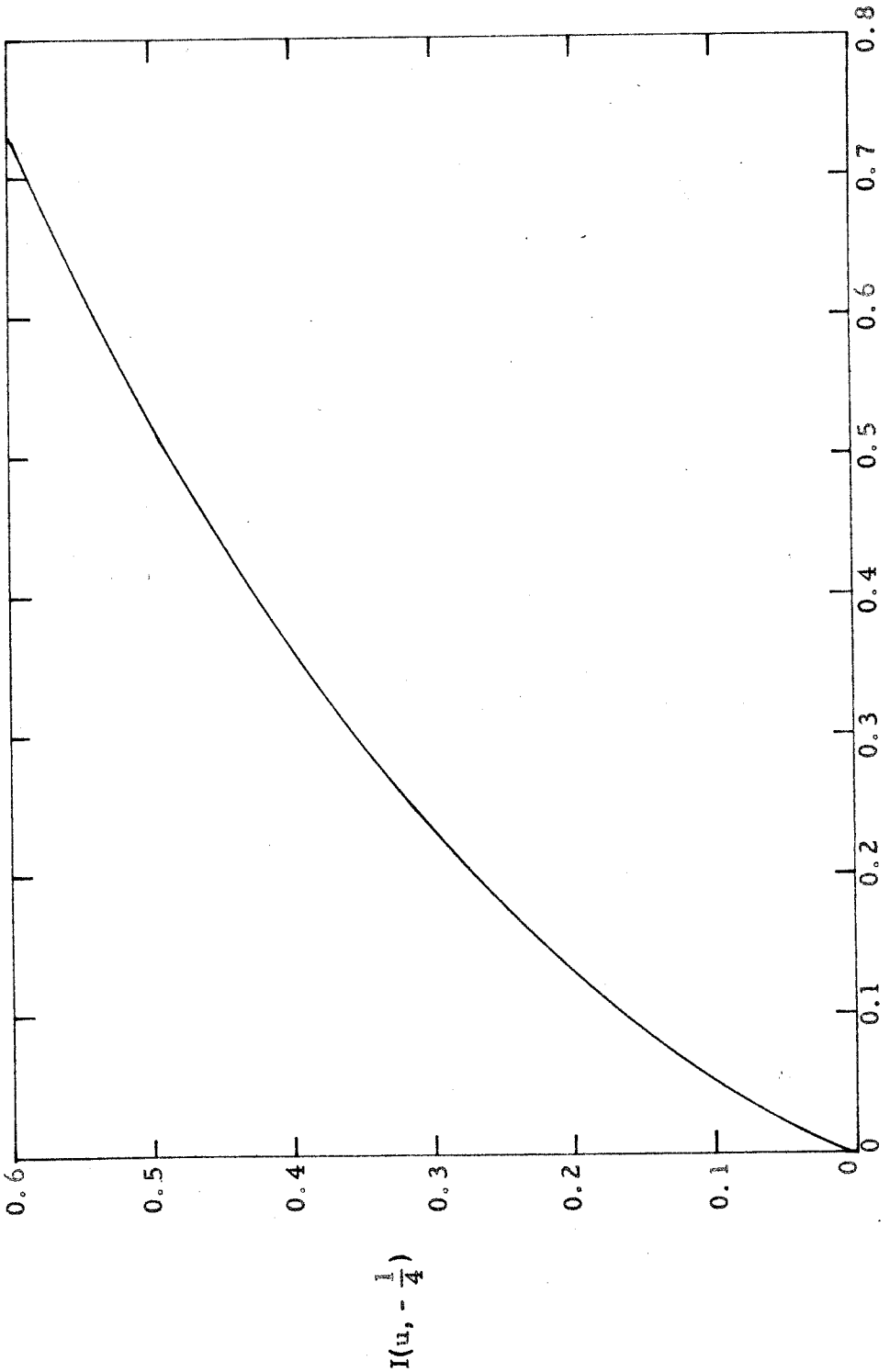

Fig. 22. The quantity $I(u, -\frac{1}{4})$ as a function of u (from Pearson[14]).

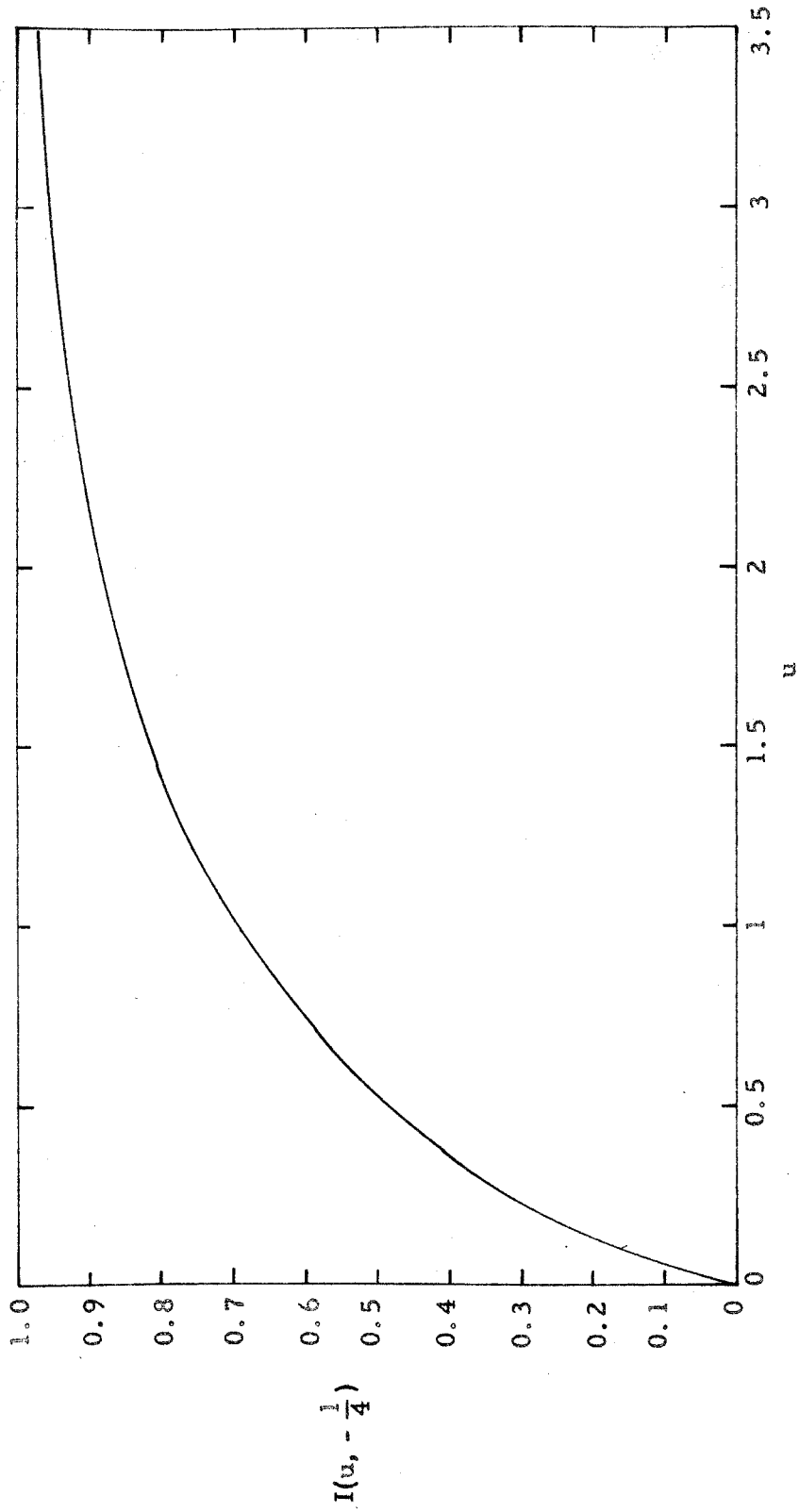

Fig. 23. The quantity $I(u, -\frac{1}{4})$ as a function of u (from Pearson[14]).

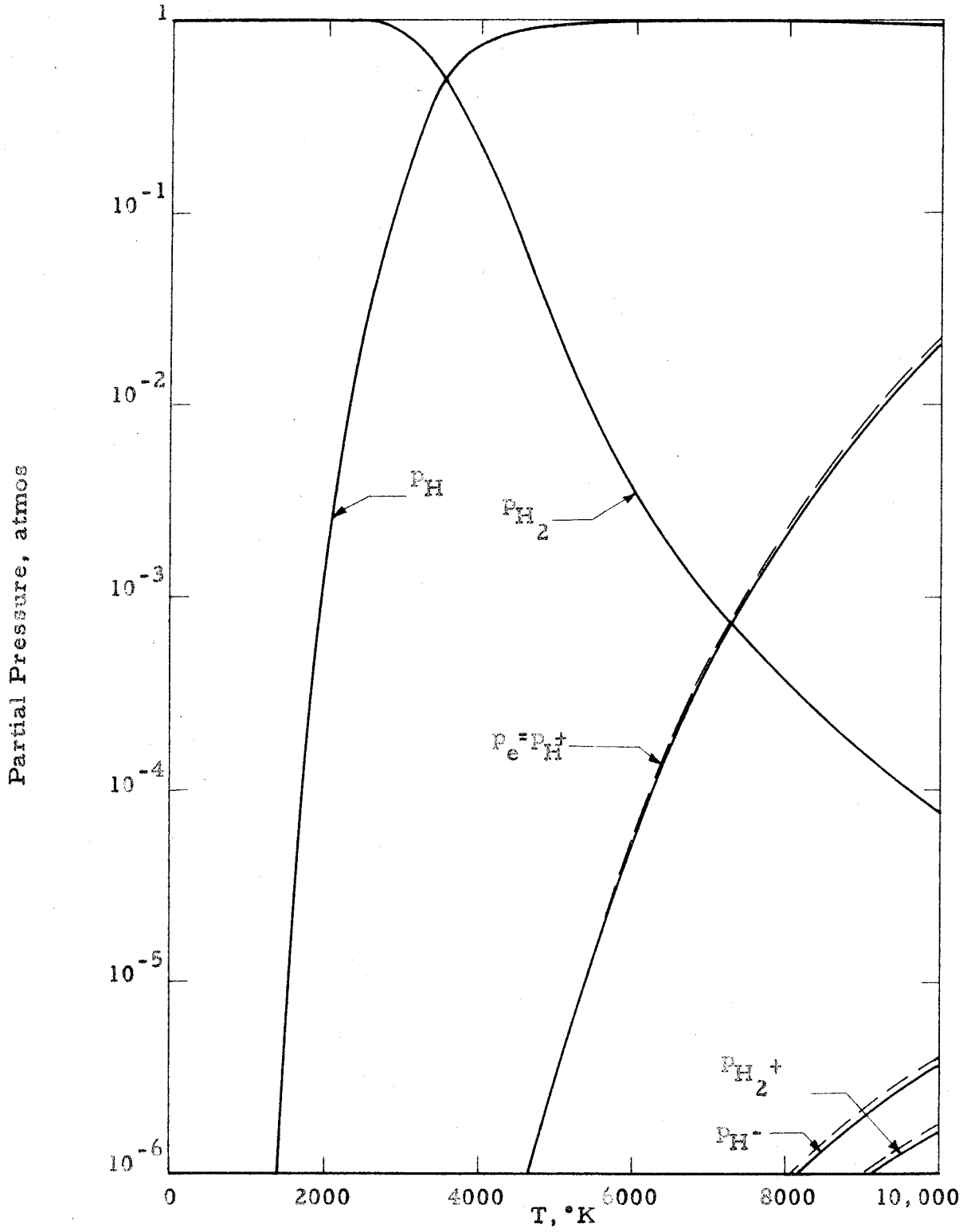

Fig. 24. Equilibrium composition as a function of temperature for p_T = 1 atmos. The difference between p_e and p_{H^+} is too small to be shown. The dashed curves include the correction for the lowering of the ionization potential.

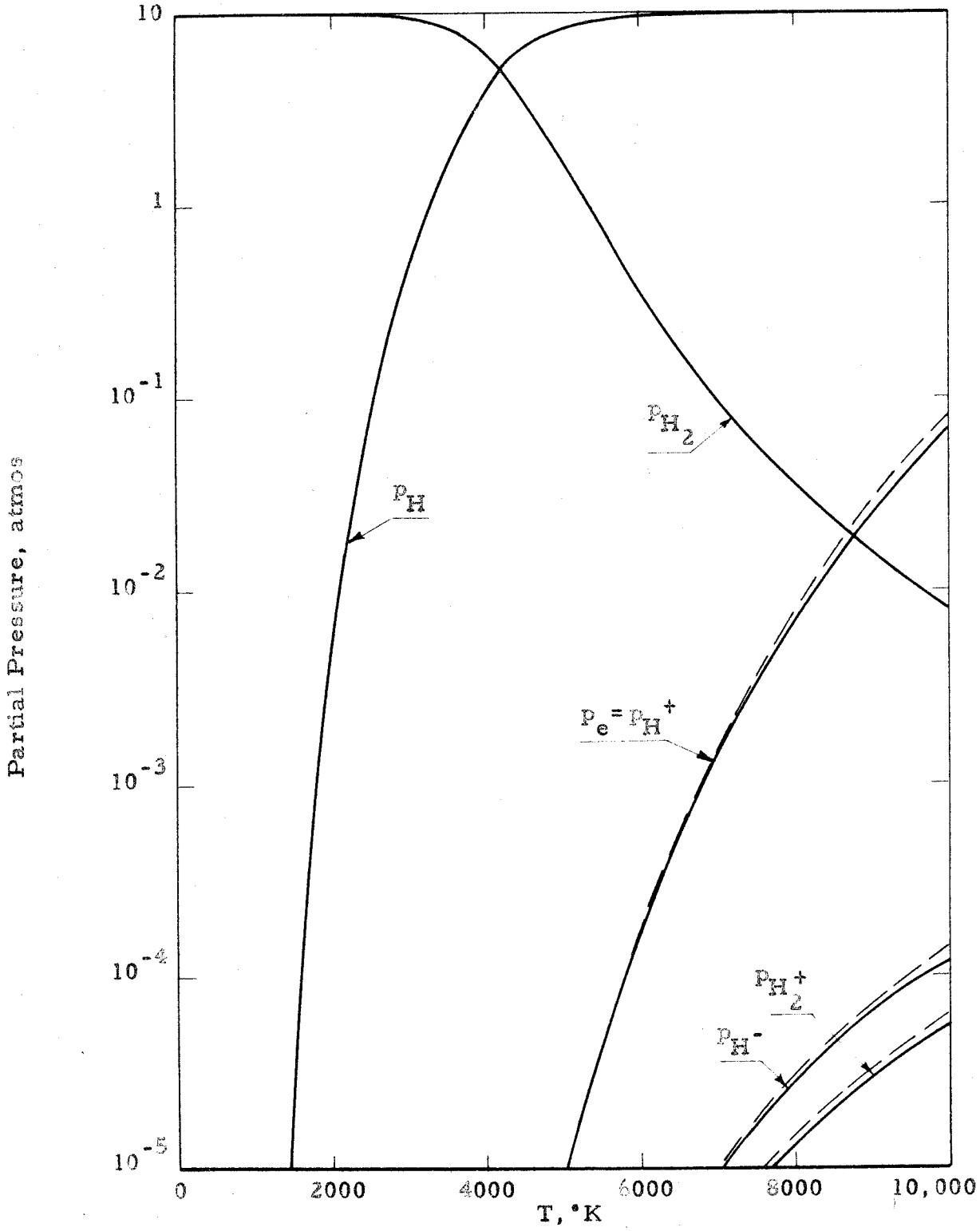

Fig. 25. Equilibrium composition as a function of temperature for p_T = 10 atmos. The difference between p_e and p_{H^+} is too small to be shown. The dashed curves include the correction for the lowering of the ionization potential.

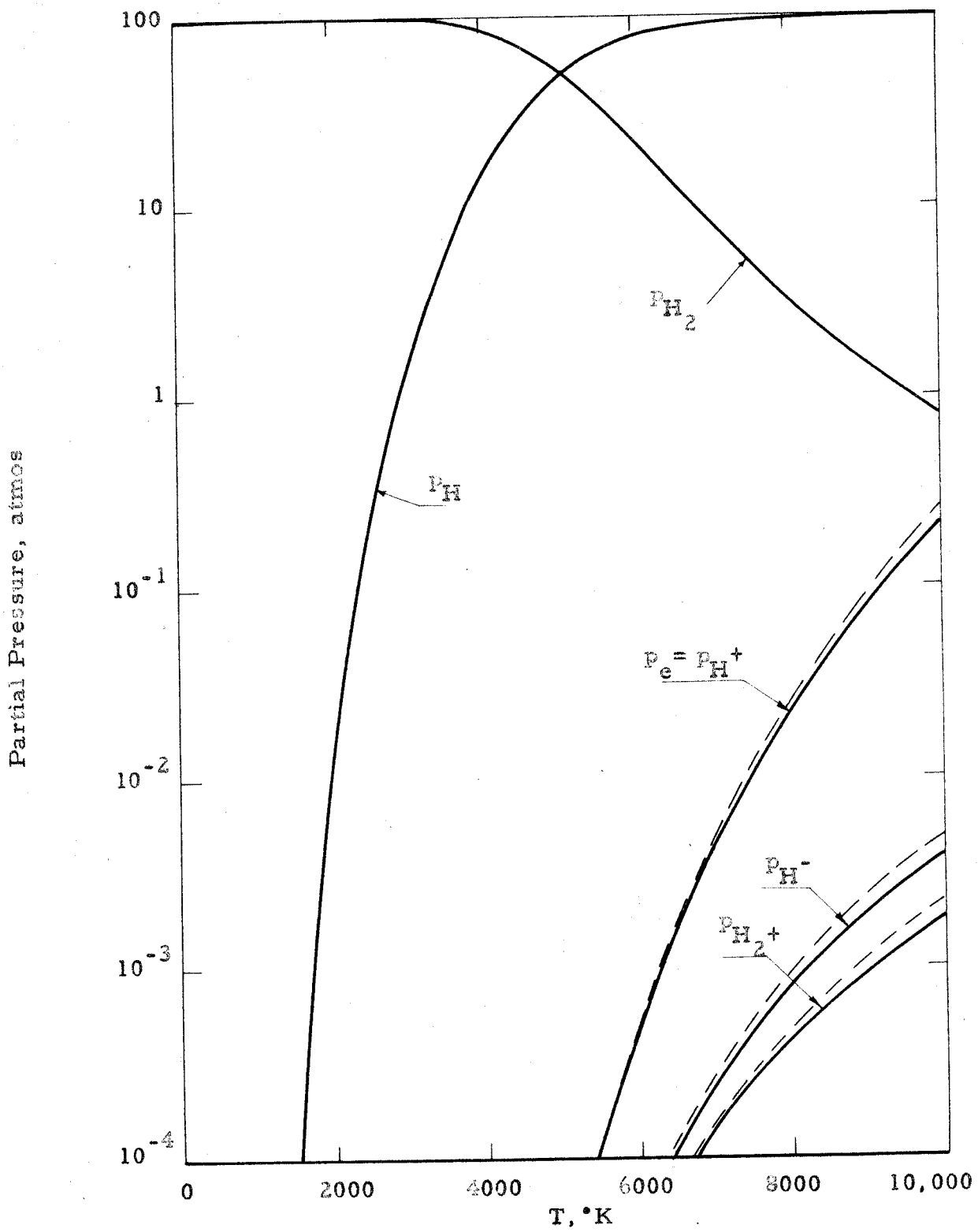

Fig. 26. Equilibrium composition as a function of temperature for p_T = 100 atmos. The difference between p_e and p_{H^+} is too small to be shown. The dashed curves include the correction for the lowering of the ionization potential.

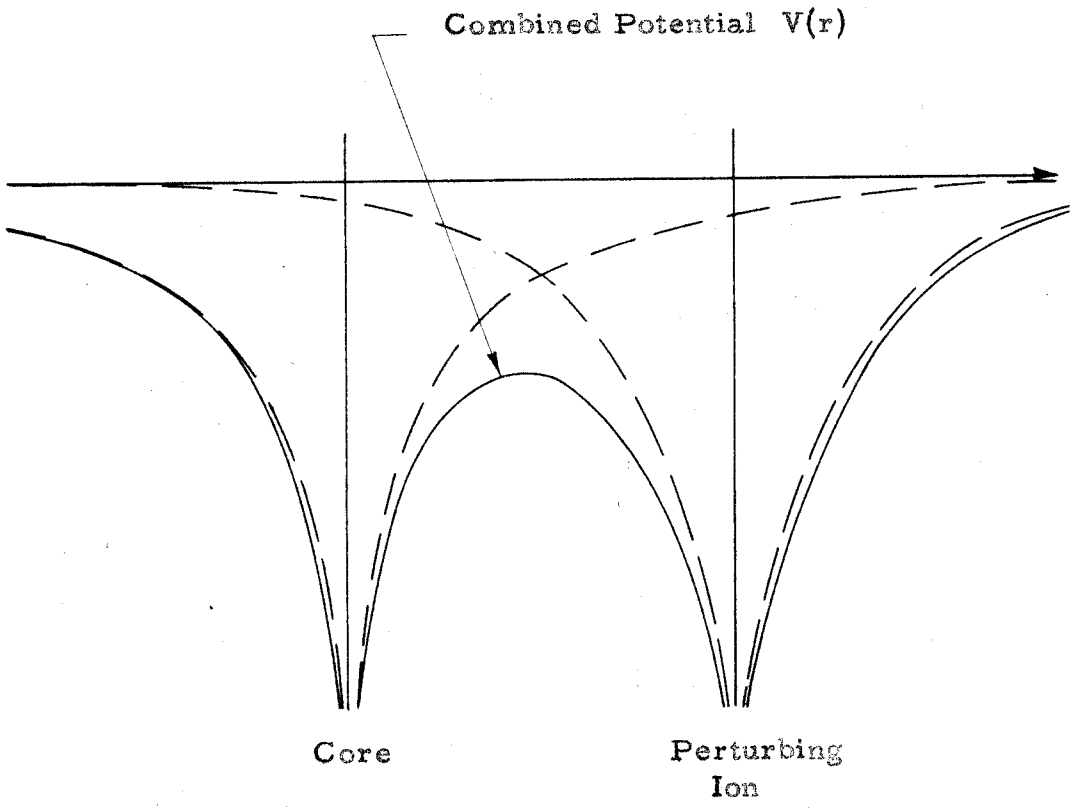

Fig. 27. Potential energy curves for an electron in the field of a particle (atom, ion, or molecule) core and an ion.

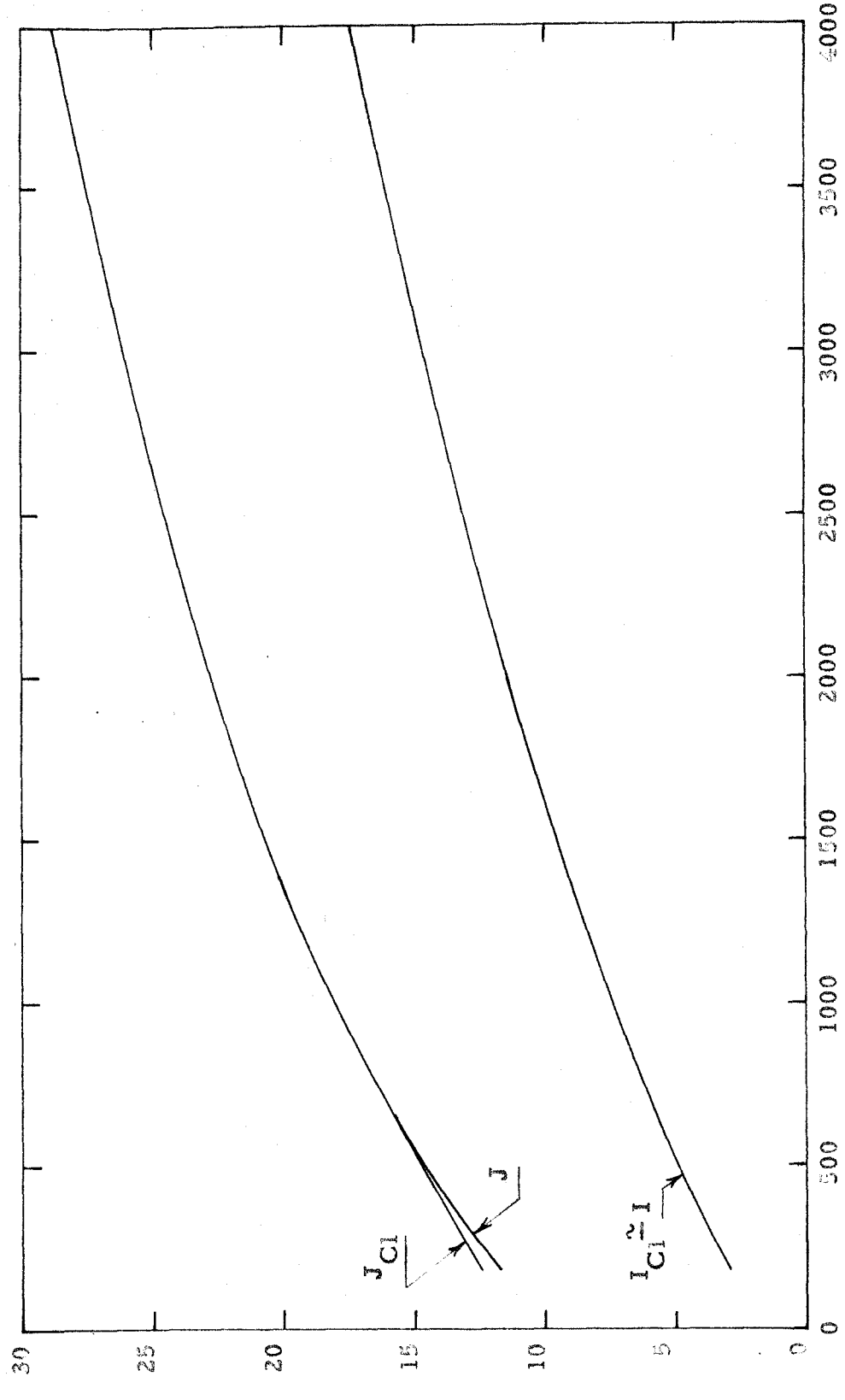

Fig. 28. The integrals I, J, I_{Cl}, and J_{Cl} for pressure-induced absorption as functions of the temperature.

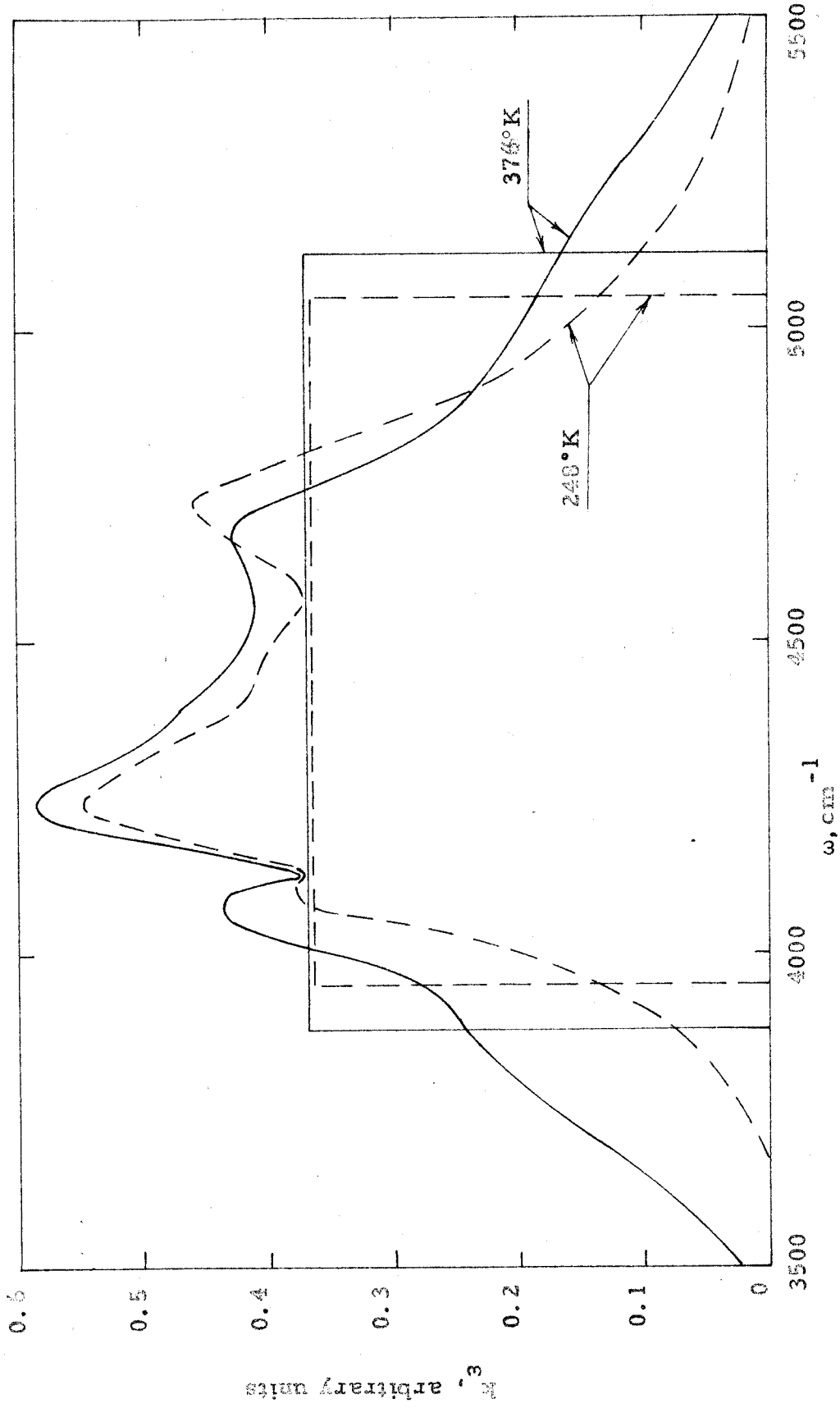

Fig. 29. Box model for the fundamental band compared with the absorption coefficients measured by Chisholm and Welsh.(27)

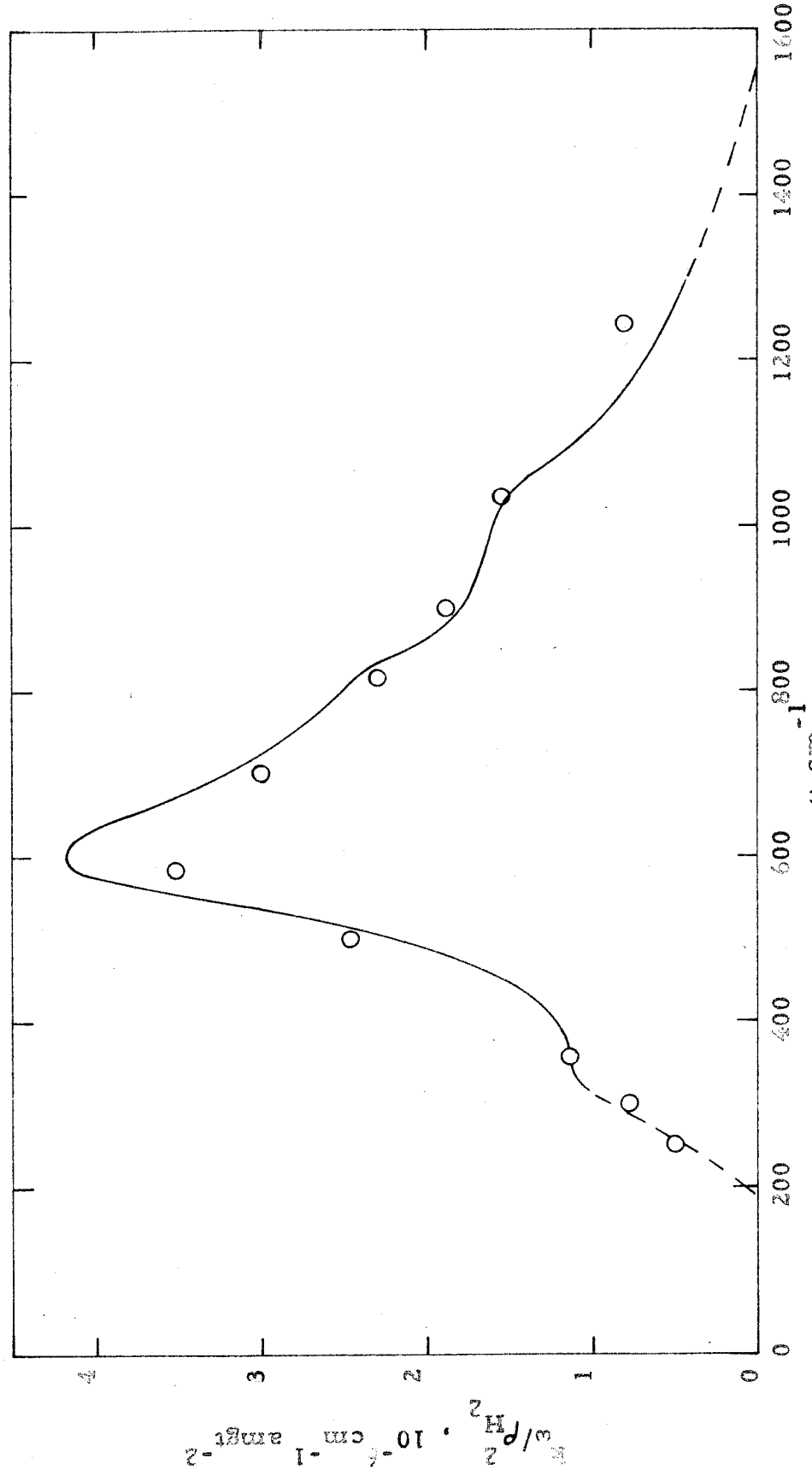

Fig. 30. The pressure-induced absorption coefficient for the rotational lines of H_2 at 300°K as measured by Kiss et al.[33] (curve) and computed from Eq. (34) (circles).

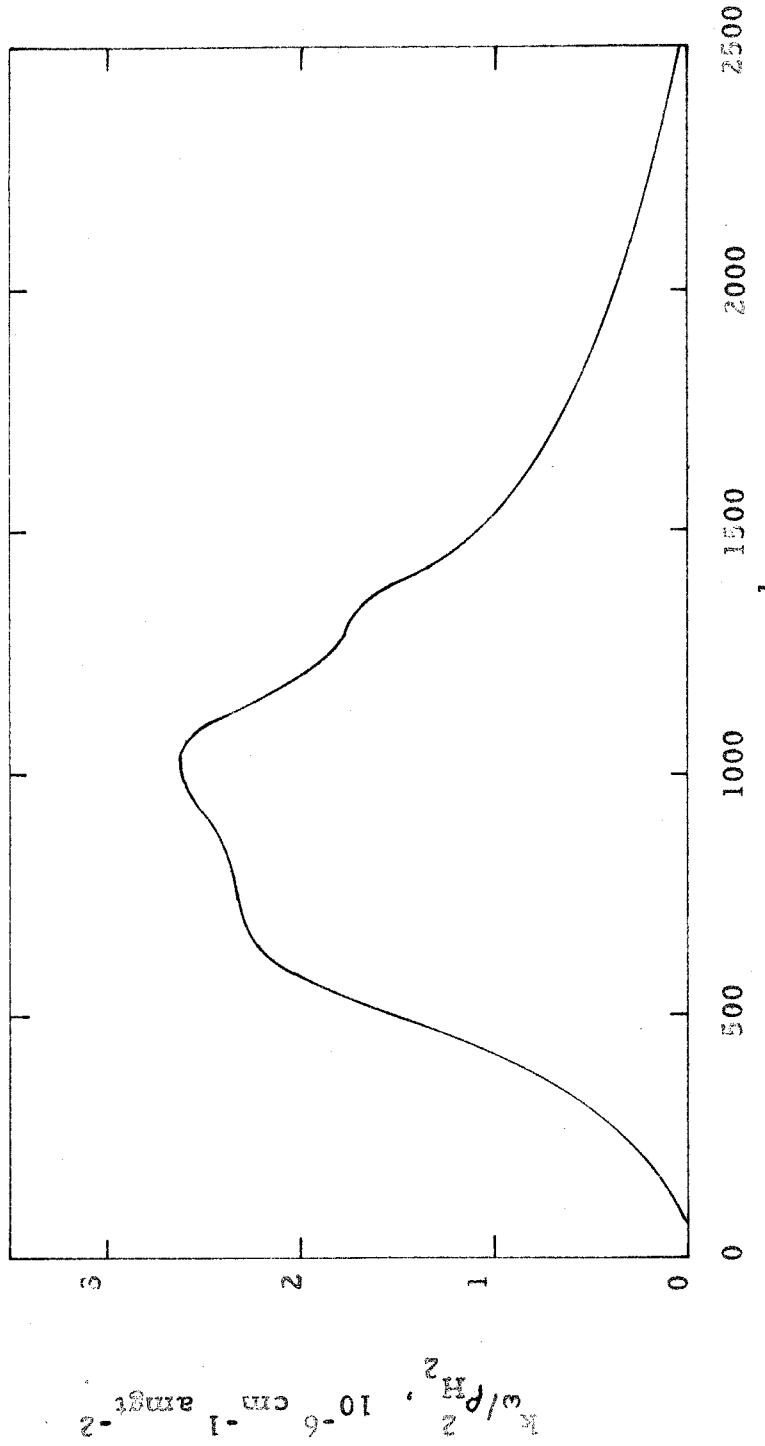

Fig. 31. The pressure-induced absorption coefficient for the rotational lines of H_2 computed from Eq. (34) for T = 300°K.

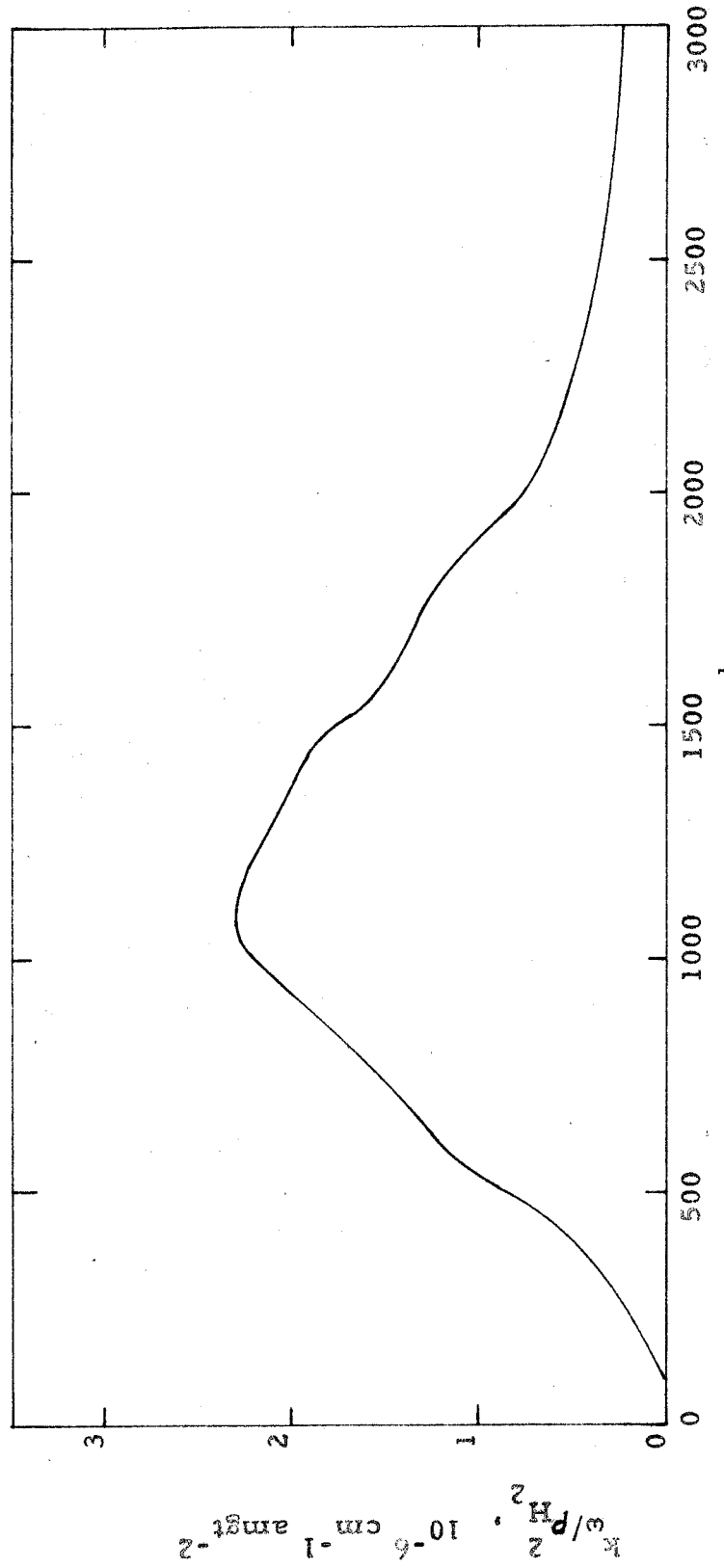

Fig. 32. The pressure-induced absorption coefficient for the rotational lines of H_2 computed from Eq. (34) for T = 1000°K.

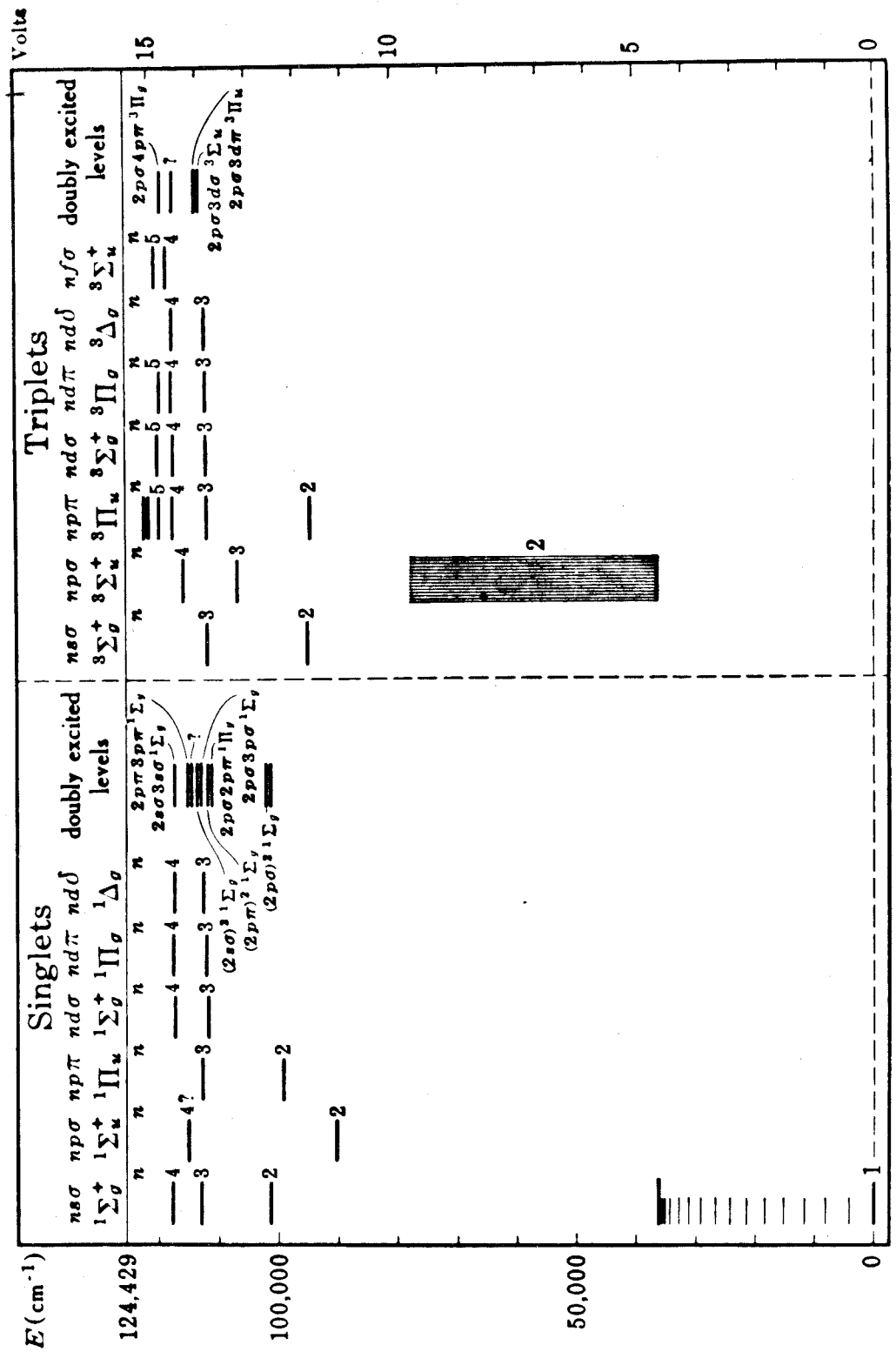

Fig. 33. Energy level diagram of the observed electronic states of the H_2 molecule (after Fig. 160 of Ref. 19).

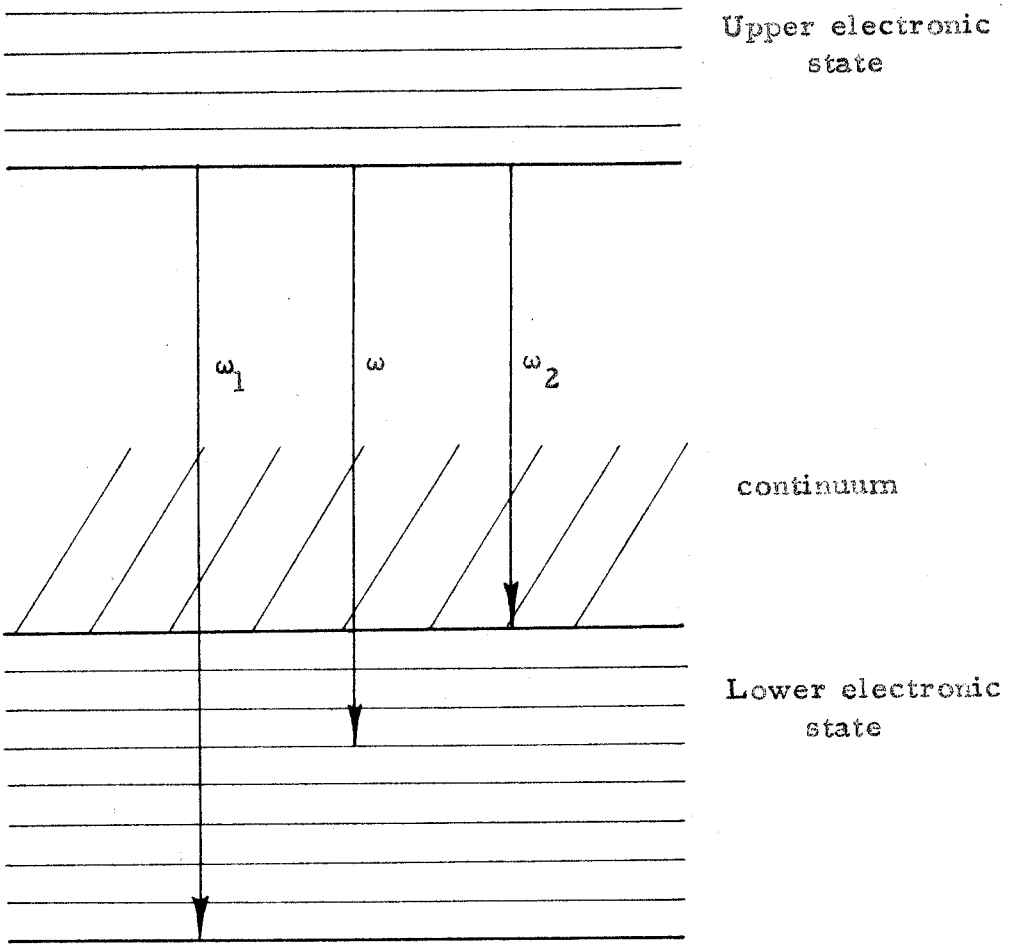

Fig. 34. Energy level diagram illustrating the model used for estimating the emissivity contributions of the Lyman and Werner bands.

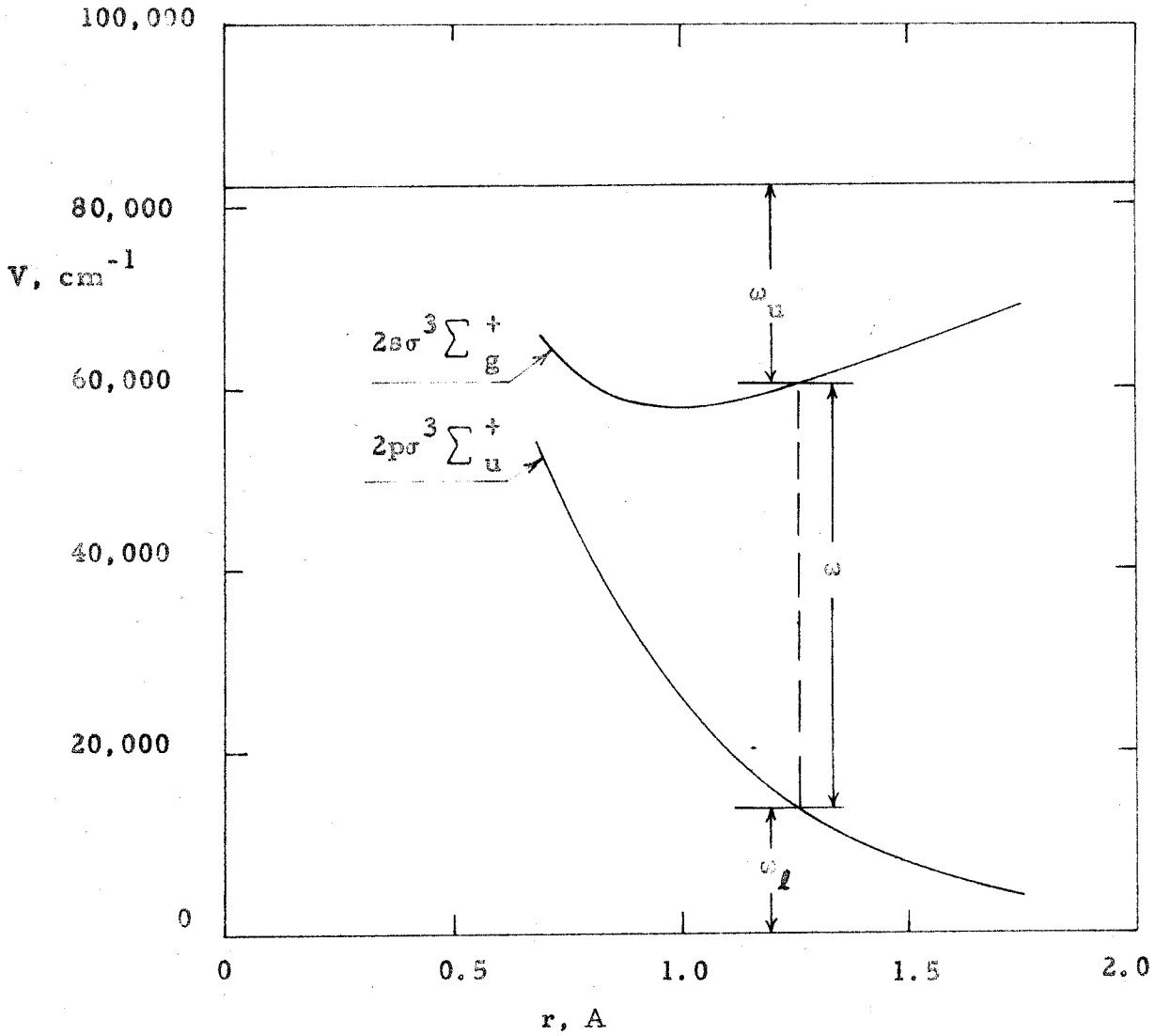

Fig. 35. Potentials of H_2 (from Ref. 66) considered in the broadening of the low wavenumber wing of the Lyman α line. A transition as described by the statistical theory is illustrated.

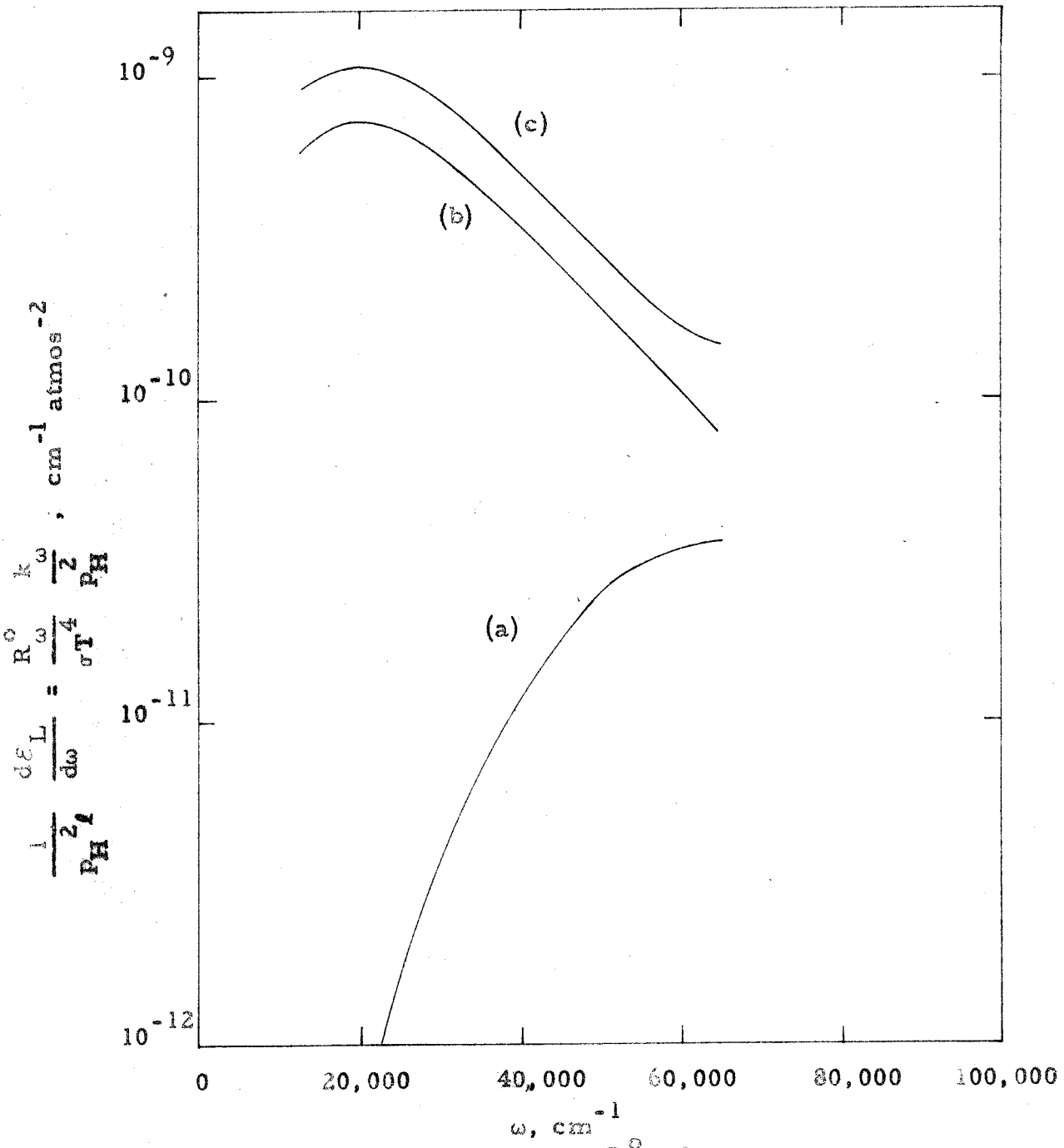

Fig. 36. The quantity $\frac{1}{p_H^2 \ell} \frac{d\varepsilon_L}{d\omega} = \frac{R^o_\omega}{\sigma T^4} \frac{k_\omega^3}{p_H^2}$ at 8000°K. Curve (a) was computed by using Eq. (72), curve (b) by using Eq. (72) with the repulsive term omitted, and curve (c) by using Eqs. (61) and (62).

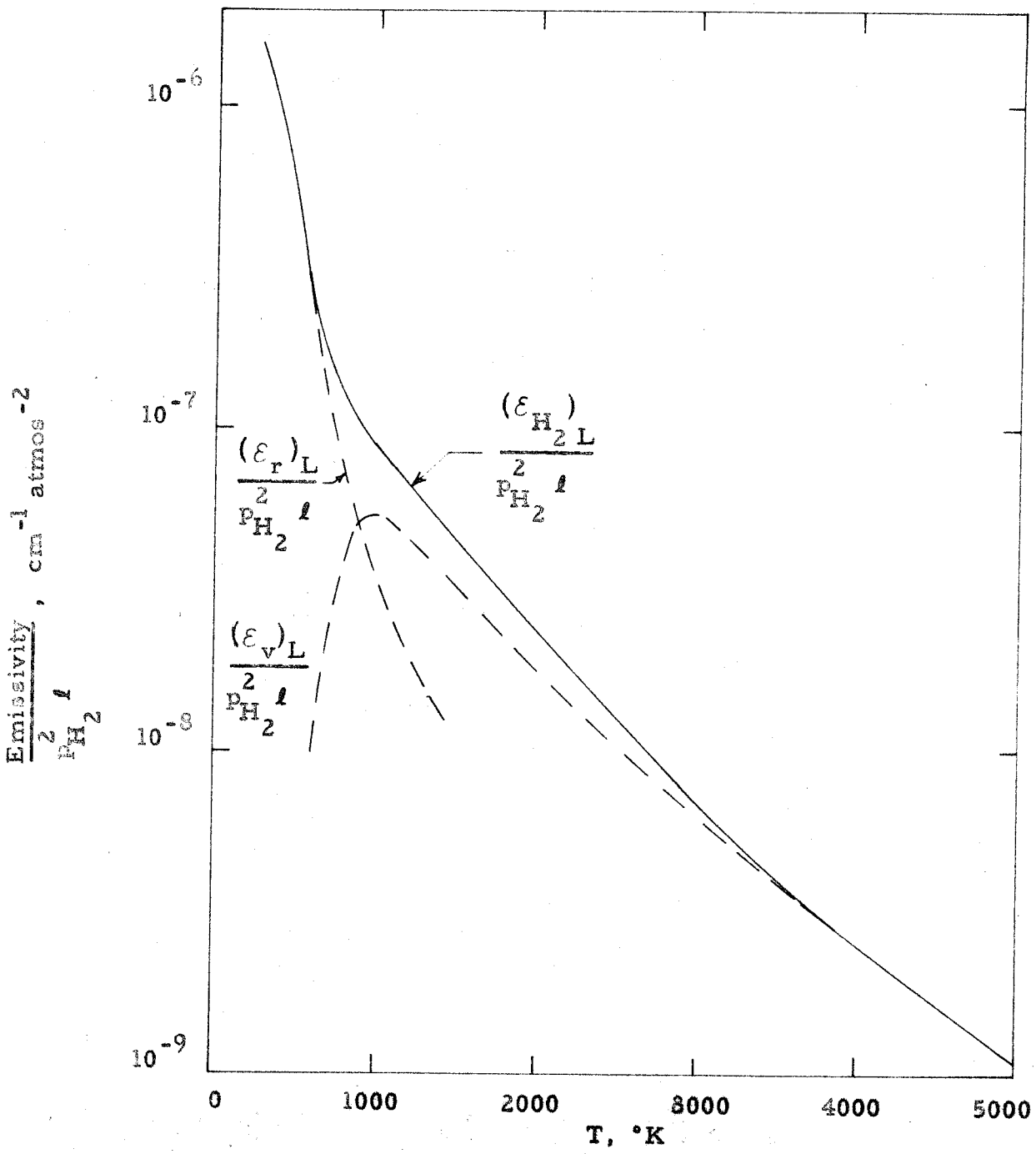

Fig. 37. The transparent gas emissivity term $(\varepsilon_{H_2})_L/p_{H_2}^2$ as a function of the temperature. This term is the sum of the contribution from the pressure-induced rotational spectrum, $(\varepsilon_r)_L/p_{H_2}^2$, and that from the pressure-induced fundamental vibration-rotation band, $(\varepsilon_v)_L/p_{H_2}^2$

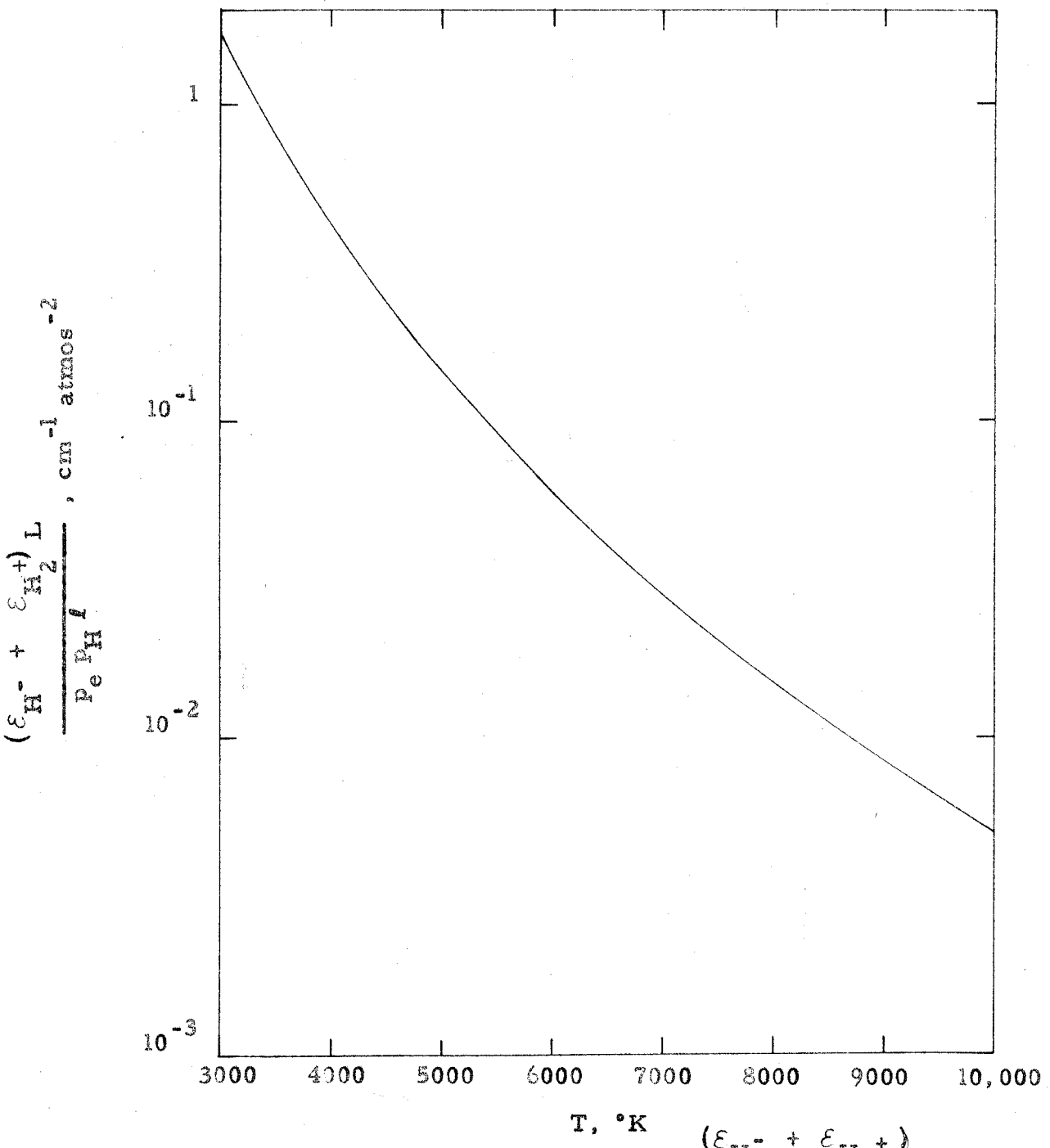

Fig. 38. The transparent gas emissivity term $\frac{(\varepsilon_{H^-} + \varepsilon_{H_2^+})_L}{P_e P_H \ell}$ as a function of temperature.

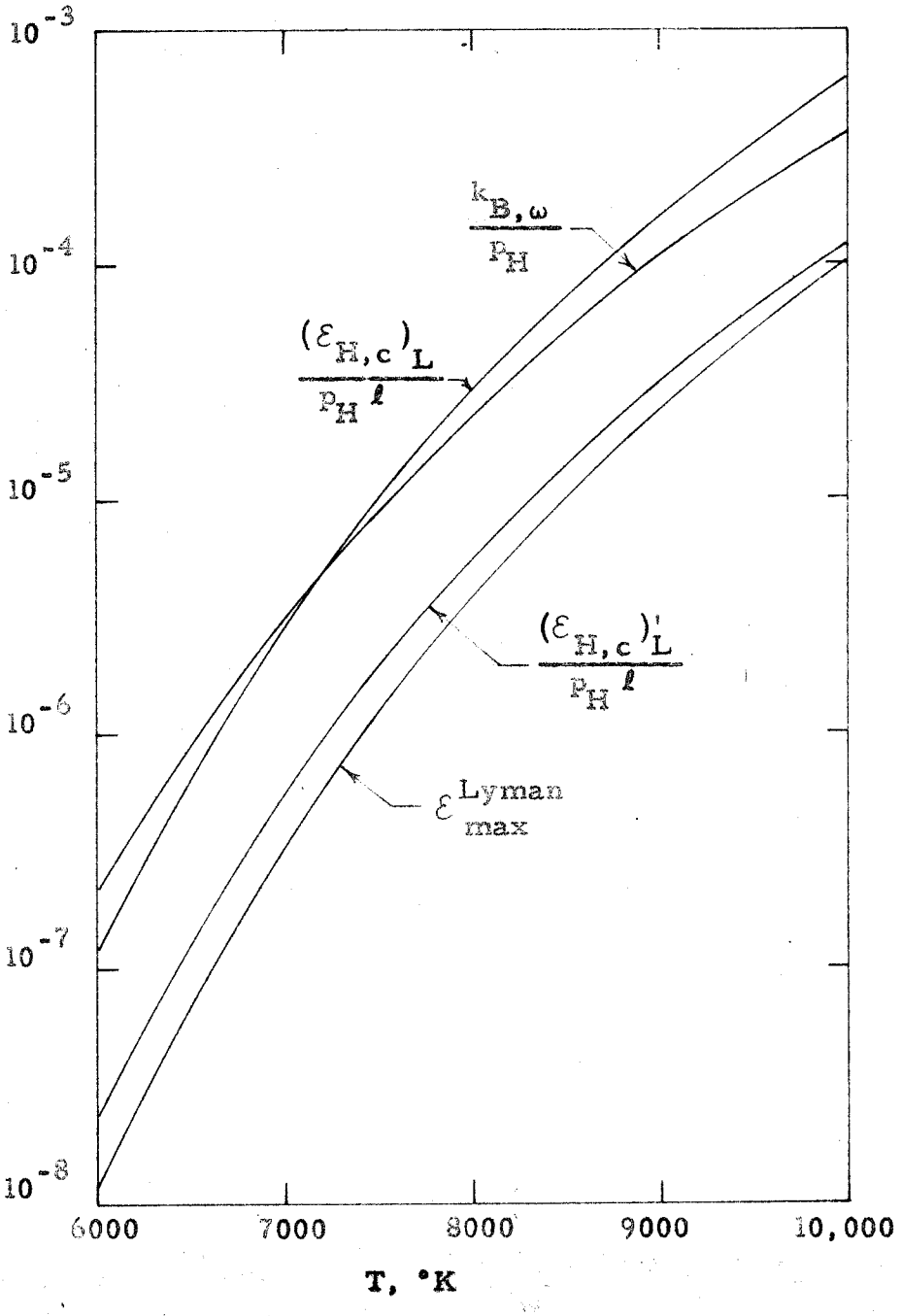

Fig. 39. The transparent gas emissivity terms $(\varepsilon_{H,c})_L/p_H$ and $(\varepsilon_{H,c})'_L/p_H$ in $cm^{-1}atmos^{-1}$, the maximum value of the Balmer continuum absorption coefficient $k_{B,\omega}/p_H$ in $cm^{-1}atmos^{-1}$, and $\varepsilon^{Lyman}_{max} = \int_{R_y}^{\infty} R^o_\omega d\omega$ as functions of the temperature.

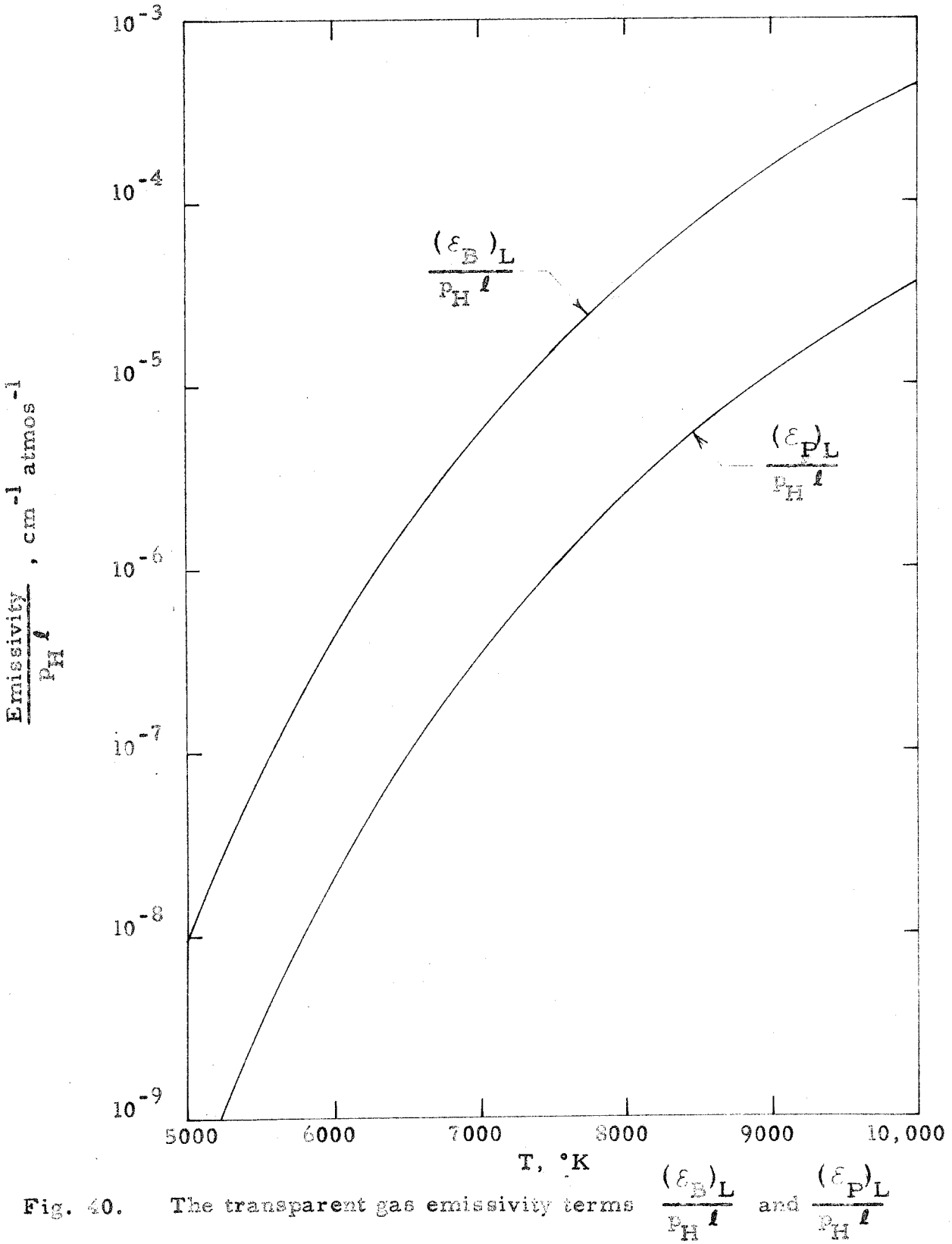

Fig. 40. The transparent gas emissivity terms $\frac{(\varepsilon_B)_L}{P_H \ell}$ and $\frac{(\varepsilon_P)_L}{P_H \ell}$ for the Balmer and Paschen lines, respectively.

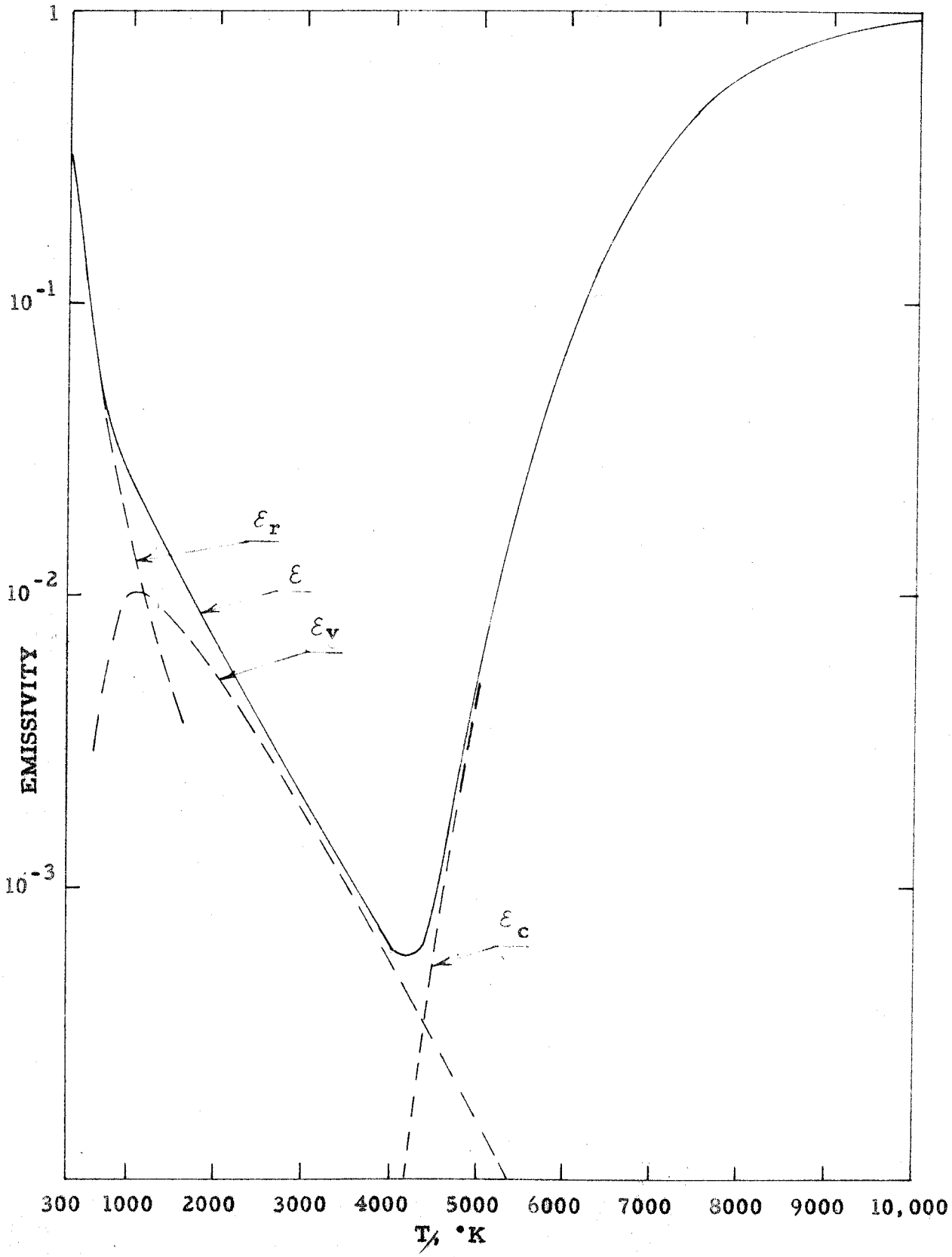

Fig. 41. The total emissivity $\mathcal{E}$ of a hydrogen plasma for p_T= 100 atmos and ℓ = 30 cm. The dashed lines indicate emissivity contributions from the pressure-induced rotational lines $\mathcal{E}_r$ and fundamental band $\mathcal{E}_v$, and from the continuum spectrum $\mathcal{E}_c$.

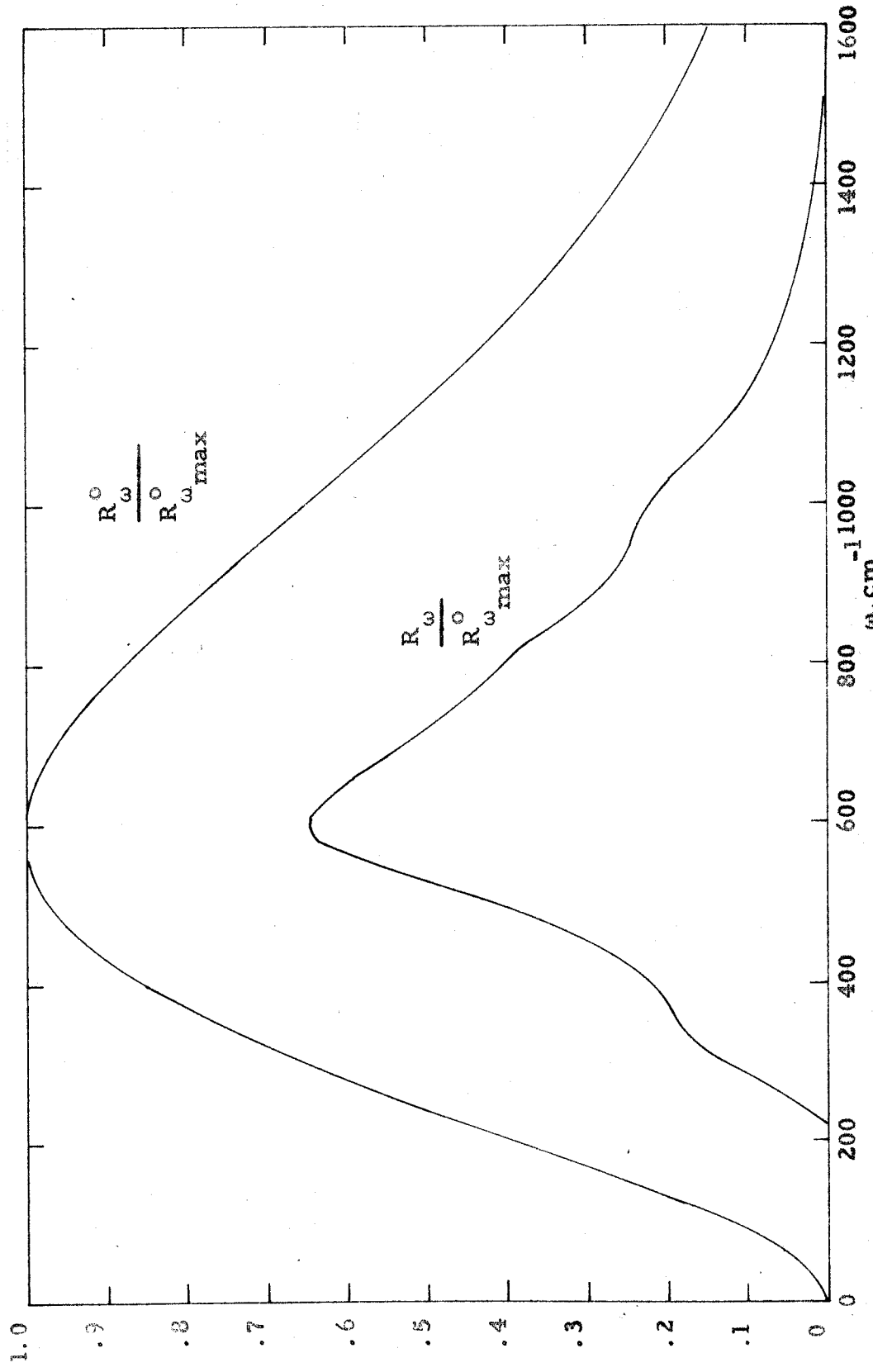

Fig. 42. The relative radiancy $R_\omega/R^o_{\omega_{max}}$ at 300°K for the pressure-induced rotational spectrum with p_T = 100 atmos and ℓ = 30 cm. The relative blackbody radiancy $R^o_\omega/R^o_{\omega_{max}}$ is shown for comparison.

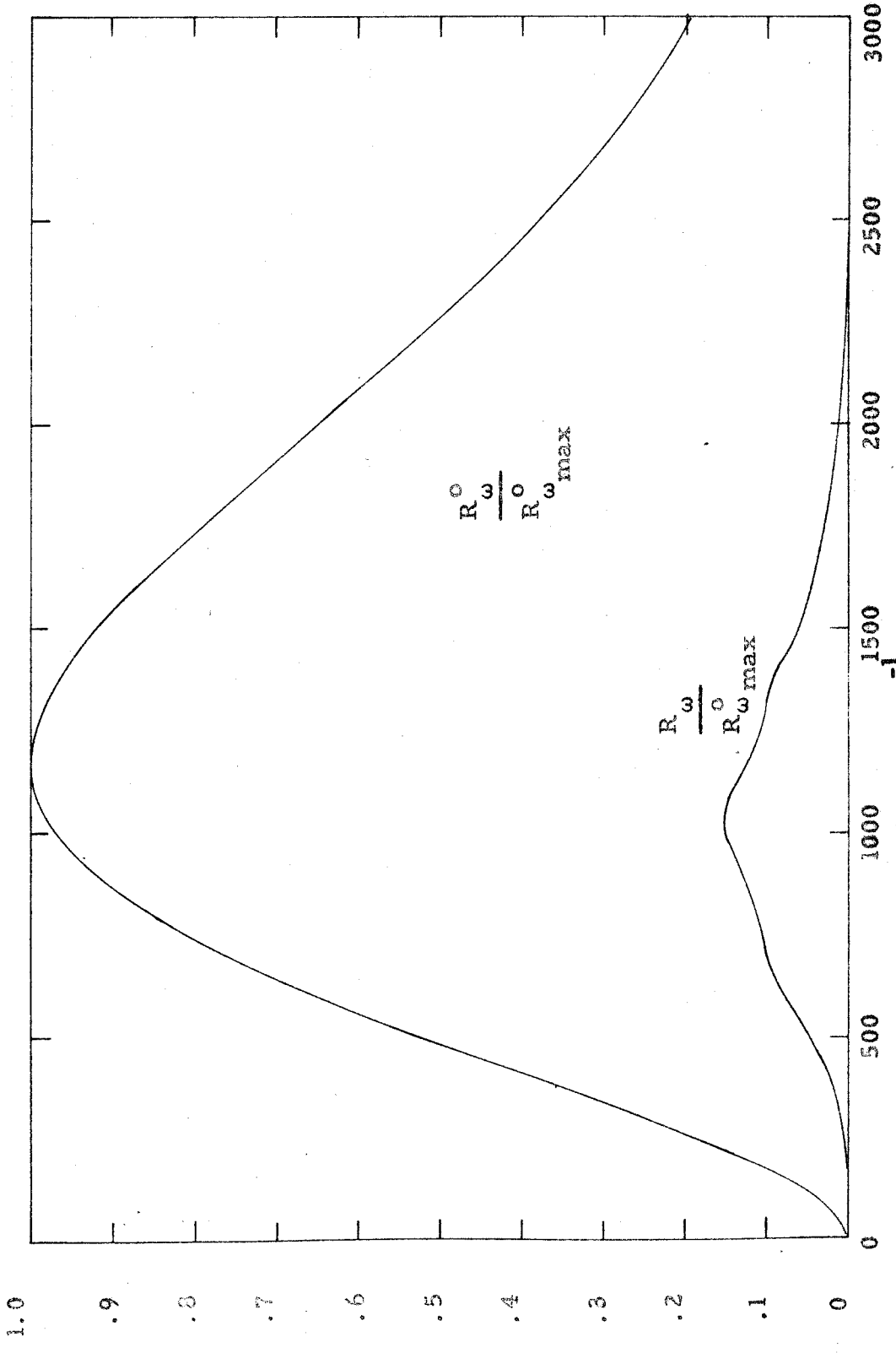

Fig. 43. The relative radiancy $R_\omega/R^o_{\omega_{max}}$ at 600°K for the pressure-induced rotational spectrum with p_T = 100 atmos and ℓ = 30 cm. The relative blackbody radiancy $R^o_\omega/R^o_{\omega_{max}}$ is shown for comparison.

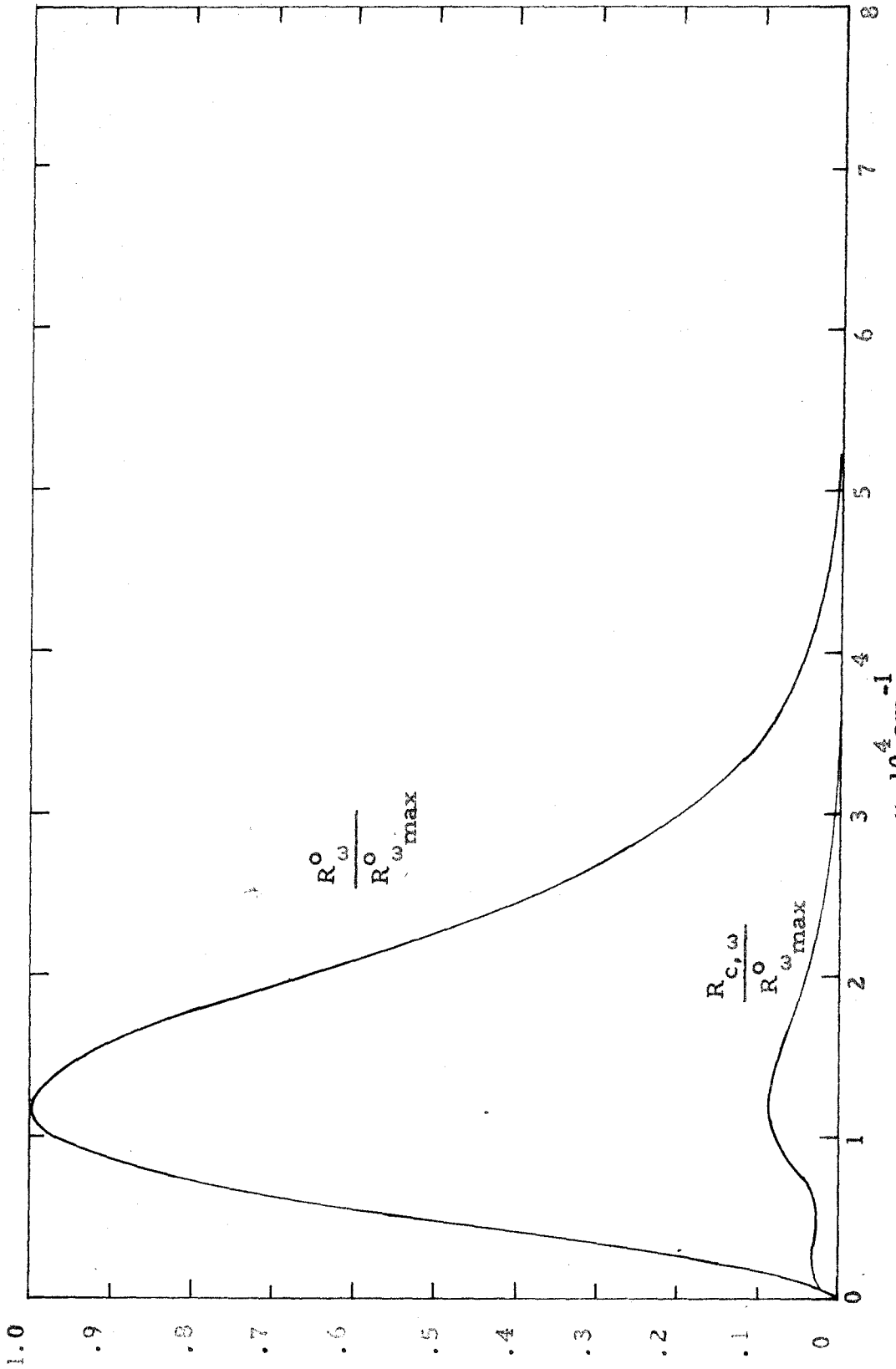

Fig. 44. The relative continuum radiancy $R_{c,\omega}/R^{o}_{\omega_{max}}$ for $T = 6000^{o}K$, $p_T = 100$ atmos, and $\ell = 30$ cm compared with the relative blackbody radiancy $R^{o}_{\omega}/R^{o}_{\omega_{max}}$.

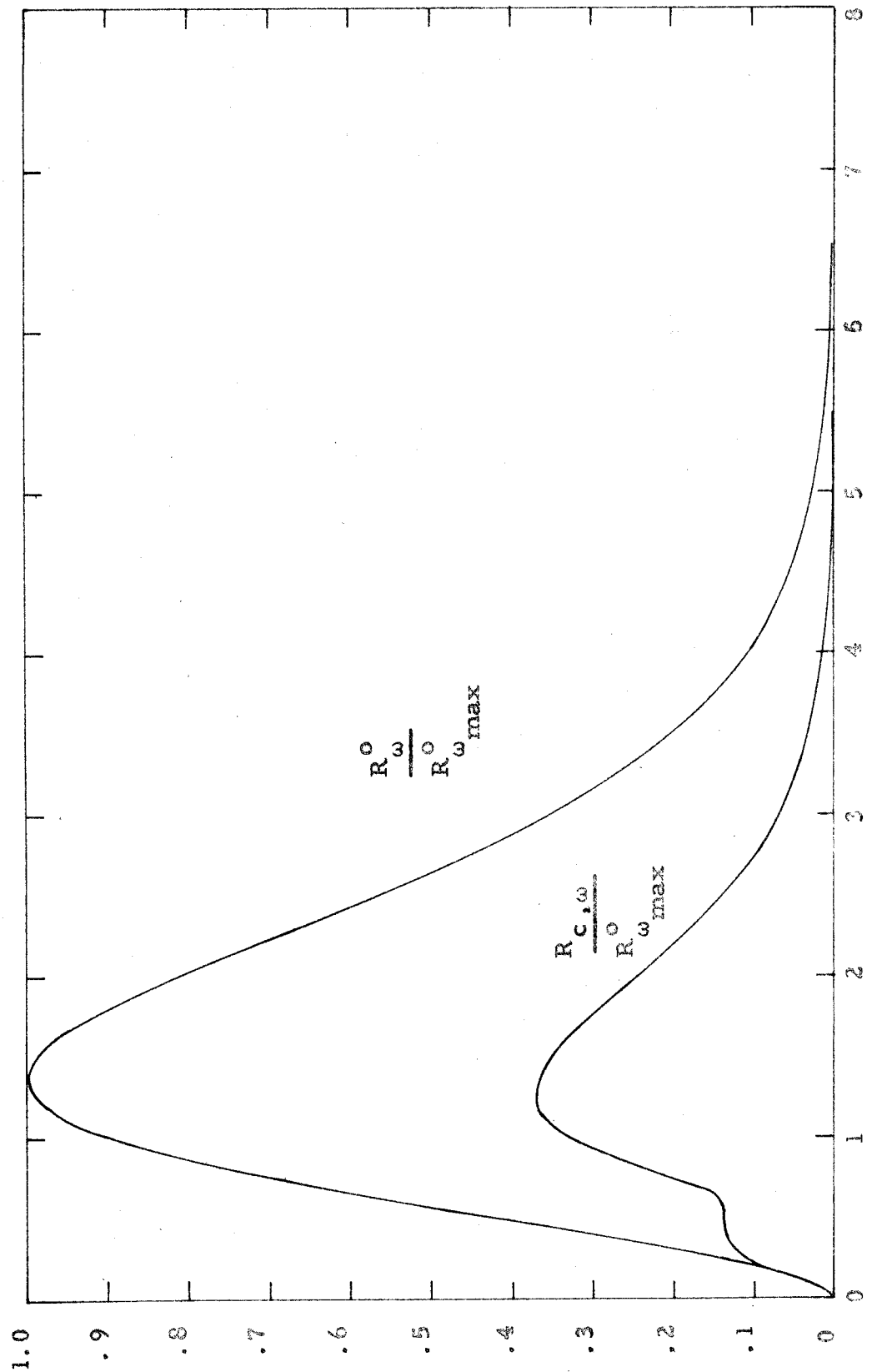

Fig. 45. The relative continuum radiancy $R_{c,\omega}/R^o_{\omega_{max}}$ for T = 7000°K, p_T = 100 atmos, and ℓ = 30 cm compared with the relative blackbody radiancy $R^o_\omega/R^o_{\omega_{max}}$.

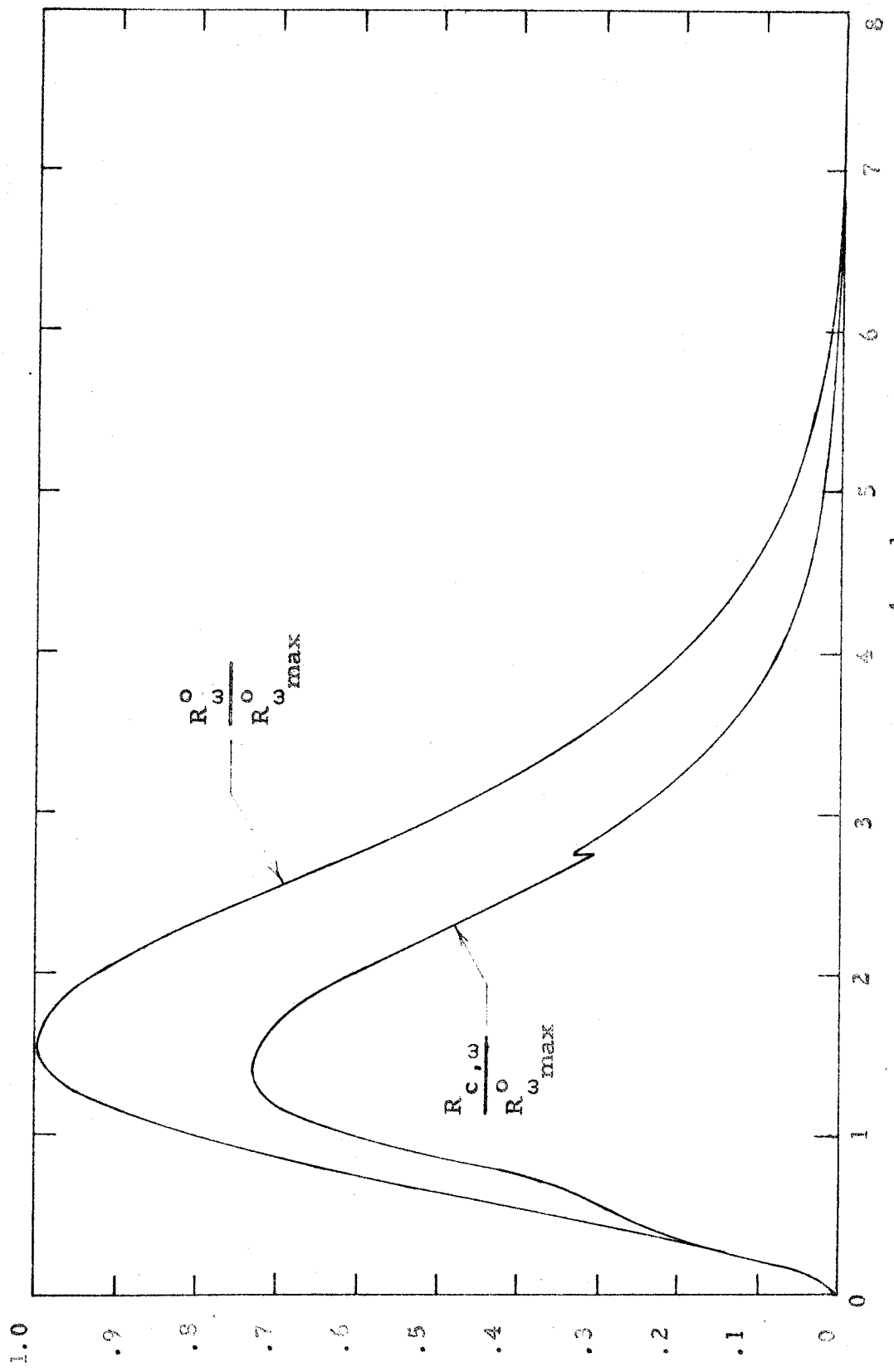

Fig. 46. The relative continuum radiancy $R_{c,\omega}/R^o_{\omega_{max}}$ for T = 8000°K, p_T = 100 atmos, and ℓ = 30 cm compared with the relative blackbody radiancy $R^o_\omega/R^o_{\omega_{max}}$.

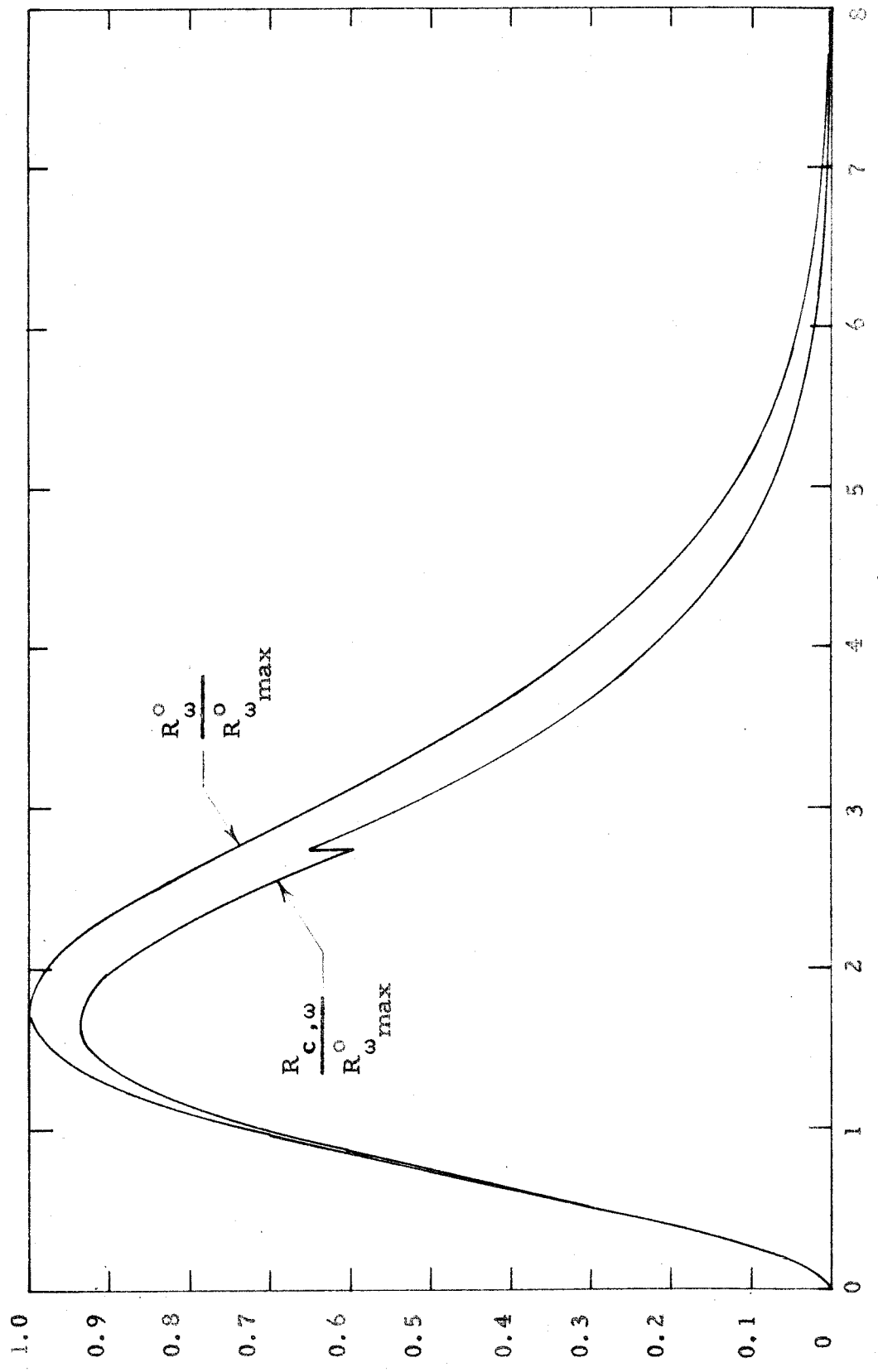

Fig. 47. The relative continuum radiancy $R_{c,\omega}/R^o_{\omega_{max}}$ for $T = 9000^oK$, $p_T = 100$ atmos, and $\ell = 30$ cm compared with the relative blackbody radiancy $R^o_\omega/R^o_{\omega_{max}}$.

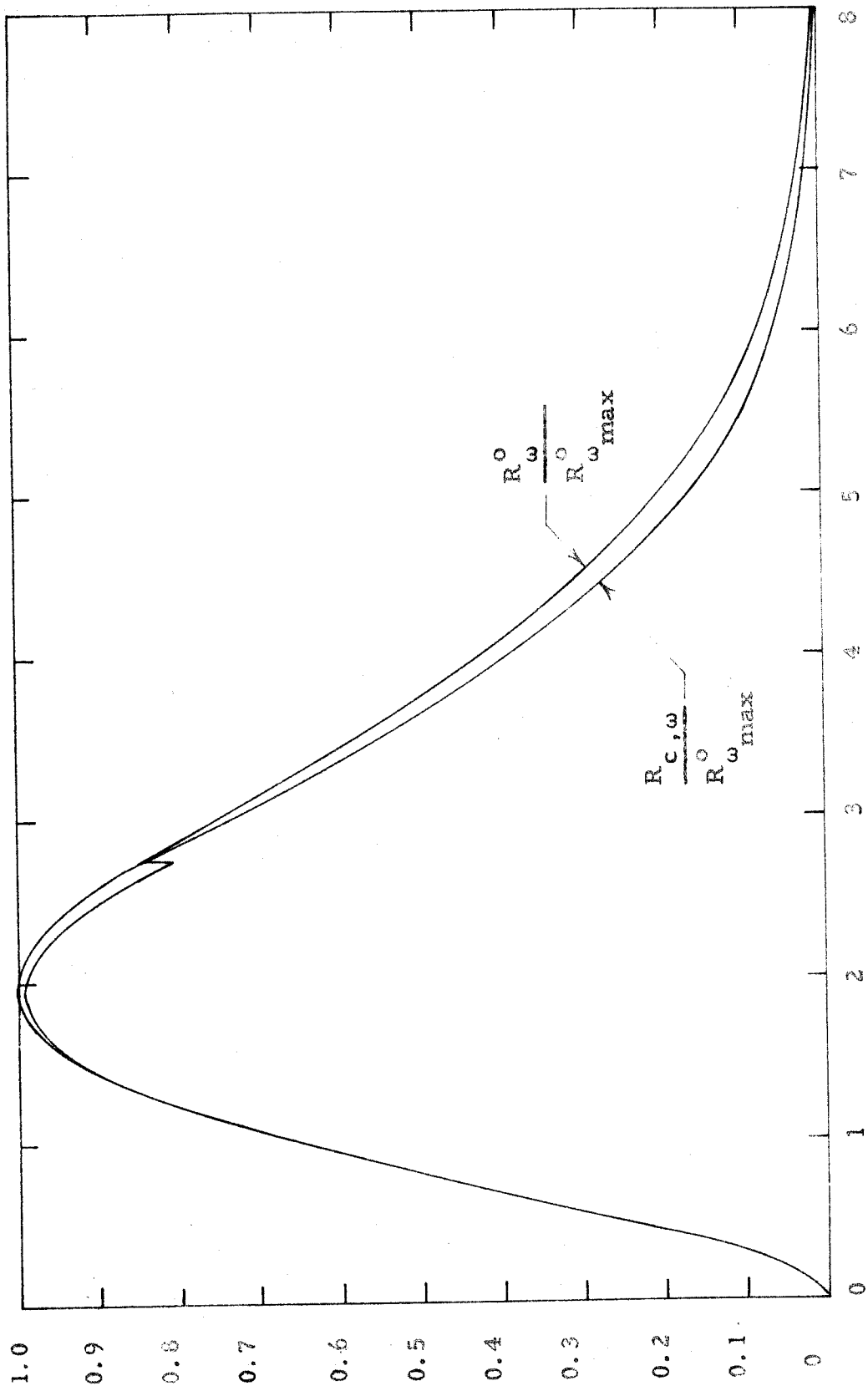

Fig. 48. The relative continuum radiancy $R_{c,\omega}/R^o_{\omega_{max}}$ for T = 10,000°K, p_T = 100 atmos, and λ = 30 cm compared with the relative blackbody radiancy $R^o_\omega/R^o_{\omega_{max}}$.